Arabidopsis Salicylic Acid-Binding Metalloendopeptidases TOP1 and TOP2 Regulate H_2O_2 Accumulation and Programmed Cell Death during the Immune Response against the Bacterial Pathogen *Pseudomonas syringae*

Honors Thesis
Presented to the College of Agriculture and Life Sciences,
Plant Science Research Honors Program,
of Cornell University
in Partial Fulfillment of the Requirements for the
Research Honors Program

by
Giulio Zampogna
May 2012

Dr. Sorina Popescu

Abstract

Salicylic acid is a phytohormone indispensable for plant immunity. Interactions between hosts and pathogens create selective pressures—a cycle whereby hosts evolve novel defenses and alarm systems while their pathogen counterparts evolve enhanced weaponry and stealth tactics. Not uncommonly, plants lose the war against pathogens and succumb to disease. If a plant does survive a pathogen attack, it may be left with battle scars that reduce vegetative growth and fruit yield and quality. Without question, human survival depends on the abilities of plants to defend themselves against and survive pathogen onslaughts. With an increased understanding of plant immunity, humans will gain the ability to modulate and augment plant defenses to minimize disease and yield losses. *Arabidopsis thaliana* thimet oligopeptidase (TOP) family TOP1 and TOP2 metalloendopeptidases bind salicylic acid and may, therefore, play critical roles in plant immunity. Our research demonstrates that TOP1 and TOP2 regulate hydrogen peroxide accumulation, programmed cell death intensity, and possibly chloroplast integrity during the hypersensitive response following infection by the hemibiotrophic bacterial pathogen *Pseudomonas syringae*. We hypothesize that TOP1 and TOP2 are central hubs in reactive oxygen species production and redox regulation, and, as such, may influence physiological responses during both abiotic and biotic stresses.

Introduction

Prelude

Plants have evolved an elaborate immune system that senses and responds to environmental stimuli to enable acclimation and increased tolerance or resistance against pathogens and disease. However, plant defense responses represent enormous energy costs. Fitness, therefore, is relative to the abilities of a plant to balance mobilization of its defensive resources under appropriate conditions (Durrant and Dong, 2004). Increased knowledge of plant immunity may forward the production of novel plant defense elicitors and, in addition, potentially uncover animalian orthologs and components of the basal eukaryotic cell defense machinery (Greenberg and Yao, 2004). Researchers must study the interactome—the proteome and the mass complexity of

interconnections and crosstalk between signaling pathways—to understand the intricacies composing plant immunity.

Salicylic Acid and Plant Immunity

Salicylic acid (SA) is an endogenous phenolic phytohormone having essential regulatory roles in plant immunity, and is necessary for normal physiological functioning and development (**Figure S1**) (Vanacker et al., 2001; Vlot et al., 2009). SA is involved in the regulation of microbe/pathogen-associated molecular pattern (MAMP/PAMP)-triggered immunity (MTI/PTI), effector-triggered immunity (ETI), and systemic acquired resistance (SAR)—collectively termed the resistance response—in angiosperm monocots and eudicots (Vlot et al., 2009). MTI is a weak, broad-spectrum form of resistance, whereas ETI is stronger, faster, and pathogen-specific. Although conceptually separated, an absolute division between MTI and ETI does not exist except for their modes of pathogen elicitor recognition: perception of MAMPs via cell surface pattern recognition receptors (PRRs) or perception of effectors via primarily intracellular Resistance (R) proteins, respectively (Coll et al., 2011; Dodds and Rathjen, 2010; Gimenez-Ibanez and Rathjen, 2010; Padmanabhan and Dinesh-Kumar, 2010).

R genes mostly encode intracellular receptor-like R proteins possessing nucleotide-binding (NB) and leucine-rich repeat (LRR) domains (Vlot et al., 2009). In general, NB-LRR proteins directly or indirectly recognize immunosuppressant pathogen effectors (avirulence proteins) secreted into the cell, and then relay signals to stimulate SA biosynthesis in chloroplasts and activate ETI (Fragnière et al., 2011; Nishimura and Dangl, 2010; Vlot et al., 2009). To activate defenses, the host plant must be able to recognize either MAMPs or effector proteins. If the host cannot recognize the effectors, then the host-pathogen interaction is compatible: the host is susceptible and the pathogen virulent and capable of causing disease. Reciprocally, host recognition of the effectors results in an incompatible interaction in which the host is resistant and the pathogen avirulent (Greenberg and Yao, 2004; Jones and Dangl, 2006).

Depending on the host-pathogen relationship, SA can promote or repress the hypersensitive response (HR)—a form of programmed cell death (PCD) similar to apoptosis in mammals—at the zone of infection (Greenberg and Yao, 2004; Vanacker et al., 2001). In *Arabidopsis thaliana*, for example, SA can promote HR-PCD after infection with the avirulent

bacterium *Pseudomonas syringae* pv. *tomato* (*Pst*) DC3000 *avrRpt2*, or—indirectly through NON-EXPRESSOR OF PATHOGENESIS-RELATED (PR) GENES 1 (NPR1)—repress cell death after infection with the avirulent *Pst* DC3000 *avrRpm1* (Rate and Greenberg, 2001; Vanacker et al., 2001). Additionally, SA can control photo-oxidative stress PCD spread by promoting the conversion of superoxide ($O_2\bullet^-$) to hydrogen peroxide (H_2O_2) and thus balance reactive oxygen species (ROS) production within chloroplasts to specifically disfavor PCD (Straus et al., 2010). Although its roles are highly debated, the HR may function by inhibiting or otherwise inducing signals that ultimately culminate in suppressing pathogen growth and dissemination (Coll et al., 2011).

ROS, such as H_2O_2, are normally produced in chloroplasts and mitochondria as a byproduct of photosynthesis and oxidative phosphorylation, respectively. Under normal growth conditions, chloroplasts are the main source of ROS in photosynthetic tissues, whereas that role is fulfilled by mitochondria in non-photosynthetic tissues (Jaspers and Kangasjärvi, 2010). However, high levels of and the specific balance between nitric oxide (NO) and different ROS produced during abiotic or biotic stress may activate PCD (Delledonne et al., 2001; Gadjev et al., 2008). During biotic stress, SA can inhibit the salicylic acid-binding proteins (SABPs) catalase (SABP1) and ascorbate peroxidase, two antioxidant enzymes in tobacco (*Nicotiana benthamiana*), to facilitate H_2O_2 accumulation from dismutated $O_2\bullet^-$ (Chen et al., 1993b; Durner and Klessig, 1995; Vicente and Plasencia, 2011). *N. benthamiana* chloroplastic carbonic anhydrase (SABP3) and its *Arabidopsis thaliana* ortholog (AtSABP3) are known to have antioxidant activities and roles in HR activation, perhaps by influencing chloroplastic ROS production; this indicates that SA-binding activity in chloroplasts may contribute to redox homeostasis (Slaymaker et al., 2002; Wang et al., 2009b).

Indeed, evidence has shown that H_2O_2 is a critically important signaling molecule that regulates chloroplastic SA biosynthesis and HR activation in response to pathogen infection (De Pinto et al., 2011; Snyrychová et al., 2009; Wolfe et al., 2000); for example, H_2O_2 can trigger mitogen-activated protein kinase (MAPK) signaling cascades, which mediate PCD primarily through interactions with WRKY transcription factors (Gadjev et al., 2008). High levels of SA may also inhibit acclimation to excessive light by reducing photosynthetic efficiency and thereby promoting ROS accumulation and PCD (Vicente and Plasencia, 2011; Vlot et al., 2009). Reciprocally, SA may act in a feedback loop to activate ROS detoxification pathways (e.g. by

mediating conversion of $O_2\bullet^-$ to H_2O_2) and thus prevent PCD, protect photosynthetic machinery, and facilitate acclimation to high light intensities (Straus et al., 2010; Torres, 2010; Vicente and Plasencia, 2011). But greater H_2O_2 accumulation relative to $O_2\bullet^-$ can initiate stress signals that promote runaway cell death (RCD), essentially an uncontrolled spread of PCD. However, as the potential for RCD increases after pathogen infection and enhanced SA activity, PCD is concomitantly restricted to the initial infection site by LESIONS STIMULATING DISEASE RESISTANCE RESPONSE 1 (LSD1) and *Arabidopsis thaliana* RESPIRATORY BURST OXIDASE HOMOLOG (AtRBOH) proteins (Dietrich et al., 1994; Torres et al., 2005). Clearly there exists a redox balance that, depending on intracellular crosstalk and epistatic signals, ultimately determines cell fate during an immune response (De Pinto et al., 2011; Miller et al., 2008; Mittler et al., 2004).

Generally during incompatible host-pathogen interactions, the HR precedes or is concomitant with SAR development; however, SAR development may not be a consequence of the HR (Liu et al., 2010b). SAR is an inducible and enduring defense system that confers broad-spectrum pathogen resistance in systemic tissues distal from the original site of infection. Upon recognizing avirulence effector proteins, NB-LRR proteins may relay SAR-induction signals and upregulate production of SA in non-infected tissues (Greenberg and Yao, 2004; Liu et al., 2010b). SAR development in *Arabidopsis* begins when SA is converted via *Arabidopsis thaliana* Benzoic Acid/Salicylic Acid Carboxyl Methyltransferase 1 (AtBSMT1) in locally infected tissue to the volatile ester methyl salicylate (MeSA), which can be transported long-distances systemically through phloem and be cleaved by *Arabidopsis thaliana* methyl/MeSA esterases (AtMSE)—orthologous to *N. benthamiana* SABP2—back into SA in uninfected tissues to initiate partial defense priming (Chen et al., 2003; Liu et al., 2010a; Park et al., 2007a; Vlot et al., 2008a; Vlot et al., 2008b). More recently, however, multiple studies have found that mobile lipid-based signals may additionally facilitate SAR development under certain conditions (Liu et al., 2011b).

Interestingly, a phenomenon termed systemic acquired tolerance has been observed in tomato and other species, and is characterized by a reduction in disease symptom development despite continued pathogen proliferation (Block et al., 2005). Mecey et al. (2011) found that *Arabidopsis thaliana STAYGREEN* (*AtSGR*) expression is upregulated during pathogen infection and promotes chlorotic cell death disease symptom development. Specifically, they found that *no*

chlorosis1 (*noc1*) mutants (*AtSGR* null) failed to develop chlorotic disease symptoms after infection with a virulent strain of *Pst*. Interestingly, *noc1* mutants sustained intercellular *Pst* populations at a high level for longer than the wild-type control, in which *Pst* population levels eventually declined (Mecey et al., 2011). Previously it was found that SGR-family proteins function during senescence by entering chloroplasts and promoting photosystem disassembly and chlorophyll catabolism, thus causing leaf yellowing (Park et al., 2007b). These findings suggest that *AtSGR* upregulation may be a default defense mechanism against virulent pathogens (Mecey et al., 2011): at the cost of decreased photosynthetic output, chlorosis may suppress pathogen persistence in infected leaves by restricting nutrient supplies. Since chlorotic cell death occurs only during compatible infection with a virulent pathogen (Katagiri et al., 2002), this suggests that pathogen recognition in incompatible interactions enables suppression of AtSGR-mediated chlorophyll degradation.

Key players in SA signaling pathways may differ between plant species, host-pathogen interactions, or under different environmental conditions (Attaran et al., 2009; Liu et al., 2011a). However, as a recurring theme during MTI and ETI, increased SA concentrations indirectly shift the intracellular redox state to a reducing environment, thus causing NPR1 oligomers to dissociate into active monomers, which are then imported from the cytosol to the nucleus and interact with transcription factors to alter gene expression (Durrant and Dong, 2004; Nishimura and Dangl, 2010; Zhang et al., 2010). Although NPR1-independent SA defense signaling is poorly understood (An and Mou, 2011), NPR1 is clearly known to be required for SA-mediated stomatal closure (during MTI), SAR development, and *Pathogenesis-Related* (*PR*) gene expression to prevent pathogen growth and dissemination in both local and systemic tissues, among other functions (Loake and Grant, 2007; Melotto et al., 2006; Spoel et al., 2009). Therefore, it is not surprising that mutants in SA-dependent resistance exhibit a mixture of phenotypes.

Defense knockout mutants typically display high susceptibility to pathogen infection due to depleted SA levels and/or reduced *PR* gene expression (Vlot et al., 2009). These mutants may display HR-PCD but are incapable of sustaining the HR and chlorophyll catabolism (Greenberg and Yao, 2004). Mutants overproducing SA typically display—either singly or in combination—enhanced resistance, spontaneous cell death lesions, curly leaves, and dwarfism (Dangl et al., 1996; Loake and Grant, 2007; Vlot et al., 2009).

Incontestably, SA is critically important for plant immunity, yet still much remains to be discovered in SA signaling networks. Identifying SABPs in plants may establish focal points for defense signaling, pinpoint the long-sought SA receptor(s), identify a protein SA-binding motif, and perhaps even uncover SABP orthologs in animals, thereby increasing our understanding of both plant and animalian physiology.

Functional Protein Microarrays and the Identification of SABPs

Protein microarrays are an emerging high-throughput technology with a powerful potential for studying proteomes—protein-protein and other protein-molecule interactions (Hall et al., 2007)—both qualitatively and quantitatively (Wolf-Yadlin et al., 2009). Klessig et al. isolated catalase, the first SABP to be identified (Chen et al., 1993b), using a [^{14}C]SA size-exclusion chromatography assay (Chen et al., 1993a; Du and Klessig, 1997). Using [^{3}H]SA, which has a higher radioactive specific activity, Klessig et al. were able to isolate the low abundant SABP2 (Du and Klessig, 1997) and SABP3 (Slaymaker et al., 2002) from tobacco extracts; therefore, detection of SA-affinity was dependent upon the initial amount of plant material, the extraction procedure, and protein stability. With functional protein microarrays (FPM), plant-purified proteins are equally accessible to probing, and the majority are also equally represented in their active full-length native conformations (Hall et al., 2007; Popescu et al., 2007). In creating the FPM-5000, Popescu et al. individually cloned 5,000 *A. thaliana* open reading frames encoding a mixture of protein kinases, transcription factors, and other proteins with known and unknown functions. After expression in and purification from leaves of *N. benthamiana*, proteins were printed and immobilized on microarray slides, ready to be assayed.

Preliminary Research

To identify low-affinity putative SABPs (pSABPs), the *Arabidopsis* FPM-5000 chip was probed using 4-Azidosalicylic acid (4-AzSA) in four independent experiments (including controls) and analyzed using three criteria: (a) the fluorescence signal is low in the absence of 4-AzSA (negative control), which ensures that there is little nonspecific cross-reaction with the anti-SA antibody; (b) the fluorescence signal is high in the presence of 4-AzSA (treatment group); and (c) the signal ratio in the treatment group versus the control group is greater than three

(**Figure 1**). Only 93 proteins fulfilled these criteria at least 50% of the time, with only three achieving over 80%. One of these three proteins, TOP1 metalloendopeptidase, is characterized in this report along with its suspected paralog, TOP2, which was recently determined using an *in vitro* cross-linking assay to also have binding specificity for 4-AzSA (data not shown).

Three independent assays were conducted using recombinant purified TOP1 (**Figure 2A**) to confirm its SA-binding ability: (a) *in vitro* 4-AzSA cross-linking to *in planta*-produced TOP1 was confirmed to be specific via separation after SA competition of the 4-AzSA-TOP1 complex by SDS-PAGE followed by Western blotting using an anti-SA antibody (**Figure 2B**); (b) [^{3}H]SA exclusion chromatography confirmed that TOP1-SA binding was specific (**Figure 2C**); and (c) Biacore™ surface plasmon resonance detected TOP1 binding to a 4-Aminoethylsalicylic acid-modified surface (data not shown). TOP1 proteolytic activity was measured in and varied depending on the presence or absence of SA and several types of divalent metal cations. SA primarily had an inhibitory effect on TOP1 activity (data not shown). Crystals of TOP1 prepared from protein isolated from *Escherichia coli* revealed that the protein exists as a homodimer (results not shown); however, TOP1-SA crystals are currently unavailable. Efforts to generate these crystals are ongoing.

TOP1 and TOP2 pSABP Metalloendopeptidases

TOP1 and TOP2 are predicted to be zincin-like metalloendopeptidases belonging to the peptidase M3 (clan MA(E)—the gluzincins)—two of the four known to exist in *Arabidopsis*—and thimet oligopeptidase (TOP) protein families (Rawlings et al., 2008). TOPs preferentially cleave medium-sized peptides upon activation with thiol-containing compounds or residues (Rawlings and Barrett, 1995). Metalloendopeptidases are hydrolases that possess a HEXXH (His-Glu-X-X-His) motif consisting of three amino acid ligands that hold and stabilize a divalent metal cation (such as Zn^{2+} or Mn^{2+}), which activates a water molecule for use in nucleophilic attack of endopeptide bonds, and a fourth amino acid that functions in catalysis (Beers et al., 2000; Jongeneel et al., 1989; Rawlings and Barrett, 1995). Metalloendopeptidases are ubiquitous in all kingdoms of life yet have largely unknown functions in plants compared to their well-characterized roles in animals (Beers et al., 2000). For example, human TOP is highly expressed in the brain, pituitary gland, and testes, and plays roles in metabolic reactions of the central and peripheral nervous systems and in preventing the accumulation of amyloid plaques responsible

for Alzheimer's disease (Ray et al., 2004). Beers et al. (2000) proposed that plant metalloendopeptidases might play a direct role in PCD (Beers et al., 2000), though, to our knowledge, this has yet to be demonstrated.

Sokolenko et al. (2002) performed a comparative analysis between the cyanobacterium *Synechocystis* sp. PCC 6803 genome and *Arabidopsis* peptidases and found that TOP1 and TOP2 are 55% and 52% homologous, respectively, with a cyanobacterial oligopeptidase. Interestingly, this study also revealed that most paralogous peptidases of bacterial origin are not functionally redundant (Sokolenko et al., 2002). Polge et al. (2009) found evidence that TOP2 may act downstream of the cytosolic 20S proteasome in *Arabidopsis* leaves by further degrading the small peptides processed after oxidative damage under cadmium (Cd^{2+}) stress. More specifically, they determined that *TOP2* expression levels and TOP2 activity increased significantly 48-144 hours after Cd^{2+} stress; however, *TOP1* expression changed only slightly (Polge et al., 2009). Analogous to mammals, in plants the ubiquitin/ATP-dependent 26S proteasome degradation pathway is essential for protein turnover and gene regulation (Aiken et al., 2011; Robert-Seilaniantz et al., 2011), and the ubiquitin/ATP-independent 20S proteasome (core protease of the 26S proteasome) seems to have a default role in degrading oxidized or misfolded proteins to prevent them from forming aggregates or functioning abnormally, all of which can disrupt cellular homeostasis and result in cytotoxicity (Aiken et al., 2011; Book et al., 2010; Dielen et al., 2010; Polge et al., 2009).

This report characterizes the possible roles of TOP1 and TOP2 metalloendopeptidases in net H_2O_2 accumulation during the oxidative burst, PCD during the HR, maintenance of chloroplast integrity during biotic stress, and sensitivity to SA-induced cell death. We hypothesize that TOP1 and TOP2 directly or indirectly function antagonistically to ultimately upregulate photosystem quality control during abiotic and biotic stresses.

Results

Predicted Characteristics of the *TOP1* and *TOP2* Genes

TOP1 and *TOP2* (**Figure 3**) are located on opposite ends of chromosome 5 and share high sequence homology (**Table 1**), possibly indicating the occurrence of a past intrachromosomal duplication event or two separate horizontal gene transfer events from the chloroplast to nuclear

genome (Huala et al., 2001; Rawlings and Barrett, 1995; Sokolenko et al., 2002; Vision et al., 2000). According to the *Arabidopsis* cis regulatory element database (AtcisDB), the *TOP1* gene promoter is predicted to span an ≈ 3.0 kilobase pair (kbp) region containing multiple regulatory elements. Interestingly, among the 48 regulatory elements predicted, there are four W-box elements—binding sites for WRKY transcription factors (Davuluri et al., 2003); WRKYs are activated in response to pathogen infection and regulate plant defense responses (Gadjev et al., 2008). According to the *Arabidopsis* eFP Browser (AeFPB), *TOP1* transcript expression levels are normally higher under diurnal light cycling and high light intensity and in leaves, pollen, and maturation zone lateral roots compared to *TOP2* transcripts, which are more abundant under continuous light and in the primary root meristem. Compared to *TOP2*, *TOP1* transcript levels are higher after exogenous SA application and exposure to Photosystem II (PSII) inhibitors. *TOP1* and *TOP2* expression levels increase in response to oxidative damage and high inoculum avirulent and virulent *Pst* DC3000 infections, but *TOP1* expression begins increasing before *TOP2* (Winter et al., 2007).

Both *TOP1* and *TOP2* encode predicted metalloendopeptidases (**Figure 4**) possessing the characteristic C-terminal HEXXH motif plus an N-terminal pro-sequence and/or regulatory domain that may be required for proper protein folding and/or intracellular transport (Eder and Fersht, 1995; Rawlings et al., 2008; Sigrist et al., 2010; Sun et al., 2009). TOP1, but not TOP2, is predicted to possess an N-terminal serine-rich region containing a C-5 cytosine-specific DNA methylase (C5-MTase) functional active site, which includes the conserved cysteine residue required for methyl transfer. Strangely, only the C5-MTase active site is present in TOP1, whereas known plant C5-MTase generally contain this site in addition to multiple conserved C5-MTase motifs that cooperate in C5-methylation (Huang et al., 2010; Pavlopoulou and Kossida, 2007). According to the SUB-cellular location database of *Arabidopsis* proteins (SUBA), TOP1 and TOP2 predicted subcellular localizations vary (**Table 2**). Both have been detected in chloroplasts using mass spectrometry, but TOP2 has additionally been detected in the cytosol (Heazlewood et al., 2005; Heazlewood et al., 2007).

Generation of the *top1*, *top2*, and *top1 top2* Mutants

Multiple lines containing T-DNA insertions in *TOP1* and *TOP2* (Krysan et al., 1999) were obtained from the *Arabidopsis* Biological Resource Center (ABRC) to explore the *in vivo*

functions of TOP1 and TOP2 (**Table S1**). *top1* mutant lines 339, 439, and E07 and *top2* mutant lines 127, 727, 509, and 554 were selfed (if required) to achieve homozygosity for each T-DNA insertion. *TOP1* line G04 lacked the T-DNA entirely and was eliminated from future analyses, and *top2*^{509} and *top2*^{554} were also excluded to reduce the number of experimental lines. *top1*^{339} and *top1*^{439} were crossed with *top2*^{127} and *top2*^{727} to generate *top1*^{339}*top2*^{127}, *top1*^{339}*top2*^{727}, *top1*^{439}*top2*^{127}, and *top1*^{439}*top2*^{727} double mutants, which were then selfed to achieve homozygosity for both T-DNA insertions (**Figure 5, Table S2**). Since *TOP1* and *TOP2* cDNAs are 88% homologous (see Table 1), primer pairs for semi-quantitative RT-PCR analysis were created with reference to a cDNA alignment in order to properly interpret the PCR results (**Figure 6**).

For the semi-quantitative RT-PCR, RNA was extracted from wild-type (WT) and single and double mutant lines, reverse transcribed into cDNA, and subjected to PCR analysis to determine transcript lengths and expression levels relative to the Col-0 WT (**Figure 7, Table S3**). *top1*^{339} had severely knocked-down (KD) expression of a truncated transcript likely approximating 1.0-1.3 kbp (330-435 amino acids) in length, *top1*^{439} had WT expression of a truncated transcript likely approximating 1.9-2.2 kbp (630-735 amino acids) in length, and *top1*^{E07} had WT expression of a full-length transcript containing the T-DNA insertion. *top2*^{127} was likely a complete knockout because the T-DNA insertion is in an intron and the 3′ *TOP2* primer pair did not yield an amplification product. *top2*^{727} had moderate to severe KD expression of a full-length transcript containing the T-DNA insertion. *top1 top2* double mutants resembled their respective single mutant expression profiles but with a couple exceptions: *top2* expression levels in the *top1*^{339}*top2*^{727} and *top1*^{439}*top2*^{727} double mutants seemed to decrease even further, an indication that TOP1 and TOP2 may reciprocally regulate each other at the transcriptional level. Also, the *top1*^{339}*top2*^{127} and *top1*^{339}*top2*^{727} double mutants yielded an extra *TOP1* 34 primer pair amplification product along with the expected-sized product. Since the 3′ *TOP1* primer pair confirmed the absence of *TOP1* transcripts in *top1*^{339} single and *top1*^{339}*top2*^{127} and *top1*^{339}*top2*^{727} double mutants, this suggested that this primer pair was specific to *TOP1* but that the *TOP1* 34 primer pair might be cross-reacting elsewhere in the genome unless the *TOP1* transcript in *top1*^{339} single mutants was not truncated until a great distance downstream of the T-DNA insertion (which is less likely due to nonsense frameshift mutations). The presence of the

extra amplification product likely indicates cross-reaction elsewhere in the genome, but it is unclear why it would be specific only to the *top1*^{339}*top2*^{127} and *top1*^{339}*top2*^{727} double mutants.

top1^{339} and *top2*^{127} are likely null mutants. The other mutants may also be null because translation of T-DNA-containing aberrant transcripts would give rise to mutant proteins with altered or defective functions (Wang, 2008); however, the same cannot be said for E07 (5′UTR insertion), though the T-DNA could influence *TOP1* expression and transcript processing. For the sake of simplicity, all mutants were thus considered dysfunctional but potentially not null.

Normal Growth Phenotypic Characterization of the *top1*, *top2*, and *top1 top2* Mutants

It is not completely definitive whether any of the *top1*, *top2*, or *top1 top2* mutants had an obvious physically abnormal phenotype under normal growth conditions. Since the AeFPB suggested that *TOP1* and *TOP2* transcripts might be differentially localized within roots, root growth of *top1*^{339}, *top2*^{127}, and *top1*^{439}*top2*^{127} mutants was observed. Preliminary experiments revealed that *top1*^{339} and *top2*^{127} potentially had more hairy roots compared to the Col-0 WT, while the normal phenotype seemed restored in the *top1*^{439}*top2*^{127} double mutant. Additionally, *top1*^{339} seemed to visibly have shorter than normal roots (results not shown). However, these phenotypes were not definitive due to significant phenotypic variation within each line (**Figure S2**), and it is possible that the other mutants (such as *top1*^{339}*top2*^{127} and *top1*^{339}*top2*^{727}, which were not available at the time) may possess growth defects.

top1 and *top2* Single Mutants are Not Definitively Impaired in MTI or ETI

SA is known to play critical roles in activating MTI and ETI (Vlot et al., 2009). *Arabidopsis* NB-LRR proteins RESISTANCE TO PSEUDOMONAS SYRINGAE PV MACULICOLA 1 (RPM1) and RESISTANCE TO PSEUDOMONAS SYRINGAE 2 (RPS2) recognize modifications to or destruction of RPM1-INTERACTING PROTEIN 4 (RIN4) by *Pst* effectors AvrRpm1 and AvrRpt2, respectively, and subsequently activate defense signaling (Dodds and Rathjen, 2010; Katagiri et al., 2002). *RPS2*-mediated resistance depends on SA biosynthesis and accumulation, while *RPM1*-mediated resistance does not (Gimenez-Ibanez and Rathjen, 2010; Katagiri, 2004). *Pst* mutants defective in the Type III Secretion System (T3SS), such as Δ*hrcC*, cannot secrete effector proteins into the host cell and elicit ETI; however, *Pst* T3SS mutants may

still be recognized through MAMPs and elicit MTI (Gimenez-Ibanez and Rathjen, 2010; Roine et al., 1997).

To characterize the potential roles of TOP1 and TOP2 in MTI and/or ETI, *top1* and *top2* single mutants (*top1 top2* double mutants were not available at the time) were challenged with *Pst* DC3000 virulent (WT), Δ*hrcC*, *avrRpt2*, or *avrRpm1* strains. Mutants were analyzed for visible disease symptoms at 4 days post-inoculation (dpi) (**Figure 8**) and changes in the amount of intercellular bacterial growth at 0, 2, and 4 dpi (**Figure 9**) to observe any defects in the resistance response compared with the Col-0 WT positive control and the *rps2* and *rpm1* negative controls. *top1* and *top2* mutants displayed normal MTI and ETI resistance phenotypes, and only *Pst avrRpt2* growth in *top1*^{E07} leaves was significantly greater compared to that in Col-0. Though it is uncertain, *top1* and *top2* single mutants may undergo slight HR-PCD after infection with a low titer of *Pst avrRpt2* that is not normally sufficient to induce the HR in Col-0. Overall, these results indicate that TOP1 and TOP2 may have overlapping or redundant functions, if any, in protecting against *Pst* DC3000 infection.

TOP1 and TOP2 Antagonistically Regulate ROS Accumulation during the Oxidative Burst

Arabidopsis plants normally undergo an oxidative burst—an increase in ROS accumulation—to trigger the HR at initial sites of infection with a high titer ($\geq 1 \times 10^6$ colony forming units/mL) of an avirulent pathogen (Mur et al., 2008; Wolfe et al., 2000; Zhang et al., 2004). SA contributes to HR induction, and H_2O_2 from the oxidative burst is known to directly influence HR activation during ETI (Levine et al., 1994; Tenhaken et al., 1995; Zhang et al., 2004). *Pst* T3SS mutants may also be recognized through MAMPs and trigger H_2O_2 production through MTI (Gimenez-Ibanez and Rathjen, 2010; Torres, 2010). ROS produced during the oxidative burst are eventually quenched by ROS-scavengers (Torres, 2010).

To determine if TOP1 and TOP2 might function in net ROS accumulation during the oxidative burst, *top1* and *top2* single mutants (*top1 top2* double mutants were not available at the time) were analyzed using 3,3′-Diaminobenzidine (DAB) staining for qualitative differences in H_2O_2 accumulation after challenge with *Pst* DC3000 virulent (WT), Δ*hrcC*, or *avrRpt2* strains at 0, 6, 9, and 12 hours post-inoculation (hpi) (**Figure 10, Figure S3**). DAB can penetrate leaf cells and enable visualization of H_2O_2 accumulation (Thordal-Christensen et al., 1997; Wolfe et al., 2000). DAB polymerizes and precipitates after oxidation by H_2O_2 in a reaction catalyzed by

peroxidase, and subsequently turns reddish-brown in color, with a darker color indicating higher H_2O_2 levels (Thordal-Christensen et al., 1997).

Compared to the Col-0 WT positive control, *top1*^{E07} potentially exhibited greater H_2O_2 accumulation at both 6 hpi and 12 hpi with *Pst avrRpt2* and Δ*hrcC*, whereas this was only observed at 6 hpi for *top2*^{127} and 9 hpi for top2^{727}. Dissimilarly, *top1*^{339} and *top1*^{439} exhibited less H_2O_2 accumulation at 6 hpi with *Pst avrRpt2*. The seemingly high H_2O_2 accumulation in *top2*^{727} at 0 hpi with *Pst avrRpt2* was likely due to severe wounding because the 0 hpi $MgCl_2$ control revealed background staining levels; however, this is not completely conclusive. H_2O_2 did not significantly differ between *top1* and *top2* mutants and Col-0 at all other hpi with *Pst* virulent or Δ*hrcC* in comparison to $MgCl_2$ control infiltrations. Overall, these results indicate that TOP1 and TOP2 may antagonistically regulate net ROS accumulation during the oxidative burst.

TOP1 and TOP2 Antagonistically Regulate HR-PCD Initiation and Spread

Sustained PCD during the HR is generally a phenomenon of ETI but not MTI (Torres, 2010), and LSD1 and AtRBOH proteins regulate ROS metabolism during secondary oxidative bursts to prevent RCD (Torres et al., 2005). Since TOP1 and TOP2 appeared to be involved in net H_2O_2 accumulation during the oxidative burst, it was hypothesized that PCD intensity and/or spread during the HR might also be altered.

Accordingly, *top1* and *top2* single mutants (*top1 top2* double mutants were not available at the time) were qualitatively analyzed via Trypan Blue (TB) staining for differences in the amount of PCD after challenge with *Pst* DC3000 virulent (WT), Δ*hrcC*, or *avrRpt2* strains at 24 hpi (**Figure 11**). TB enables visualization of dead cells, which, due to loss of membrane integrity, can take up and retain the stain; this is useful for qualitatively detecting HR-PCD triggered during incompatible interactions with an avirulent pathogen (Keogh et al., 1980). *top1* and *top2* mutants showed similar amounts of HR-PCD as the Col-0 WT positive control after infection with avirulent *Pst avrRpt2*. However, the *top2* single mutants showed severe collapse in the infiltrated leaf halves before staining (results not shown). As expected, HR-PCD was not triggered during the compatible interaction (*Pst* virulent) or during MTI (*Pst* Δ*hrcC*). These results indicate that HR-PCD intensity and spread was not affected in the mutants; however, it is possible that a qualitative PCD phenotype was not observed because—at 24 hpi—HR-PCD may

have reached indistinguishable levels due to staining saturation. Additionally, PCD lesions may only become visible at an even later time.

Therefore, a small-scale ion leakage experiment was conducted to allow quantitative HR-PCD comparisons between *top1*^{339}, *top2*^{727}, and *top1*^{439}*top2*^{127} at 0, 8, and 16 hpi with *Pst* DC3000 *avrRpt2* (**Figure 12A**). Ion leakage measures the relative amount of ions released by dead and dying cells as a result of membrane permeabilization caused by abiotic or biotic stress, and is, therefore, a conductivity measurement that can be used to quantify HR-PCD (Watanabe and Lam, 2006). *top2*^{727} had significantly higher conductivity levels at 8 hpi compared to Col-0, indicative of accelerated or higher intensity PCD. Dissimilarly, *top1*^{339} and *top1*^{439}*top2*^{127} mutants had statistically normal conductivity levels, though this may have been an artifact of the small sample size. Variation was too great at 16 hpi in both the mutants and controls to establish any significant differences.

Infected leaves were assessed for the development of characteristic HR-PCD lesions at 2-3 dpi (**Figure 12B, Figure S4**). *top1*^{339} and *top2*^{727} mutants displayed higher intensity and spread of HR-PCD compared to Col-0, indicating that the mutants may be defective in PCD initiation and/or RCD restriction. Intriguingly, *top1*^{439}*top2*^{127} resembled the *rps2* negative control: it displayed chlorosis, indicative of cell death. However, the chlorosis did not resemble the chlorotic cell death disease symptoms indicative of a compatible interaction. *top1*^{439}*top2*^{127} also showed signs of HR-PCD, albeit at a much lower intensity, surrounded by chlorosis; this phenotype suggested that ETI might not be completely impaired. Overall, these results indicate that TOP1 and TOP2 may antagonistically regulate HR-PCD and function together to enforce chloroplast integrity.

top2 Mutants are Less Sensitive to SA-induced Cell Death

High concentrations of exogenously applied SA (1-5 mM) can trigger cell death in leaves (Mur et al., 2008; Postel et al., 2010), likely by disrupting thylakoid membranes and photosynthesis to cause a hyperaccumulation of H_2O_2 while reducing chlorophyll content and, consequently, photosynthetic rate (Moharekar et al., 2003; Pancheva and Popova, 1998; Rao et al., 2012; Vicente and Plasencia, 2011). Contrastingly, low concentrations of exogenously applied SA (< 10 μM) can increase photosynthetic efficiency, possibly by upregulating AtSABP3 antioxidant activity (Fariduddin et al., 2003; Vicente and Plasencia, 2011).

Since TOP1 and TOP2 are pSABPs, *top1*, *top2*, and *top1 top2* mutants were analyzed for differences in SA-induced cell death sensitivity (**Figure 13**). Both *top2* single mutants had significantly less SA-induced cell death compared to the Col-0 WT when infiltrated with 5 mM SA, whereas *top1* and *top1 top2* mutants appeared phenotypically normal. Compared with Col-0, no significant differences were observed in plants infiltrated with 10 mM SA, possibly because such high phytohormone levels were more disruptive to cellular homeostasis. Results from this experiment suggest that *top2* mutants have decreased sensitivity to exogenous SA, which is relieved in the double mutants.

Transgenic *TOP1* Arabidopsis Lines are Available for Future Analyses

TOP1 expression clones for complementation, native and constitutive subcellular localization, native tissue-specific localization, native protein complex pull-down, inducible overexpression, and constitutive, inducible-constitutive, and inducible-quantitative RNAi gene silencing were created and stably transformed into specific *Arabidopsis* backgrounds using *Agrobacterium tumefaciens* GV2260 (**Figure 14, Table S4**). However, the native subcellular localization expression clones—dpGreen BarT (Pro-cDNA(ns)-mGFP) and dpGreen BarT (Pro-Genomic(ns)-mGFP)—were obtained but could not, even after multiple attempts, be transformed into GV2260; therefore, native TOP1 subcellular localization cannot yet be analyzed *in planta*. Stable *Arabidopsis* transformants carrying these clones are currently undergoing selection. Once obtained, they will be used to confirm and further characterize the localization(s) of TOP1 and the *in vivo* functions of TOP1 and TOP2.

Discussion

Analysis of T-DNA-tagged Mutant Genotypes and Normal Growth Phenotypes

The *top1*, *top2*, and *top1 top2* mutants varied in transcript expression levels and truncation relative to the Col-0 WT. Recall that *top1*^{439} was determined to have normal *TOP1* expression levels of a partly truncated transcript (possibly translated into a 636-726 amino acid length protein), and *top2*^{727} had markedly reduced expression of a full-length transcript containing the T-DNA insertion. These differences in transcript length and expression may manifest as loss-of-function, gain-of-function, or dominant negative mutations, thus complicating our observations.

For example, TOP1 and/or TOP2 may complex with other proteins to perform specific activities, but decreased TOP2 levels may not be adequate for efficient completion of a particular process. Moreover, truncated TOP1 may be missing a critical functional or regulatory domain, such as one containing a site for post-translational modifications. Interestingly, phosphorylation of TOP1 at serine residue 754 and TOP2 at serine residue 686 was detected by mass spectrometry and peptide chip analysis (van Bentem et al., 2008). Since *top1*^{339} and *top1*^{439} expressed *TOP1* transcripts that were truncated before these potential phosphorylation sites, if translated they may give rise to dysfunctional TOP1. Dissimilarly, *top1*^{E07} expressed full-length *TOP1* containing the T-DNA insertion at wild-type levels under normal growth conditions. It is not clear why *top1*^{E07} seemed to potentially hyperaccumulate H_2O_2 and support significantly more *Pst* DC3000 *avrRpt2* growth compared with Col-0. These two observations suggest that the *top1*^{E07} 5′UTR T-DNA insertion may alter *TOP1* expression and/or translation, thus making the results difficult to interpret. RNAi lines should be included as controls in future experiments to confirm our observations. Nonetheless, both single and double mutants displayed phenotypes representative of altered ROS homeostasis.

TOP1 and TOP2 Regulate Cellular Redox Homeostasis and HR-PCD

SA and ROS regulate development, cellular growth, and immune responses in plants (Swanson and Gilroy, 2010; Vlot et al., 2009). For example, ROS signaling is intimately involved in cell wall extensibility during development, notably in root hair meristems and pollen tubes (Swanson and Gilroy, 2010). Interestingly, *TOP1* expression was detected during pollen germination and pollen tube growth using RNA hybridization to *Arabidopsis* Affymetrix GeneChips (Wang et al., 2008), and phosphorylated and glycosylated TOP2 was detected in regenerating protoplast cell walls by 2-D PAGE followed by MALDI-TOF/MS (Kwon et al., 2005). Since *top1* pollen was used successfully to make crosses with *top2*, TOP1 must not be essential for pollen germination and tube growth. If TOP2 influences cell wall development and extensibility, it also must not be essential because *top2* mutants were viable. *top1 top2* double mutants were also viable and could reproduce successfully, indicating that TOP1 and TOP2 may have nonessential functions. Regardless, TOP1 and TOP2 may be involved in redox homeostasis.

Previous indirect evidence linked TOP2 to oxidative stress regulation downstream of the 20S proteasome: Polge et al. (2009) found *TOP2* expression levels and TOP2 activity to

significantly increase after Cd^{2+} stress, while *TOP1* expression changed only slightly (Polge et al., 2009). In a different study, TOP2 protein abundance increased in cell cultures exposed to high concentrations of Cd^{2+}, as determined by 2-D PAGE followed by MALDI-MS or NanoLC-MS/MS (Sarry et al., 2006). According to Jaspers and Kangasjärvi (2010), only a few reports have highlighted the connection between ROS signaling and the proteasome (Jaspers and Kangasjärvi, 2010). The presence and amount of oxidation of certain amino acid residues, such as methionine, may serve as markers that target oxidized proteins for degradation by the 20S proteasome, which—unlike the 26S proteasome—remains active in the presence of H_2O_2 (Aiken et al., 2011; Davies, 2005; Polge et al., 2009). Cd^{2+} can inhibit PSII and antioxidant enzyme activities, resulting in uncontrolled ROS production and chlorophyll destruction. Concomitantly, detoxification or tolerization machinery are upregulated to prevent protein oxidation (Villiers et al., 2011; Zhang and Chen, 2011). Most protein oxidation is functionally damaging and irreversible, necessitating that damaged proteins be catabolized to prevent the transfer of damaging modifications to other cellular targets and the formation of protein aggregates, all of which can trigger cell death or other pathologies (Polge et al., 2009; Villiers et al., 2011).

Since Polge et al. (2009) found evidence that TOP2 may act downstream of the cytosolic 20S proteasome, it is possible that TOP2 may participate in the degradation of oxidized proteins to ultimately prevent PCD and alter redox homeostasis. In addition, Nakagami et al. (2006) demonstrated that H_2O_2-induced MAPK kinase kinase 1 (MEKK1) activation is regulated through proteasome-mediated turnover, and Miao et al. (2007) found that MEKK1 transcriptionally activates and directly phosphorylates WRKY53 (also H_2O_2-inducible) to regulate senescence-induced PCD (Gadjev et al., 2008; Jaspers and Kangasjärvi, 2010; Miao et al., 2007; Nakagami et al., 2006). Recall that the predicted *TOP1* promoter contains W-box elements, binding sites for WRKY transcription factors; therefore, TOP1 may also regulate PCD. Interestingly, Zhang and Chen (2011) found that exogenous SA could alleviate Cd^{2+}-induced autophagic-PCD and photosynthetic damage in *Arabidopsis*, presumably by reducing ROS overproduction and thereby preventing oxidative stress (Yoshimoto et al., 2009; Zhang and Chen, 2011). Liu et al. (2005) determined that autophagic-PCD could negatively regulate HR-PCD to restrict lesion spread in *N. benthamiana* (Liu et al., 2005); reciprocally, autophagic-PCD inhibition by ROS may be necessary for rapid HR-PCD activation in order to quickly contain an infection (Love et al., 2008; Van Breusegem et al., 2008). All these findings are consistent with

our observations that TOP1 and TOP2 antagonistically regulate ROS accumulation and HR-PCD during incompatible *Pst* infection: *top1* mutants hypoaccumulated H_2O_2 while *top2* mutants hyperaccumulated H_2O_2 during the oxidative burst, and *top1*^{339} and top2^{727} had increased HR-PCD spread and intensity at 2-3 dpi while *top1*^{439}*top2*^{127} displayed chlorosis and had weakened HR-PCD.

Interestingly, proteasomal degradation of NPR1 and RPM1 is necessary for proper SAR development and HR activation, respectively (Boyes et al., 1998; Dielen et al., 2010; Kawasaki et al., 2005; Spoel et al., 2009). It is possible that signaling oligopeptides may be produced through proteasomal degradation of these proteins (Cunha et al., 2008). Recall that TOP1 and TOP2 have been detected in chloroplasts using mass spectrometry, but TOP2 has additionally been detected in the cytosol; therefore, TOP2 may alternatively function by regulating degradation of these signaling oligopeptides in the cytosol to influence redox homeostasis and suppress PCD. Changes in the balance between NO and ROS in the cytosol may subsequently alter TOP1 and/or TOP2 activities in chloroplasts. *Pst* also secretes effectors that specifically target and disrupt thylakoid membranes in chloroplasts to suppress SA biosynthesis (Jelenska et al., 2007; Padmanabhan and Dinesh-Kumar, 2010); therefore, TOP1 and/or TOP2 may function to ultimately maintain chloroplast integrity during such attacks.

TOP1 and TOP2 may Regulate Chloroplast Integrity during Immune Responses

PSII is essential for splitting H_2O and facilitating oxidative photosynthesis, but the PSII complex reaction center consists of multiple subunits that are highly susceptible to oxidative damage by ROS. To ensure that PSII functions properly, chloroplasts possess photosystem quality control repair machinery (Chi et al., 2012; Yoshioka and Yamamoto, 2011). Interestingly, Filamentous temperature sensitive H (FtsH) family proteins include the only known thylakoid membrane-localized metalloproteases, and are responsible for repairing photodamaged PSII (Yoshioka and Yamamoto, 2011). For example, FtsH complexes can initiate degradation of the commonly photodamaged D1 subunit (essential for H_2O-splitting) to facilitate its replacement with functional D1 (Nixon et al., 2005). FtsH protease complexes release peptide fragment degradation products into the chloroplast stroma, where it is suspected that secondary proteolysis occurs to complete the degradation process and maintain chloroplast homeostasis (Chi et al., 2012). Interestingly, ROS may inactivate repair mechanisms by halting translation of PSII

subunit transcripts, such as those encoding the D1 protein (Takahashi and Murata, 2008). High ROS levels during stress, however, may also increase FtsH expression and, through redox regulation, facilitate FtsH complex formation and activation (Yoshioka and Yamamoto, 2011). Not surprisingly, suppressed FtsH levels have been associated with accelerated HR-PCD during pathogen infection (Padmanabhan and Dinesh-Kumar, 2010; Seo et al., 2000).

Under normal conditions, TOP1 and/or TOP2 may function downstream of FtsH by further degrading damaged PSII subunit peptide fragments in the chloroplast stroma. However, when SA biosynthesis and PSII damage increase during certain abiotic or biotic stresses, SA may inhibit TOP1 and/or TOP2 to prevent degradation of these peptide fragments. Accumulation of these peptides may then be sensed as a stress signal that subsequently results in activation of photosystem quality controls, such as increased FtsH expression. Although chloroplasts are the main source of H_2O_2 in photosynthetic tissues, H_2O_2 may be produced in other organelles and the apoplast (Jaspers and Kangasjärvi, 2010) and is highly diffusible throughout the cell (Mubarakshina et al., 2010). Therefore, when H_2O_2 accumulates under stressful conditions, TOP2 may indirectly sense excess ROS in the cytosol and subsequently activate ROS-scavenging pathways. Decreased ROS accumulation would then relieve photoinhibition and ensure chloroplast integrity. These hypotheses are supported by the observations that *top1* mutants hypoaccumulated H_2O_2 while *top2* mutants hyperaccumulated H_2O_2 during the oxidative burst, and *top1*^{339} and *top2*^{727} single mutants had higher intensity HR-PCD while the *top1*^{439}*top2*^{127} double mutant displayed chlorosis (chlorophyll degradation) and lower intensity HR-PCD following infection with a high titer of *Pst* DC3000 *avrRpt2*. This suggests that TOP1 and TOP2 jointly enforce photosystem quality control—possibly through regulating net ROS production and redox homeostasis—which then directly influences HR-PCD initiation, intensity, and spread.

Another possibility is that TOP1 and TOP2 may regulate AtSGR translocation into chloroplasts. Recall that AtSGR family proteins function in photosystem disassembly and chlorophyll catabolism during senescence (Park et al., 2007b), a process that is also regulated by SA (Vlot et al., 2009), and AtSGR expression is upregulated during compatible but not incompatible host-pathogen interactions (Park et al., 2007b). Interestingly, Mur et al. (2010) found that AtSGR-mediated photosystem disassembly contributes to net ROS production and HR induction during *Pst* DC3000 *avrRpm1* infection. Specifically, they found that increased

AtSGR expression accelerates HR-PCD, whereas decreased expression suppresses HR-PCD (Mur et al., 2010). Consequently, TOP1 and TOP2 may regulate AtSGR activity in and/or transport into chloroplasts during incompatible infections. For example, SA may inhibit TOP1 and TOP2 proteolytic activities, which may be involved in cleaving the AtSGR chloroplast transit peptide to prevent AtSGR translocation into chloroplasts. In other words, when SA levels rise during an incompatible infection, TOP1 and/or TOP2 may be inhibited to allow AtSGR transit into chloroplasts. Since the *top1* and *top2* single mutants displayed higher intensity HR-PCD and spread after infection with a high titer of *Pst* DC3000 *avrRpt2*, the absence of either TOP1 or TOP2 may enhance AtSGR activity. Dissimilarly, the chlorosis and weakened HR-PCD phenotype in *top1*^{439}*top2*^{127} suggests that the absence of both TOP1 and TOP2 may simultaneously compromise photosystem quality controls during enhanced AtSGR activity, thus altering redox homeostasis to disfavor PCD.

Potential Functions of the TOP1 C5-MTase Functional Active Site

It is unknown whether or not the C5-MTase functional active site is actually accessible in the putative TOP1 homodimer. If it is not, SA-binding to TOP1 might trigger a conformational change (perhaps causing dissociation of the homodimer), thus exposing the C5-MTase site. Regardless, TOP1 may use the C5-MTase site to somehow maintain chloroplast integrity, perhaps by binding to methylated cytosine residues on chloroplast plasmids (Ahlert et al., 2009) or RNA transcripts and subsequently recruiting true C5-MTases and/or activating transcription factors to modulate the expression of photoprotective chloroplast genes. Although Fojtová et al. (2001) did not detect the occurrence of chloroplast DNA methylation, Ahlert et al. (2009) found evidence that chloroplast DNA cytosine methylation could potentially occur in certain regions and under specific conditions, but is unlikely to affect gene expression (Ahlert et al., 2009; Fojtová et al., 2001). Nonetheless, it is possible that TOP1 could be recruited to methylated cytosines under certain stressful conditions to form a complex that somehow modulates photosystem quality controls. Alternatively, TOP1 may be involved in SAR development.

A recent study by Liu et al. (2011) revealed that the MeSA requirement for SAR development in *Arabidopsis* depends on the duration of light exposure a plant receives following pathogen infection; regardless, MeSA was shown to be necessary for optimal SAR development (Liu et al., 2011a). The C5-MTase site of TOP1 may be directly involved in the conversion of

SA to MeSA or vice versa. All C5-MTases are known to use *S*-adenosyl-L-methionine as a methyl donor (Huang et al., 2010), including AtBSMT1 as it catalyzes the formation of MeSA from SA (Liu et al., 2010a). Therefore, TOP1 may form a complex with AtBSMT1 to participate in this enzymatic conversion, or TOP1 may complex with AtMSEs in systemic tissues and participate in MeSA cleavage to SA. Another possibility is that TOP1 uses its C5-MTase site to directly bind SA (which structurally resembles cytosine) and enhance MeSA—SA conversions. How these functions might link to photosystem quality controls is unclear. Perhaps TOP1 plays roles in both photosystem quality control and SAR development.

Working Model of TOP1 and TOP2 *in vivo* Functions

We propose that, through interactions with SA, TOP1 and TOP2 ultimately cooperate in enforcing photosystem quality control to maintain chloroplast integrity and prevent photoinhibition, especially from damages caused by ROS overproduction during MTI and ETI. Our findings may be summarized as follows. (1) *top1*^{339} and *top1*^{439} mutants hypoaccumulated H_2O_2 while the *top2*^{127} and *top2*^{727} mutants hyperaccumulated H_2O_2, suggesting that TOP1 and TOP2 antagonistically regulate net ROS production. (2) Conductivity measurements at 8 hpi with *Pst* DC3000 *avrRpt2* revealed that *top2*^{727} had higher intensity HR-PCD, while both *top1*^{339} and *top1*^{439}*top2*^{127} had normal HR-PCD levels; this suggests that TOP1 may be epistatic to TOP2 (i.e. TOP2 is upstream of TOP1), and indicates that TOP1 and TOP2 may antagonistically regulate HR-PCD, possibly through regulating net ROS production. (3) *top1*^{339} and *top2*^{727} single mutants displayed more HR-PCD lesions and spread 2-3 dpi with a high titer of *Pst* DC3000 *avrRpt2*, whereas *top1*^{439}*top2*^{127} displayed chlorosis and weakened HR-PCD; this suggests that TOP1 and TOP2 may together support chloroplast integrity—possibly through regulating net ROS production—which consequently influences HR-PCD initiation, intensity, and spread. (4) *top2* mutants were desensitized to SA-induced cell death while *top1 top2* mutants were not. However, the higher H_2O_2 accumulation in *top2* mutants contradicts this result because autophagic-PCD would be inhibited, relieving negative feedback on HR-PCD and thereby allowing the lesion zone to expand. Therefore, these results might indicate that TOP2 inhibits autophagic-PCD while TOP1 is epistatic to TOP2 and promotes autophagic-PCD (again, possibly through regulating net ROS production). (5) Lastly, though it is not definitive, the *top1*^{339} and *top2*^{727} single mutants may have had more hairy roots compared to Col-0, whereas

the *top1*^{439}*top2*^{127} double mutant seemed normal; this supports the role of TOP1 and TOP2 in net ROS production, and thus in developmental processes.

Together, our findings support a model in which SA directly modulates the activities of TOP1 and TOP2 to influence net ROS production and thereby restrict PCD intensity and RCD, notably during biotic stress (**Figure 15A**). These interactions may additionally facilitate metabolic changes conducive to SAR development (**Figure 15B**). In this way, TOP1 and TOP2 may be considered central hubs in ROS signaling networks and redox regulation, and thereby control several physiological responses during both abiotic and biotic stresses.

Future Research

Several experiments will be conducted to further characterize TOP1 and TOP2 functions *in vivo* and to reinforce and optimally restructure our model: (1) DAB and TB staining, bacterial growth, and resistance response analyses in all the double mutants; (2) large-scale ion leakage analysis incorporating all the single and double mutants; (3) SAR development, root growth, light stress, and senescence analyses in both the single and double mutants; and (4) subcellular and tissue-specific localization, constitutive overexpression, and complex-pull down analyses of TOP1. Constitutive, inducible-constitutive, and/or inducible-quantitative RNAi gene silencing of *TOP1* and *TOP2* can be used to confirm the double mutant phenotypes. Quantitative RT-PCR should be conducted to confirm *TOP1* and *TOP2* expression levels and determine whether they are reciprocally influenced, and to analyze differences in *PR*, *FtsH*, and *AtSGR* gene expression. If our model is valid, then TOP1 and/or TOP2 (and their homologs in other plant species) may potentially be targeted by necrotrophic pathogens to induce ROS accumulation and/or trigger PCD, and consequently suppress SAR development; therefore, it may be worthwhile to analyze immune responses of both the single and double mutants to challenge with *Botrytis cinerea*.

Significance of SABPs in Humans

Considering the importance of SA in plant immunity, it is not surprising that SA is present, albeit in small quantities, in most vegetables and fruits. Consequently, SA is a daily component of the human diet (Paterson et al., 2006). SA quantification from different food items has yielded variable results. But whereas fresh, unprocessed tomato fruit may contain between 1.6-3.6 µg

SA/g fruit, for example, a single tablet of the synthetic SA derivative acetylsalicylic acid (Aspirin) equates to 75-80 mg (Meher et al., 2011; Paterson et al., 2006; Scotter et al., 2007). Aspirin is a non-steroidal anti-inflammatory drug that has renowned medicinal applications as an antithrombotic, antipyretic, and analgesic (Miner and Hoffhines, 2007; Vane and Botting, 2003), and may even counteract the severity of arthritis and the incidence of heart attack, stroke, and certain cancers (Miner and Hoffhines, 2007; Vane and Botting, 2003; Vlot et al., 2009). Although SA and Aspirin have slightly different structures, both molecules affect mammalian biology in extremely similar ways; this is because Aspirin is deacetylated to SA within the liver and blood, and transported throughout the body (Paterson et al., 2006). Although the quantity of SA within tomato fruit is extremely low compared to a tablet of Aspirin, daily consumption of tomato and other fresh plant edibles may culminate in physiologically significant SA levels that endow the aforementioned health benefits.

Surprisingly, however, SA biochemistry and metabolism in humans is poorly understood. Studies have shown that salicylates—Aspirin in particular—modulates eicosanoic acid metabolism to suppress inflammation and reduce pain (Mitchell et al., 1993). Identifying SABPs in plants has the additional potential to uncover SABP orthologs in animals and provide a better understanding of SA influences on human physiology.

In mammalian cells, the main protein turnover pathway begins with protein degradation by the 20S proteasome into 3-24 amino acid peptides. Endopeptidases (e.g. human TOP) cleave 9-17 amino acid peptides into < 6 amino acid peptides, and these small peptides may then be completely catabolized into free amino acids by aminopeptidases and either degraded or reused for protein synthesis (Polge et al., 2009; Saric et al., 2004). Alternatively, the 20S proteasome can process peptide antigens for presentation via the major histocompatibility complex class I, and human TOP appears to function by either degrading these antigenic peptides or generating new epitopes, thus limiting or promoting antigen presentation, respectively (Kessler et al., 2011; Kim et al., 2003; Kloetzel and Ossendorp, 2004; Rock et al., 2004; Silva et al., 1999; York et al., 2003).

Human TOP and its close homolog neurolysin have been implicated in angiogenesis and tumor growth (Paschoalin et al., 2007; Wang et al., 2009a) and are known to degrade several peptides, including the vasoactive peptides neurotensin and bradykinin (Norman et al., 2003; Paschoalin et al., 2005; Ray et al., 2004). TOP also degrades endogenous opioids—natural pain

killers—and, as previously stated, has been implicated in preventing Alzheimer's disease (Kest et al., 1991; Ray et al., 2004).

Intriguingly, TOP1 and TOP2 share considerable homology with human and mouse TOP and neurolysin (**Table S5**). Perhaps SA can modulate TOP and/or neurolysin activity, thus altering neurotensin, bradykinin, and endogenous opioid levels and, consequently, promote or repress vasodilation and blood clotting, pain perception, cancer, and/or neurological disorder development. And since TOP is involved in antigen processing, SA may also have immunomodulatory effects on humans. It would be interesting to see whether human or mouse TOP-SA and neurolysin-SA crystals can be obtained.

Comparative Immunology

Genome comparisons between species may identify developmental pathways involved in the evolution of analogous structures and systems; therefore, comparative immunology may provide insight into the potentials and limitations of immune system evolution.

Analogous to interactions between nucleotide oligomerization domain (NOD) proteins and the Nuclear Factor-Kappa B (NFκB) transcription factor (and its cofactor IκB) in animals, SA and NPR1 signaling pathways in plants interact to regulate immune responses and cell growth, division, and apoptosis (Ausubel, 2005; Spoel et al., 2009; Vanacker et al., 2001). NPR1, like NFκB and IκB, also contains an ankyrin-repeat motif (An and Mou, 2011; Cao et al., 1997), and one study found that salicylates could suppress NFκB activation (McCarty and Block, 2006). NFκB is also known to regulate mammalian proteasome expression and activity during oxidative stress (Aiken et al., 2011). Perhaps SA has the ability to modulate proteasome activity in *Arabidopsis* through interactions with TOP1 and/or TOP2, or indirectly through NPR1.

PCD is essential for proper development in plant and animalian species (Eckardt, 2006), and SA and the phytohormone auxin are known to negatively interact in regulating plant development (Canet et al., 2010). Therefore, immunity may have evolved with or from and be intimately linked with developmental pathways (Vanacker et al., 2001). Nonetheless, the evolutionarily conserved MAPK signaling pathways, and the convergent evolution of analogous immune machinery and responses—such as transmembrane PRRs and the oxidative burst and

PCD, respectively (Ausubel, 2005; Coll et al., 2011; Torres et al., 2005)—provide evidence of common evolutionary solutions to selective pressures imposed on immune systems.

It is intriguing that two completely different TOP lineages—potentially having evolved from the mitochondrial processing peptidase (MPP) conserved among all eukaryotes (Rawlings and Barrett, 1995; Sokolenko et al., 2002)—may have proteolytic functions in modulating immunity in both plants and mammals. Could the MPP have given rise to components of the basal eukaryotic cell defense machinery, which have since evolved immunomodulatory functions in complex organisms?

Perspectives

By determining how SA and other phytohormone signaling pathways function and interact in physiological development, metabolism, and defense responses (Kunkel and Brooks, 2002; Loake and Grant, 2007), it may be possible to engineer plants having durable resistance, prolific symbiotic interactions with beneficial microbes, optimal resource allocation, high productivity, and unmatched vigor. Human manipulation and strengthening of plant immunity is also a possibility via the application of plant defense activators: the benzothiadiazole acibenzolar-*S*-methyl (Actigard®), a functional analog of SA, is one example of an environmentally safe synthetic chemical used in agricultural practices to stimulate plant immunity (Dao et al., 2009; Vallad and Goodman, 2004; Walters et al., 2005). Idealized crop phenotypes may one day be achievable, and the identification of SABPs brings us one step closer.

Methods

Plant Material and Growth Conditions

Arabidopsis thaliana plants were grown in sterilized Pro-Mix® BX soil at an average density of 3 plants per 3X3 inch pot. Seed dormancy was broken by incubating sown seeds at 4°C for 2-3 days before transfer to a growth chamber. Normal growth conditions: 22°C and 60% relative humidity under a 16-hour photoperiod and photon flux density of 135-175 μmol $m^{-2}s^{-1}$. Growth conditions after *Pst* DC3000 infection: 22°C and 50% relative humidity under a 16-hour photoperiod and photon flux density of 145-185 μmol $m^{-2}s^{-1}$. Columbia-0 (Col-0) ecotype served

as the wild-type positive control for all experiments, whereas *rps2* (Col-0 background) and *rpm1* (Col-5(gl1-1) background) resistance (R)-gene mutants served as negative controls. *top1* and *top2* T-DNA-tagged mutant SALK and SAIL lines were obtained from the *Arabidopsis* Biological Resource Center (ABRC) at The Ohio State University. T-DNA-tagged mutant line specifications are listed in Table S1. T-DNA insertion presence was confirmed via PCR (32 cycles) using primers listed in Table S2. Pollen from $top1^{339}$ and $top1^{439}$ was used to make crosses with $top2^{127}$ and $top2^{727}$ to generate $top1^{339}top2^{127}$, $top1^{339}top2^{727}$, $top1^{439}top2^{127}$, and $top1^{439}top2^{727}$ T-DNA-tagged double mutant lines.

Bacterial Strains and Growth Conditions

Escherichia coli strains DB3.1 and DH5-α were cultured in liquid LB (MQH_2O + 1% NaCl + 1% tryptone + 0.5% yeast extract; pH 7.0, adjusted using HCl or NaOH) or on 1.5% LB medium at 37°C for 12-24 hours. *Agrobacterium tumefaciens* strain GV2260 was cultured in liquid LB or on 1.5% LB medium at 29°C for 1-2 days. *Pseudomonas syringae* pv. *tomato* (*Pst*) strains DC3000 virulent, DC3000 *avrRpt2* avirulent, DC3000 *avrRpm1* avirulent, and DC3000 Δ*hrcC* disarmed virulent were cultured on 1.75% KB medium (MQH_2O + 2% Proteose Peptone #3 + 0.15% K_2HPO_4*$2H_2O$ + 0.15% $MgSO_4$*$7H_2O$ + 10 mL 100% glycerol; pH 7.0-7.2, adjusted using HCl or NaOH) at 29°C for 2 days, and then rinsed twice with and suspended in 10 mM $MgCl_2$ before being infiltrated into *Arabidopsis* leaves. *Pst* dilutions were prepared starting from OD_{600} = 0.2 (≈ 1 x 10^8 CFU/mL). *Pst* extracted from *Arabidopsis* leaves were cultured on 1.5% LB medium at 29°C for 2 days. Appropriate antibiotics for selection were added to all media.

Plant DNA and RNA Extraction

DNA was extracted from rosette leaves of 2-weeks-old plants using DNA extraction buffer (200 mM Tris pH 7.5 + 250 mM NaCl + 25 mM EDTA pH 8.0 + 0.5% SDS) followed by precipitation using isopropanol. RNA was extracted from rosette leaves of 2-weeks-old plants using TRIzol® Reagent (Invitrogen; Carlsbad, CA, USA) following the manufacturer's instructions. RNA was subject to DNase treatment using RQ1 RNase-Free DNase (Promega; Madison, WI, USA) following the manufacturer's instructions, and then re-extracted using

TRIzol® Reagent. RNA quality was determined by visualizing ribosomal RNA subunits via gel electrophoresis using a method described by Masek et al. (2005).

Semi-quantitative RT-PCR

RNA was reverse transcribed into cDNA using SuperScript® II Reverse Transcriptase (Invitrogen; Carlsbad, CA, USA) following the manufacturer's instructions. Semi-quantitative PCR (28-29 or 34-35 cycles) was conducted using cDNAs as templates and specific primer pairs numbered 1-6 (see Primers methods section and refer to Figure 14 and Figure 6 to determine primers that correspond with each *TOP1* clone or RT-PCR amplification fragment, respectively). Expected PCR product sizes for wild-type *TOP1* and *TOP2* cDNAs are listed in Table S3 for each primer pair. *Actin 1* was amplified as an endogenous control. Semi-quantitative PCR analysis was conducted in duplicate (2 plants per line) for every line except *top1*^{339}*top2*^{127} and *top1*^{339}*top2*^{727}, which were analyzed singly. Primer pairs for 5′ *TOP1*, 3′ *TOP1*, and 3′ *TOP2* seemed to amplify the intended regions specifically, whereas *TOP1* 34, 5′ *TOP2*, and *TOP2* 17 primer pairs seemed to cross-react between *TOP1* and *TOP2*, or possibly elsewhere in the genome. However, it is important to note that this cross-reaction could alternatively represent changes in *TOP1* or *TOP2* expression levels when one or the other is mutated; this can be confirmed using quantitative RT-PCR. Additionally, transcript level differences could represent epigenetic influences.

TOP1 Cloning

TOP1 expression clones were all created using either traditional Gateway® cloning technology (Invitrogen; Carlsbad, CA, USA), MultiSite Gateway® cloning technology (Invitrogen; Carlsbad, CA, USA), or restriction fragment digestion-ligation cloning (New England BioLabs; Ipswich, MA, USA) following the manufacturers' instructions. *TOP1* genomic DNA and 2 kb of the predicted promoter region were separately PCR-amplified from the BAC clone K21L13 (obtained from the ABRC), whereas *TOP1* cDNA was PCR-amplified from a pLIC-C-TAP plasmid vector carrying *TOP1* cDNA (contains a silent A to G mutation at nucleotide 114). The 500 bp *TOP1* cDNA sequence used for RNAi cloning was determined using the Basic Local Alignment Search Tool (BLAST) to share 88% homology with *TOP2* but no homology greater

than 19 bp with any other sequence within the *Arabidopsis* genome. Refer to Figure 14, Table S2, and Table S4 to follow through the cloning process, including the primers used, PCR fragments amplified, entry/intermediate and destination/final vectors used, entry and expression clones created, and the *Arabidopsis* backgrounds transformed with each expression clone. For more details regarding cloning procedures and the vectors used, refer to manufacturer instruction manuals and reports that describe the vectors (see Table S4).

PCR fragments were amplified using the Phusion® High-Fidelity DNA Polymerase (Finnzymes; Espoo, Finland), gel-purified using the Zymoclean™ Gel DNA Recovery Kit (Zymo Research; Irvine, CA, USA), and then used for cloning. Note: all Pro-cDNA and Pro-Genomic *TOP1* clones (except the MultiSite Gateway® clones) were created via overlapping PCR by using attB1-Pro-5′ORF and 3′Pro-ORF-attB2 as templates together in the same polymerization reaction for 5 cycles before adding primers (see Table S2 for more details). Entry clones were transformed into DH5-α via electroporation, selected transformants confirmed via colony PCR (bacteria from a single colony were added directly to the PCR reaction mixture), and plasmids extracted using the Zyppy™ Plasmid Miniprep Kit (Zymo Research; Irvine, CA, USA) and sequenced. For Gateway® cloning, entry clones were recombined with target destination vectors to generate expression clones, whereas for restriction fragment digestion-ligation cloning the sense and antisense arms were excised as single units and ligated into the target destination vectors (see Figure 14 and Table S2 for more details). Expression clones were transformed into DH5-α and selected and sequenced as described previously. Sequencing-confirmed expression clones were then transformed into GV2260 to generate host strains for *A. tumefaciens*-mediated transformation of *Arabidopsis*.

Agrobacterium tumefaciens-mediated Stable Transformation of *Arabidopsis*

Arabidopsis Col-0 wild-type, *top1*^{339}, *top1*^{439}, *top1*^{339}*top2*^{127}, and *top1*^{339}*top2*^{727} were stably transformed via *A. tumefaciens* strain GV2260 (carrying a particular expression clone) using a method adapted from Clough and Bent (1998) and Logemann et al. (2006). Flower bolts of 4-week-old plants were clipped to stimulate rapid lateral bolting. Lateral shoot inflorescences were prepared for transformation 1 week later by removing all but those that displayed a cluster of few unopened floral buds. GV2260 host strains from 2-day-old culture plates were

resuspended in inoculation medium (MQH_2O + 5% sucrose + 0.05% Silwet L-77) to give OD_{600} = 0.8. Inflorescences were immersed in inoculation medium with gentle agitation for about 6-8 seconds, or inoculation medium was dripped via pipetting onto inflorescences to mimic a rain event. After inoculation, plants were covered with a dome for 24 hours to maintain high humidity. Slightly immature siliques were harvested 1.5-2 weeks after inoculation and air-dried for 3-4 weeks to allow seed maturation before proceeding with transformant selection via tissue culture. Selected transformants will be confirmed via semi-quantitative RT-PCR of *TOP1* or both *TOP1* and *TOP2*.

Plant Tissue Culture

Seed sterilization: Arabidopsis seeds were mixed with 70% EtOH for 1.5 minutes. After EtOH removal, seeds were shaken in 30% bleach solution (MQH_2O + 30% NaClO + 0.05% Tween® 20) for 5 minutes to complete sterilization. After bleach solution removal, seeds were washed at least 5 times with MQH_2O and then resuspended in 0.1% Murashige and Skoog (MS) medium (MQH_2O + 0.433% MS salts + 0.055% MES monohydrate + 1% sucrose; pH 5.7-5.8, adjusted using KOH) or 0.1% Basic Agar medium (MQH_2O + 0.01% KNO_3; pH adjustment unnecessary) before plating on growth media. *Root analyses:* seeds were plated on 0.8% MS, plates sealed with Micropore™ tape and incubated in darkness at 4°C for 2 days to break seed dormancy, and then transferred to a growth chamber. Eight similarly-sized seedlings per line of 10- to 12-days-old were transferred to fresh media for optimal root visualization and comparative analyses at day 20. *Transgenic line selection: Arabidopsis* transformants carrying the *bar* resistance gene were selected on 0.8% MS + 0.867% glufosinate ammonium (Crescent Chemical Company; Islandia, NY, USA) using a method described by Nakamura et al. (2010), those carrying *nptII* gene were selected on 0.8% MS + 5% kanamycin using a method described by Xiang et al. (1999), and those carrying the *hpt* gene were selected on 0.8% Basic Agar + 2% hygromycin using a method described by Nakazawa and Matsui (2003). Plates were sealed with Micropore™ tape and incubated in darkness at 4°C for 2 days to break seed dormancy, and then transferred to a growth chamber. Transformants displaying 4 adult leaves were transplanted to Pro-Mix® BX soil to complete growth.

Resistance Response and Bacterial Growth Bioassays

MTI and ETI resistance response phenotypes and *in planta* bacterial growth were analyzed following pathogen challenge using a method adapted from Katagiri et al. (2002). Plants of 3- to 4-weeks-old were syringe-infiltrated, 3 leaves per plant, to saturation with 1 x 10^5 CFU/mL *Pst* DC3000 virulent, *avrRpt2*, *avrRpm1*, or Δ*hrcC* suspended in 10 mM $MgCl_2$. Plants infiltrated with 10 mM $MgCl_2$ served as controls for symptom background caused by $MgCl_2$ and/or wounding caused by infiltration. The phenotypes of *top1* and *top2* mutant lines were compared with the Col-0 positive control and *rps2* or *rpm1* negative controls. *Resistance response analyses:* chlorotic cell death disease symptoms signified increased susceptibility toward the infecting *Pst* DC3000 strain. Average phenotypes were documented for each line 4 days post-infiltration (dpi) and displayed in Figure 8. *Bacterial growth bioassays:* 3 leaf discs from infected leaves were collected from each of 8 plants per line at 0, 2, and 4 dpi, and then shaken at 300 rpm for 1 hour at room temperature in extraction solution (10 mM $MgCl_2$ + 0.01% Silwet L-77 surfactant + appropriate antibiotics). Dilutions (1:10, 1:100, 1:1000, 1:10000, 1:100000) using MQH_2O were prepared and plated for colony growth analysis, thus giving 8 replicates per dilution per line for each dpi. Colony growth was observed and recorded for each line at the most discernible dilution ranges after 2 days incubation at 29°C, and mean colony forming units (CFU)/cm^2 leaf tissue subsequently calculated. CFU/cm^2 leaf tissue = ((# colonies)(dilution factor used to count)(dilution factor of plating)) ÷ ((disc area, πr^2)(# discs)).

3,3′-Diaminobenzidine Staining

H_2O_2 production during the oxidative burst was qualitatively analyzed by 3,3′-Diaminobenzidine (DAB) staining using a method adapted from Hatsugai et al. (2009), Snyrychová et al. (2009), Thordal-Christensen et al. (1997), and Torres et al. (2002). Plants of 3- to 4-weeks-old were syringe-infiltrated, 4 half-leaves per plant, with 5 x 10^7 CFU/mL *Pst* DC3000 virulent, *avrRpt2*, or Δ*hrcC* suspended in 10 mM $MgCl_2$ to elicit the oxidative burst. Plants infiltrated with 10 mM $MgCl_2$ served as controls for symptom background caused by $MgCl_2$ and/or wounding caused by infiltration. Leaves were fully stained with 1 mg/mL DAB (pH 6.5-6.8) at 0, 6, 9, and 12 hours post-inoculation via infiltration of leaf halves opposite that of $MgCl_2$ or *Pst* DC3000 infiltration. DAB-infiltrated leaves were collected immediately and incubated within a moisture chamber for

8-12 hours, and then shaken in fixation solution (60% EtOH + 20% lactic acid + 20% glycerol) at 120 rpm for 5 hours before de-staining in 2.5 g/mL chloral hydrate. De-stained leaves were fixed to microscope slides using 50% glycerol, and then photographed within 1 week. *top1* and *top2* mutant lines were compared with the Col-0 positive control and *rps2* negative control. DAB staining solution was prepared by dissolving DAB (97% purity; Sigma-Aldrich; St. Louis, MO, USA) in acidic MQH_2O (pH 3.8 or lower, adjusted using HCl); just prior to use, pH was raised to 6.5-6.8 using NaOH. Experiment was conducted once with 4 replicates per experimental or $MgCl_2$ control group per time point per line. DAB stained leaves resembling the average phenotype for each treatment and *Arabidopsis* line were selected for display in Figure 10.

Trypan Blue Staining

HR-PCD was qualitatively analyzed by Trypan Blue (TB) staining using a method adapted from Hatsugai et al. (2009), Keogh et al. (1980), and Koch and Slusarenko (1990). Plants of 3- to 4-weeks-old were syringe-infiltrated, 3 half-leaves per plant, with 1 x 10^6 CFU/mL *Pst* DC3000 virulent, *avrRpt2*, or Δ*hrcC* suspended in 10 mM $MgCl_2$ to elicit the HR. Plants infiltrated with 10 mM $MgCl_2$ served as controls for symptom background caused by $MgCl_2$ and/or wounding caused by infiltration. Infiltrated leaves were collected 24 hours post-inoculation and boiled in 0.33 mg/mL TB staining solution for 5-8 minutes, and then incubated at room temperature for 12 hours before de-staining in 2.5 g/mL chloral hydrate. De-stained leaves were fixed to microscope slides using 50% glycerol, and then photographed within 1 week. *top1* and *top2* mutant lines were compared with the Col-0 positive control and *rps2* negative control. TB stock solution (0.67 mg/mL) was prepared by dissolving 30 g phenol crystals in 30 mL 85% lactic acid, and then mixing in 30 mL 80% glycerol, 30 mL MQH_2O, and 0.06 g Trypan Blue (Sigma-Aldrich; St. Louis, MO, USA). TB working solution (0.33 mg/mL) was prepared by diluting the stock solution with 96% EtOH in a 1:2 v/v ratio. Experiment was conducted once with 9 replicates per experimental group per line and 6 replicates per $MgCl_2$ control group per line. TB stained leaves resembling the average phenotype for each treatment and *Arabidopsis* line were selected for display in Figure 11.

Ion Leakage Analysis

HR-PCD was quantitatively measured by ion leakage conductivity using a method adapted from Watanabe and Lam (2006), Watanabe and Lam (2008), and Watanabe and Lam (2011). Plants of 3- to 4-weeks-old were syringe-infiltrated, 5 leaves per plant, to saturation with 1 x 10^6 CFU/mL *Pst* DC3000 *avrRpt2* suspended in 10 mM $MgCl_2$ to elicit the HR. Plants infiltrated with 10 mM $MgCl_2$ served as controls for symptom background caused by $MgCl_2$ and/or wounding caused by infiltration. For each replicate, 5 leaf discs—1 per each of the 5 inoculated leaves—were collected from non-infiltrated leaf halves at 0, 8, and 16 hours post-inoculation (hpi) and floated abaxial side up on 4 mL MQH_2O. Leaf discs were shaken at 100 rpm at room temperature for 2 hours before measuring conductivity of the bathing solutions. *top1*^{339}, *top2*^{727}, and *top1*^{439}*top2*^{127} mutant lines were compared with the Col-0 positive control and *rps2* negative control. This small-scale experiment was conducted only once: 1 replicate per line at 0 hpi and 2-3 replicates per line at 8 and 16 hpi for the experimental group, and 1 replicate per line at 0, 8, and 16 hpi for the $MgCl_2$ control group. Conductivity was measured using a PC 700 pH/mV/Conductivity/°C/°F Bench Meter (Oakton Instruments; Vernon Hills, IL, USA) and calculated as µSiemens/cm leaf tissue. *Pst*-inoculated leaves resembling the average phenotype for each *Arabidopsis* line were selected for display in Figure 12, and whole plants are displayed in Figure S4.

Salicylic Acid Leaf Infiltration

SA-induced cell death was qualitatively analyzed by SA leaf infiltration using a method adapted from Brodersen et al. (2005) and Martinez et al. (2000). SA crystals (ReagentPlus®, ≥99% purity; Sigma-Aldrich; St. Louis, MO, USA) were dissolved in 100% EtOH. SA stock solution and 100% EtOH were diluted in 5 mM BIS-TRIS buffer (MQH_2O + 0.105% BIS-TRIS) to prepare 5 mM SA and 10 mM SA working solutions and their respective controls, 0.5% EtOH and 1% EtOH. All working solutions were adjusted to pH 6.5-6.8 using HCl or NaOH. SA working solutions and EtOH controls were spot-infiltrated into separate 18-day-old plants (3 leaves per plant, 5-8 plants per line per SA treatment and 4 plants per line per EtOH control treatment) in the center (adjacent to the midvein) of each leaf. *top1* and *top2* mutant lines were compared with the Col-0 positive control and analyzed for the amount of time elapsed before

SA-induced cell death symptoms appeared, the degree of cell death spread from the original site of infiltration, and the number of leaves showing cell death symptoms 1 week post-infiltration on a severity scale of 0 (no symptoms) to 2 (total leaf collapse) in 0.5 increments. Mean hypersensitive cell death severity for each line and SA treatment group was calculated as the average cell death severity score of all of the leaves analyzed. Model leaves representing phenotypes along the SA-induced cell death severity scale were selected for display in Figure 13.

Primers

Primers listed in Table S2 were synthesized by Eurofins MWG Operon. Refer to the *TOP1* Cloning and *Semi-quantitative RT-PCR* results sections for more details, and to Figure 14 and Figure 6 to determine the primers that correspond with each *TOP1* clone or RT-PCR amplification fragment, respectively.

Microscopy

Plant tissues were visualized under white light using an Olympus SZX12 Stereo Microscope. *Magnifications used for photos:* 60X for roots, 10X for whole leaves, and 90X for zoomed-in leaves.

DNA Sequencing

Sanger(3730XL) DNA sequencing services were provided by the Cornell University Core Laboratories Center. Sequencing results were analyzed using the DNASTAR Lasergene® SeqMan Pro™ program.

Statistical Analyses

Significance values for all quantitative assays were calculated using Student's *t* test. *Significance parameters:* two-tailed distribution; two-sample unequal variance; and ★ = $p < 0.01$, ★★ = $p < 0.001$, and ★★★ = $p < 0.0001$.

Accession Numbers

Sequence data from this article can be found in the *Arabidopsis* Genome Initiative or GenBank/EMBL databases under accession numbers At5g65620 (*TOP1*) and At5g10540 (*TOP2*).

Supplemental Data

Supplemental Figure 1. Salicylic acid functions and hypothetical signaling pathways.
Supplemental Figure 2. Root phenotypes of *top1*, *top2*, and *top1 top2* mutants.
Supplemental Figure 3. DAB staining replicate sets at 6 hours post-infiltration.
Supplemental Figure 4. HR phenotypes of *top1*, *top2*, and *top1 top2* mutants.
Supplemental Table 1. *TOP1* and *TOP2* T-DNA-tagged mutant lines.
Supplemental Table 2. Primers used for T-DNA insertion check, semi-quantitative RT-PCR, cloning, colony PCR check, and sequencing.
Supplemental Table 3. Expected semi-quantitative RT-PCR product sizes for wild-type *TOP1* and *TOP2*.
Supplemental Table 4. Vectors used for *TOP1* cloning.
Supplemental Table 5. TOP1 and TOP2 homology with *Homo sapiens* and *Mus musculus* proteins.

Acknowledgments

Giulio Zampogna deeply thanks Sorina Popescu for research advising and mentorship, Christopher Bowen and Hyoung Yool Lee for fundamental lab training, Rodney Tucker for assistance during the leaf staining experiments, Medeea Popescu for assistance with routine lab tasks, Hong-Gu Kang for valuable advice, Miaoying Tian for conducting Biacore™ surface plasmon resonance, the Ji-Young Lee lab (especially Jose Sebastian) for assistance with MultiSite Gateway® cloning, the Plant Cell Imaging Facility staff for providing microscope training, the Greenhouse Staff and Popescu and Klessig lab members for their cooperation, and the Plant Science Research Honors Program committee and thesis reviewers for their dedication and greatly respected, invaluable comments. This research was supported by the S. Ann and Robert R. Morley Student Research Grant and Jane E. Brody Undergraduate Research Award to

Giulio Zampogna, start-up funds to Sorina Popescu from the Boyce Thompson Institute for Plant Research, and the National Science Foundation grant
IOS-0820405 to Sorina Popescu.

Author Contributions

Giulio Zampogna designed the research and Sorina Popescu provided guidance. Giulio Zampogna performed the research and conducted statistical analyses. Giulio Zampogna and Sorina Popescu analyzed data. Giulio Zampogna wrote and Sorina Popescu edited the report. Sorina Popescu, Daniel Klessig, and Magali Moreau designed and conducted the pioneering research. Giulio Zampogna worked with Magali Moreau in conducting some of the preliminary research.

Figures

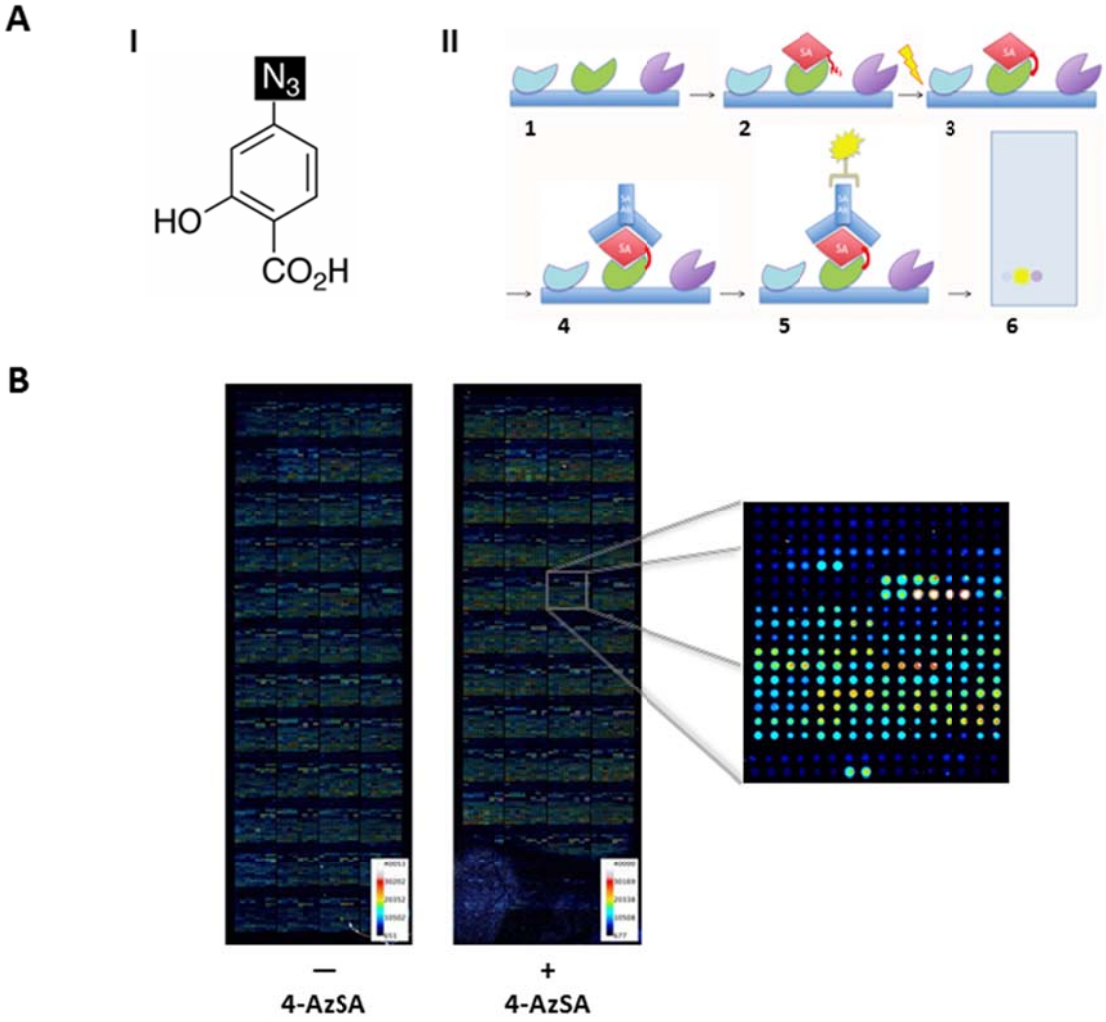

Figure 1: Screening for pSABPs using the functional protein microarray FPM-5000.
(A) Detection of protein-4-AzSA interaction using the anti-SA antibody. **(I)** Molecular structure of 4-AzSA. **(II)** Method used to probe for pSABPs. (1) Printing: *Arabidopsis* proteins were adhered to the chip surface. (2) Probing: 4-AzSA fit into the binding pockets of compatible proteins. (3) UV light triggered cross-linking between the 4-AzSA azide group (N_3) and the bound protein; chips were washed to remove unbound and weakly bound 4-AzSA. (4) and (5) Hybridization: the anti-SA antibody recognized 4-AzSA, and the Cy5 secondary antibody recognized IgG. (6) Scanning: chip was scanned at 633 nm. Schematic created by Dr. Moreau. **(B)** Detection of 4-AzSA cross-linked to proteins on the FPM-5000. Microarrays were incubated with or without 1 mM 4-AzSA for 1 hour, cross-linked under 500 mJ UV light, and probed with

the anti-SA antibody. Proteins printed on the microarray surface are clearly visible as distinct dots within the amplified box; proteins that bound 4-AzSA are colored yellow to white, whereas those that did not are colored green to violet (see color scale). Photos taken by Dr. Moreau. Abbreviations: 4-AzSA = 4-Azidosalicylic acid, pSABP = putative salicylic acid-binding protein, and IgG = immunoglobulin G.

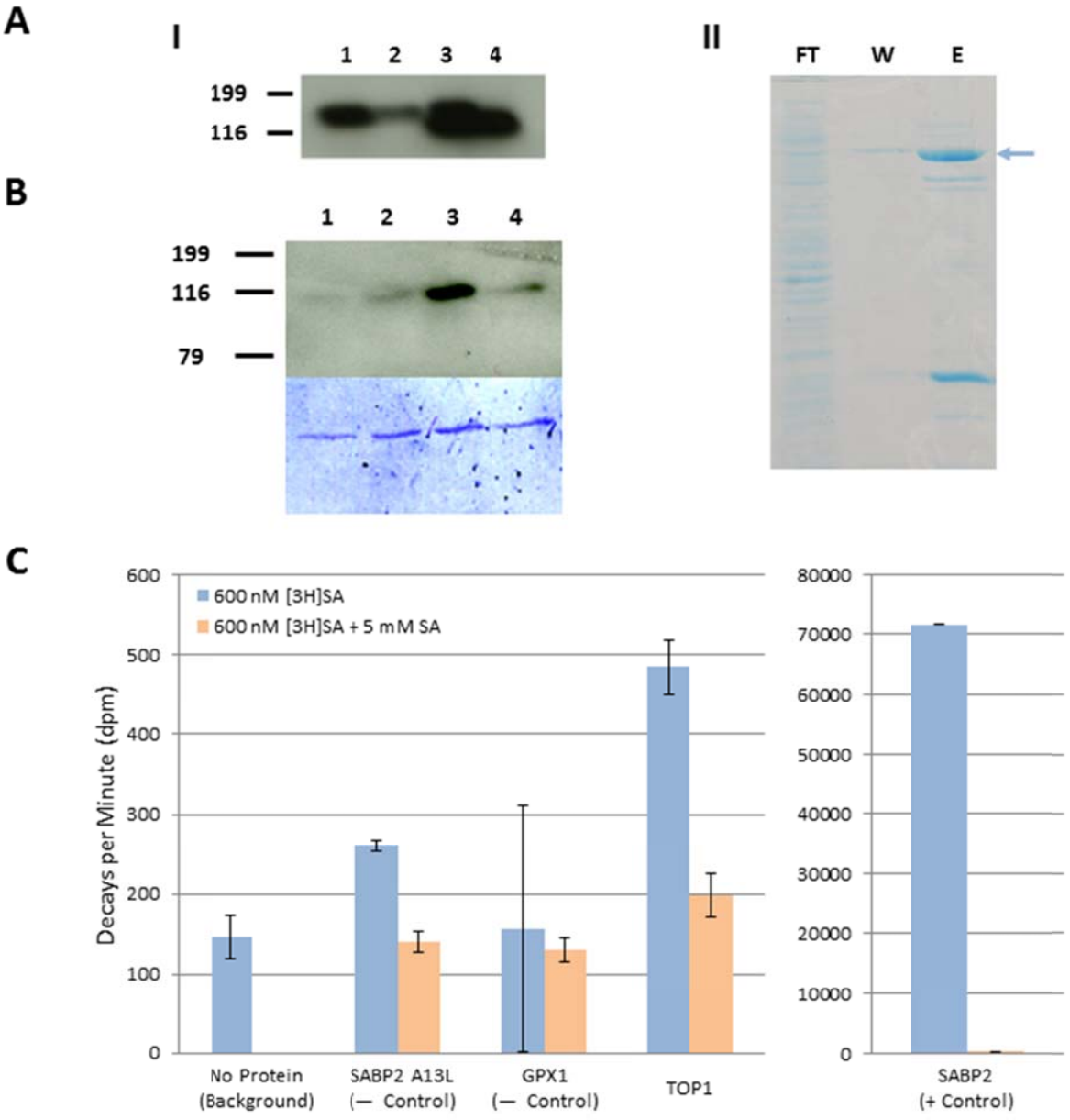

Figure 2: Recombinant TOP1 binds 4-AzSA and SA with specificity. (A) Recombinant TOP1 purification from *Nicotiana benthamiana* and *Escherichia coli*. **(I)** Western blot following the

purification of TOP1 from *Agrobacterium*-infiltrated *N. benthamiana* leaves. Lane 4 shows purified recombinant TOP1 (MW ≈ 89 + 25 kDa). Lanes 1-3 show the intermediate purification steps: 1 = crude extract, 2 = supernatant after TOP1 pull-down using IgG beads, and 4 = IgG beads after cleavage. **(II)** SDS PAGE gel following metal affinity chromatography purification of recombinant TOP1 (arrow; MW ≈ 89 kDa) from transgenic *E. coli* BL21 cells. Purification steps: FT = flow-through, W = wash, and E = eluted protein. Protein purifications were performed by Dr. Moreau and Giulio Zampogna. **(B)** SA can compete with 4-AzSA for binding recombinant TOP1. Recombinant TOP1 (MW = 89 + 25 kDa) purified from *N. benthamiana* was incubated with 500 µM 4-AzSA and cross-linked under 50 mJ UV light (3). After separation using SDS PAGE, the anti-SA antibody was used to probe for 4-AzSA. Control incubations lacking 4-AzSA (2) or without UV exposure (1) were also performed. Cross-linking in the presence of 20 fold excess SA (4) revealed the specificity of the 4-AzSA-TOP1 interaction. Relative protein concentrations are represented in the Coomassie Brilliant Blue-stained membrane. Experiment conducted by Dr. Moreau. **(C)** TOP1-SA binding may be too weak to accurately calculate specificity using [^{3}H]SA exclusion chromatography. Incubations consisting of 20 µg protein in the presence of 600 nM [^{3}H]SA (total binding) were conducted on ice for 1 hour. Incubations in the presence of 8,000 fold excess SA (+ 5 mM SA) were performed to quantify nonspecific binding. Radioactivity was counted after gel filtration. Tobacco Salicylic Acid-binding Protein 2 (SABP2) serves as a positive control, whereas the SABP2 A13L deletion mutant and non-SABP glutathione peroxidase-like protein-1 (GPX1) serve as negative controls. The difference in dpm for TOP1 between the 600 nM [^{3}H]SA and 600 nM [^{3}H]SA + 5 mM SA treatments is not significantly different than that of the negative controls (Student's *t*-test parameters: two-tailed distribution, two-sample unequal variance, ★ = $p < 0.01$). Experiment was conducted by Dr. Moreau, with statistical analysis by Giulio Zampogna. Note: this experiment was repeated by Dr. Moreau and yielded significant results that confirm TOP1-SA binding specificity (data not shown).

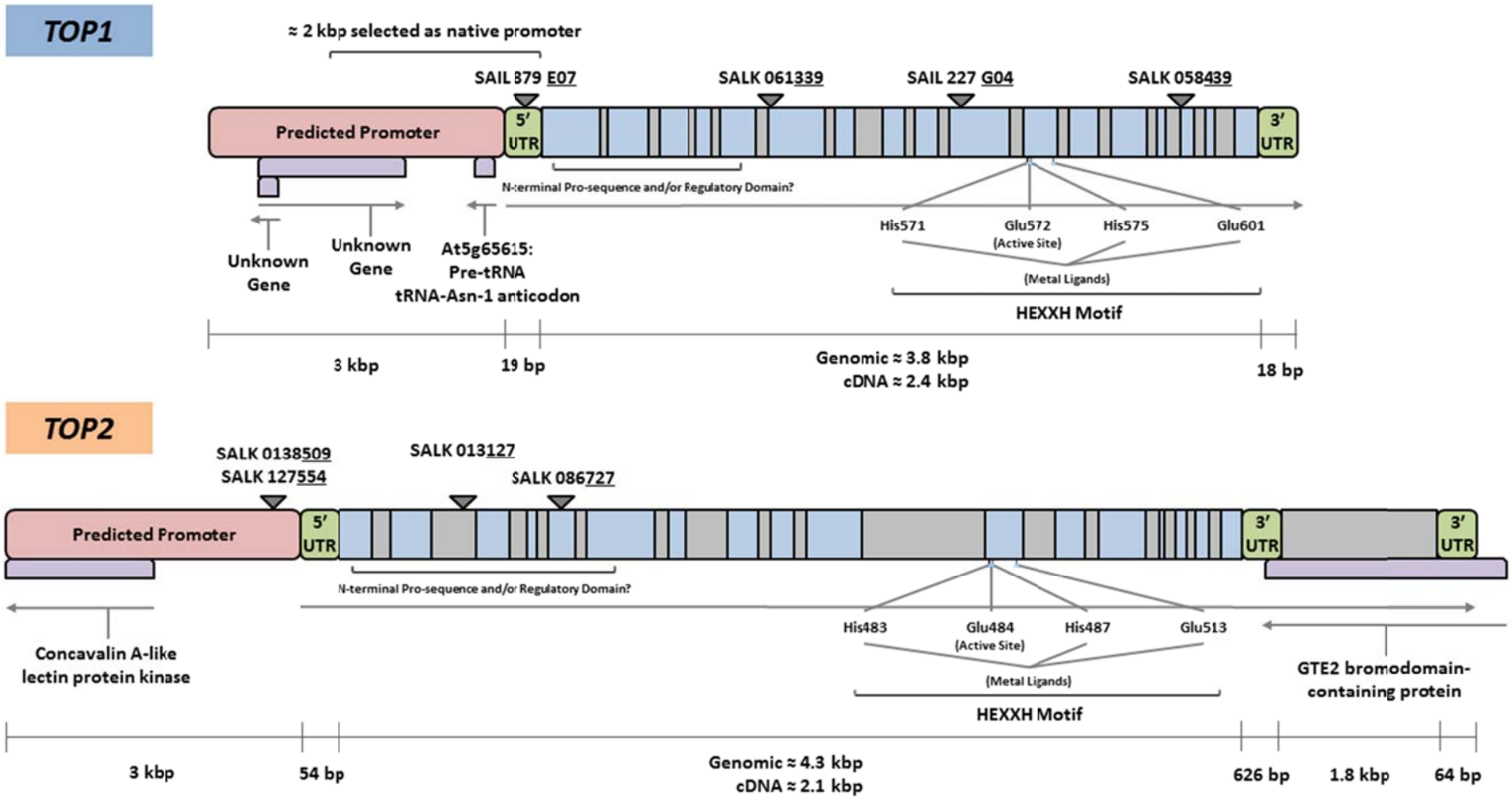

Figure 3: *TOP1* and *TOP2* gene structures and characteristics. Triangles depict T-DNA insertion locations. Arrows indicate transcriptional direction. Blue = exons. Gray = introns. Purple = overlapping genes. Diagram is approximately to scale. Figure information was adapted from The *Arabidopsis* Information Resource (TAIR), *MEROPS* the Peptidase Database, the *Arabidopsis* Gene Regulatory Information Server (AGRIS), and Beers et al. (2000). Abbreviations: UTR = untranslated region, bp = base pair, and kbp = kilobase pair.

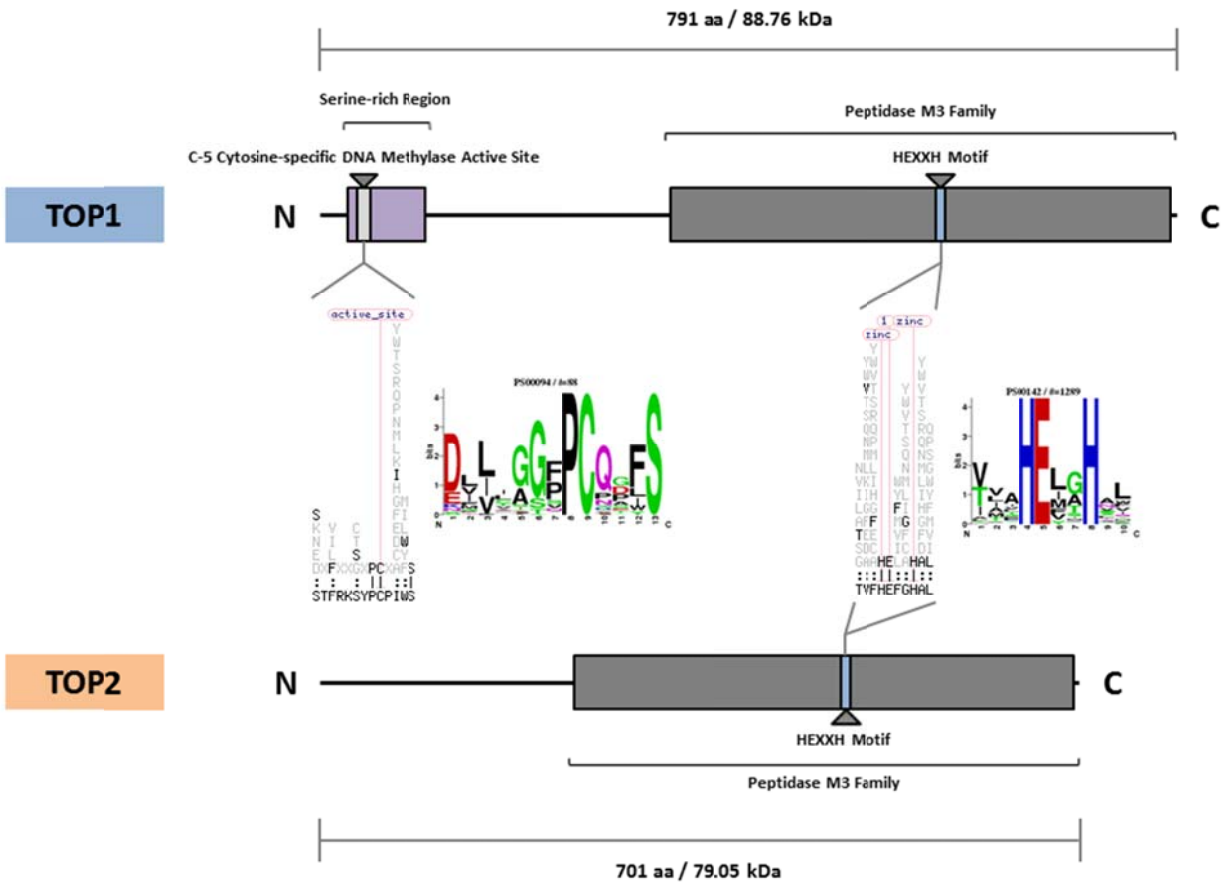

Figure 4: Predicted TOP1 and TOP2 protein structures. Diagram is to scale. Figure information was adapted from The *Arabidopsis* Information Resource (TAIR), *MEROPS* the Peptidase Database, and PROSITE Motif Scan. Motif logos and consensus sequence patterns were copied directly from PROSITE Motif Scan (http://myhits.isb-sib.ch/cgi-bin/motif_scan). Abbreviations: aa = amino acid, kDa = kilodalton, C = C-terminus, and N = N-terminus.

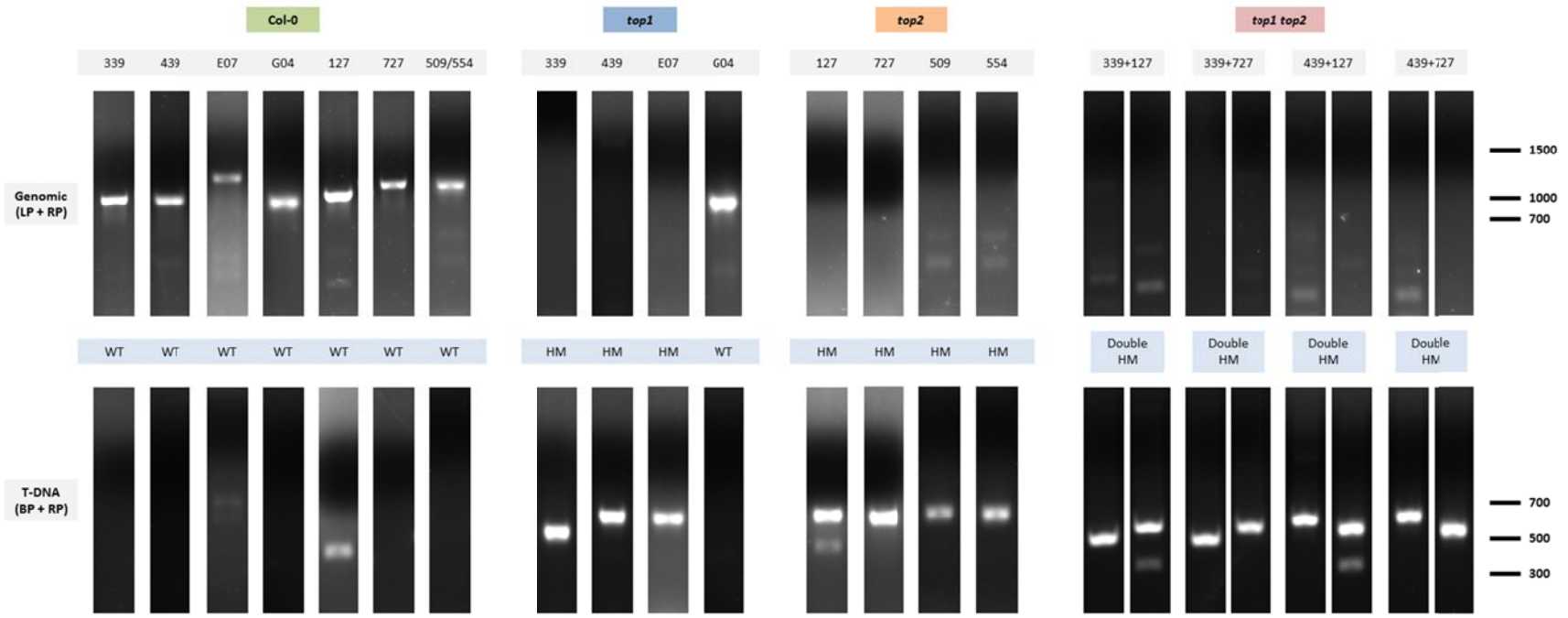

Figure 5: *top1*, *top2*, and *top1 top2* T-DNA-tagged mutant line zygosities. See Figure 2 and Table S2 for T-DNA insert locations and expected PCR product sizes. DNA was extracted from rosette leaves of 2-weeks-old plants. PCR reactions to confirm T-DNA insertions in *top2*^{127}, *top1*^{339}*top2*^{127}, and *top1*^{439}*top2*^{127} revealed a second smaller, fainter DNA band below the expected-sized brighter band; this is most likely a cross-reaction of the T-DNA BP and 127 RP primer pair elsewhere in the genome rather than amplification of a second T-DNA insertion. DNA marker is shown in base pairs. Abbreviations: LP and RP = left and right genomic DNA primers, BP = T-DNA border primer, WT = wild-type, and HM = homozygous for the T-DNA insertion(s).

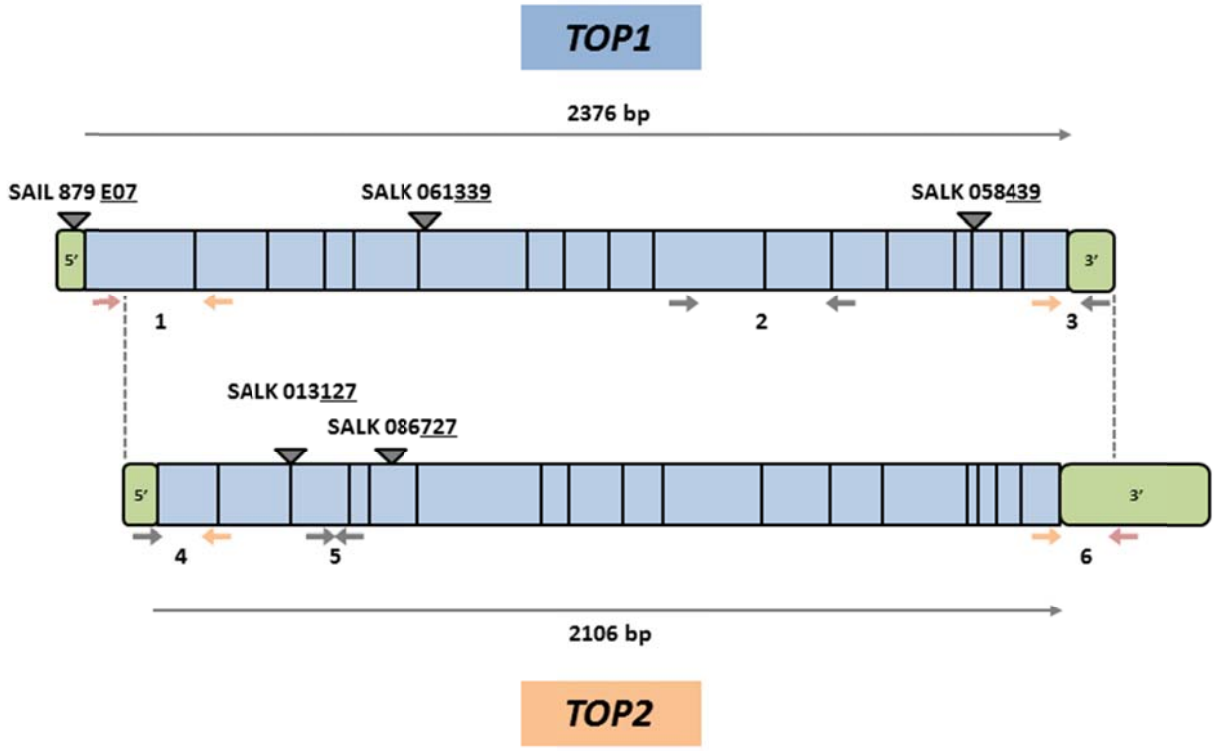

Figure 6: *TOP1* and *TOP2* cDNA alignment and semi-quantitative RT-PCR primer pair locations. Small arrows represent primers, and numbers 1-6 designate primer pairs used for semi-quantitative RT-PCR: (1) = 5′ *TOP1*, (2) = *TOP1* between 339 and 439 insertions, (3) = 3′ *TOP1*, (4) = 5′ *TOP2*, (5) = *TOP2* between 127 and 727 insertions, and (6) = 3′ *TOP2*. Red arrows represent primers that are unique to either *TOP1* or *TOP2*, whereas orange arrows represent primers that are identical between *TOP1* and *TOP2*. Diagram is approximately to scale. Figure information adapted from The *Arabidopsis* Information Resource (TAIR) and a *TOP1*—*TOP2* cDNA sequence alignment using the DNASTAR Lasergene® MegAlign™ (Clustal W alignment) program. Abbreviations: 5′ = 5′ untranslated region, 3′ = 3′ untranslated region, and bp = base pair.

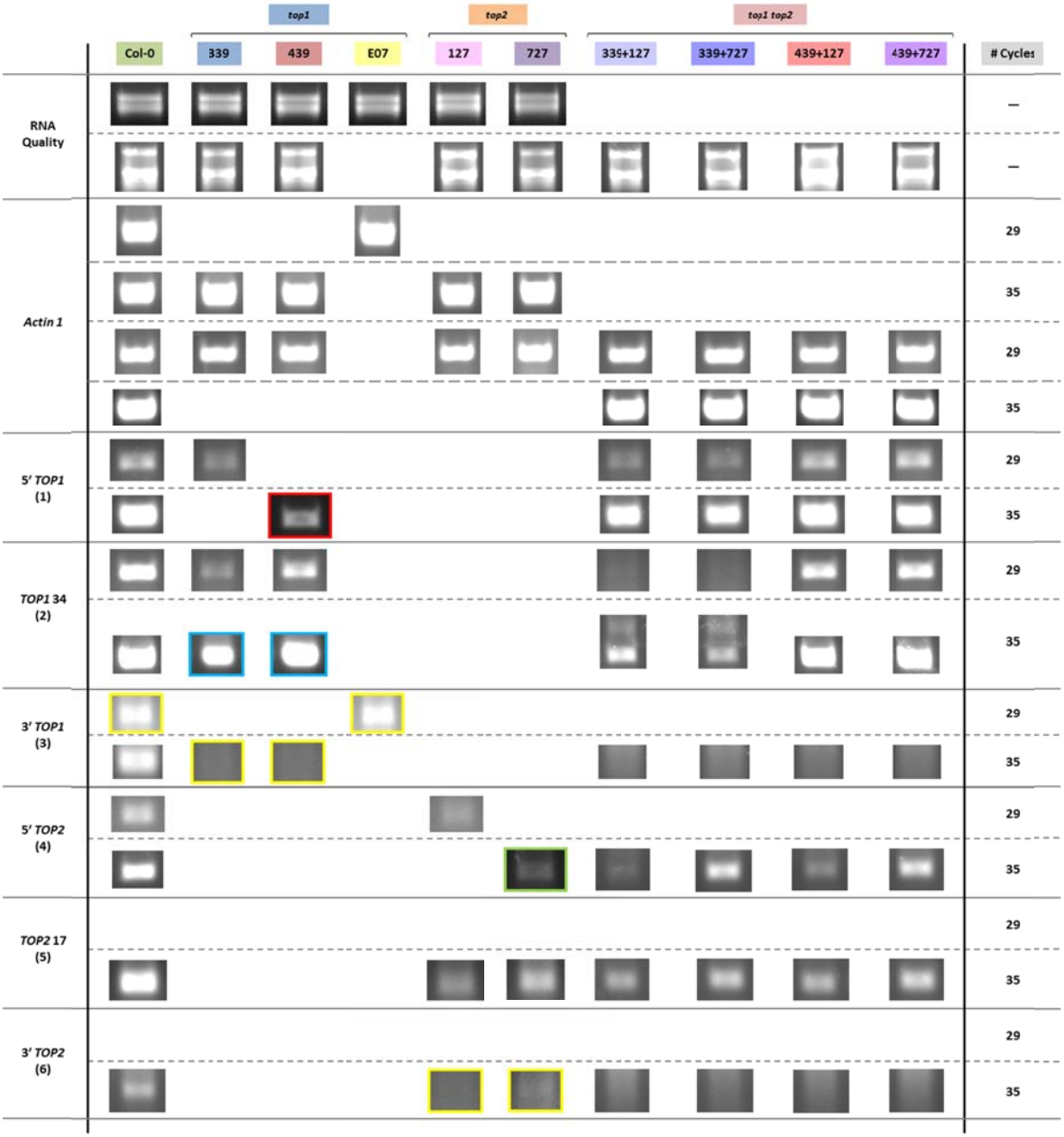

Figure 7: Semi-quantitative RT-PCR of *top1*, *top2*, and *top1 top2* T-DNA-tagged mutant lines. RNA was extracted from rosette leaves of 2-weeks-old plants. Numbers 1-6 designate primer pairs used for semi-quantitative RT-PCR (see Figure 5). See Table S3 for expected PCR product sizes. Color outlines: red = no Col-0 wild-type control, blue = no *Actin-1* control, green = no Col-0 wild-type and *Actin-1* controls, and yellow = cDNA amplification products derived from the first row of RNA extracts. All PCR fragments without a yellow outline were derived from the second row of RNA extracts.

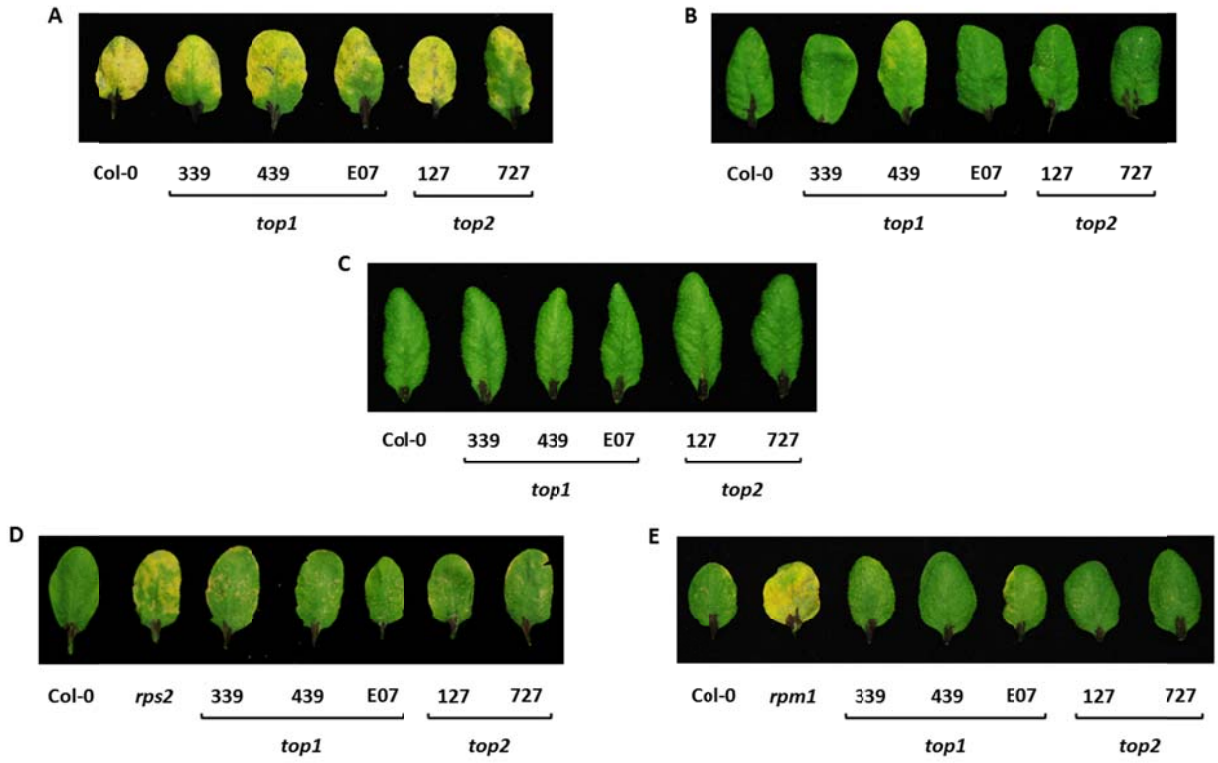

Figure 8: *top1* and *top2* single mutants do not display resistance phenotypes due to defects in MTI or ETI. Plants of 3- to 4-weeks-old were syringe-infiltrated, 3 leaves per plant, to saturation with either 10 mM $MgCl_2$ **(C)** or 1 x 10^5 CFU/mL *Pst* DC3000 virulent **(A)**, *Pst* DC3000 Δ*hrcC* **(B)**, *Pst* DC3000 *avrRpt2* **(D)**, or *Pst* DC3000 *avrRpm1* **(E)**. Pictures were taken at 4 dpi. Chlorotic cell death disease symptoms signify susceptibility toward the infecting *Pst* strain. Col-0 wild-type = positive control and *rps2* and *rpm1* = negative controls. *Pst* DC3000 virulent = test for disease symptom defects or altered resistance. *Pst* DC3000 Δ*hrcC* strain = test for MTI defects. *Pst* DC3000 avirulent *avrRpt2* and *avrRpm1* = test for ETI defects. Plants infiltrated with 10 mM $MgCl_2$ served as controls for symptom background caused by $MgCl_2$ and/or wounding caused by infiltration. Abbreviations: CFU = colony forming units, dpi = days post-inoculation, ETI = effector-triggered immunity, MTI = microbe/pathogen-associated molecular pattern-triggered immunity, and *Pst* DC3000 = *Pseudomonas syringae* pv. *tomato* DC3000.

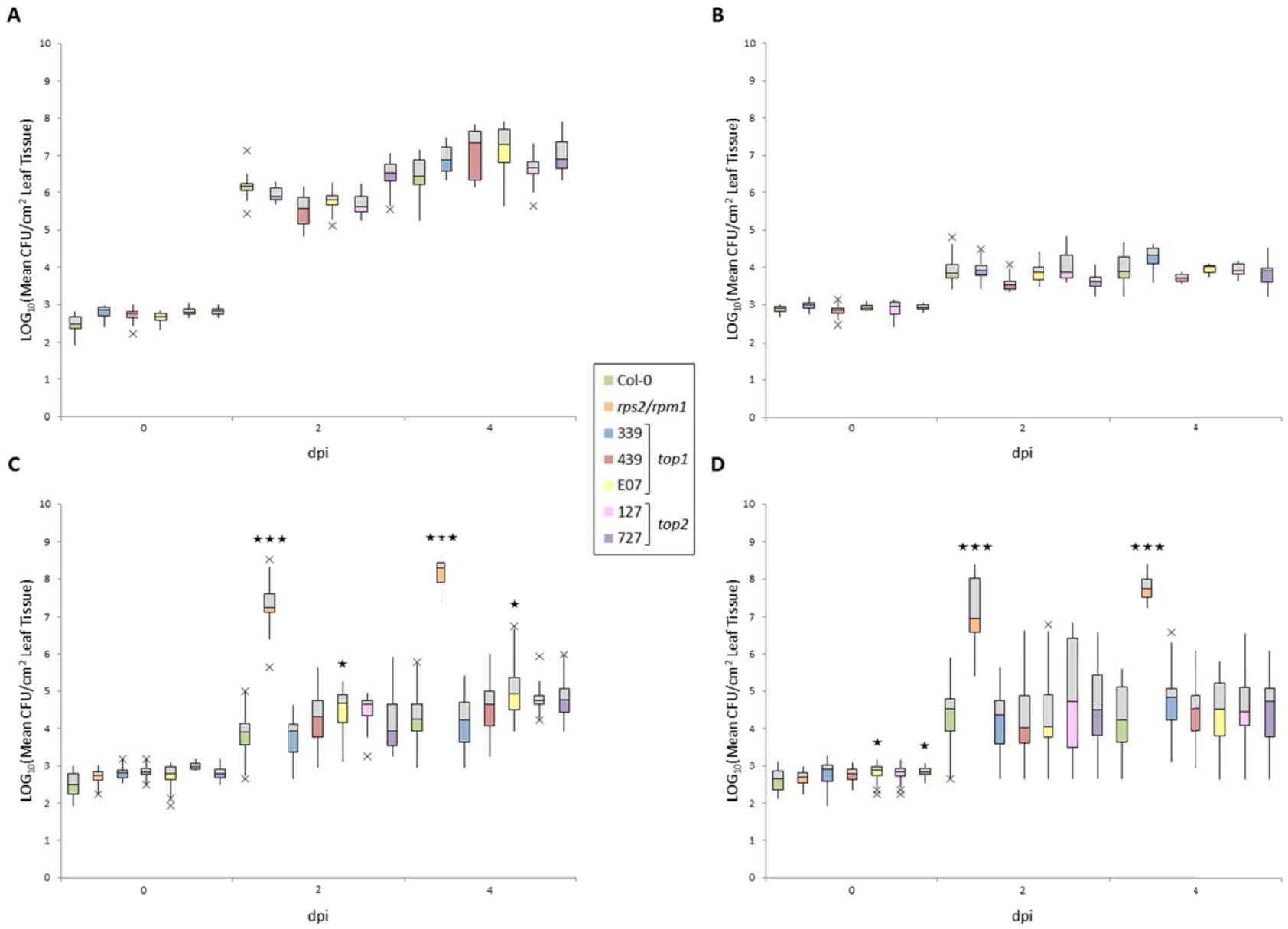

Figure 9: *Pst* DC3000 bacterial growth in *top1* and *top2* single mutant leaves is comparable to the wild-type. Plants were inoculated as described in Figure 8. Three leaf discs were collected from each of 8 plants per line at 0, 2, and 4 dpi and shaken at 300 rpm for 1 hour at room temperature in 10 mM $MgCl_2$ + 0.01% Silwet L-77 surfactant + appropriate antibiotic(s) to extract the bacteria. Dilutions were prepared and plated for colony growth analysis, thus giving 8 replicates per dilution per line for each dpi. Colony growth was observed and recorded for each line at the most discernible dilution ranges after 2 days incubation at 29°C. Mean CFU/cm^2 leaf tissue was calculated and plotted as above for **(A)** *Pst* DC3000 virulent, **(B)** *Pst* DC3000 Δ*hrcC*, **(C)** *Pst* DC3000 *avrRpt2*, and **(D)** *Pst* DC3000 *avrRpm1*. Experiments were repeated once (6-8 replicates) for (A), (B), and $top2^{127}$ and $top2^{727}$ in (C), and three times (20-24 replicates) for (C) and (D). Stars represent significant differences in comparison to Col-0 wild-type plants (Student's *t*-test parameters: two-tailed distribution, two-sample unequal variance, ★ = $p < 0.01$, ★★ = $p < 0.001$, and ★★★ = $p < 0.0001$). Abbreviations: CFU = colony forming units, dpi = days post-inoculation, rpm = revolutions per minute, and *Pst* DC3000 = *Pseudomonas syringae* pv. *tomato* DC3000.

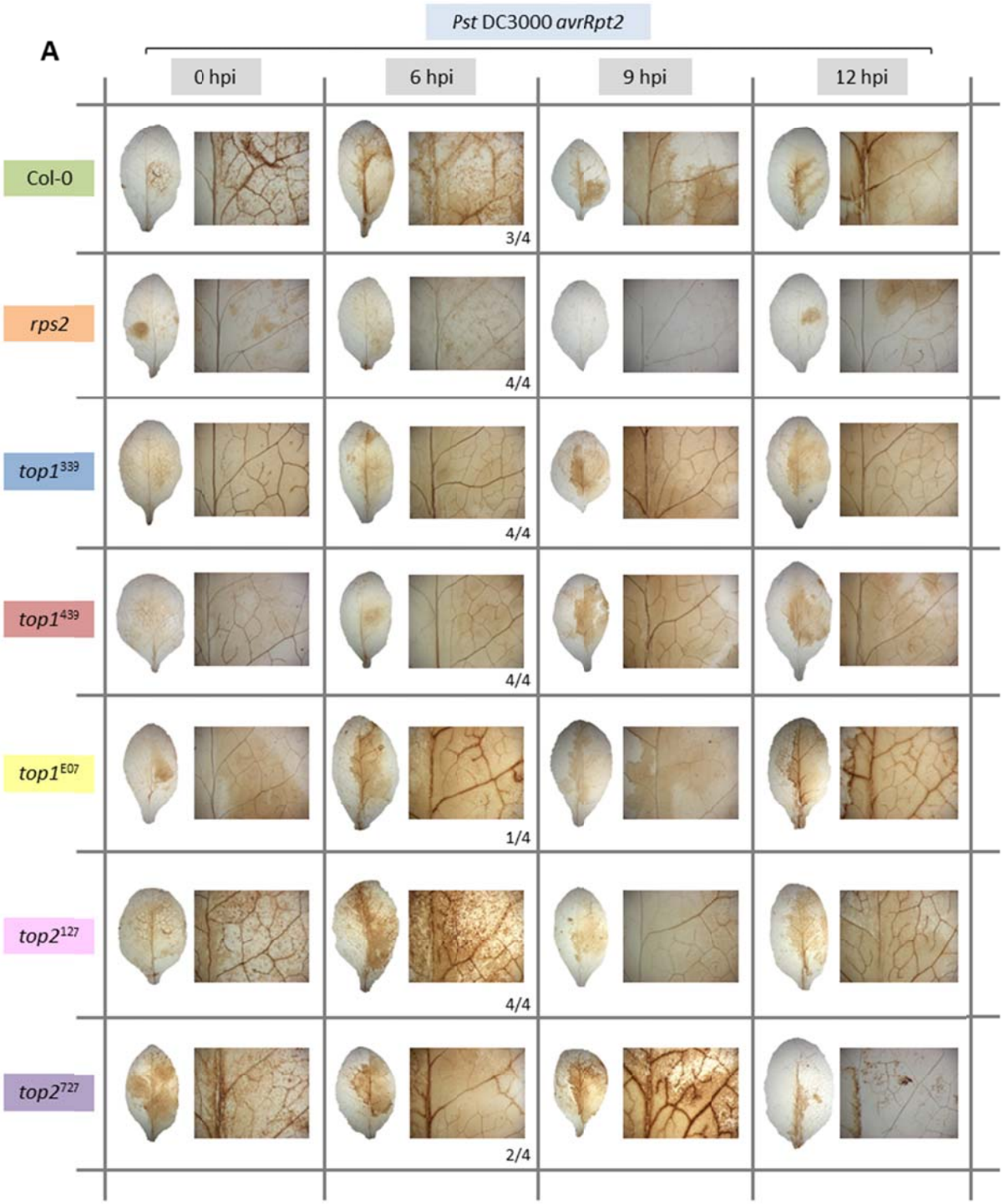

Figure 10: TOP1 and TOP2 may antagonistically regulate H_2O_2 accumulation during the oxidative burst. Figure set is continued on the next 3 pages. Plants of 3- to 4-weeks-old were syringe-infiltrated, 4 half-leaves per plant, with either 10 mM $MgCl_2$ **(D)** or 5 x 10^7 CFU/mL *Pst* DC3000 *avrRpt2* **(A)**, virulent **(B)**, or Δ*hrcC* **(C)**. Leaves were stained with 1 mg/mL (pH 6.5-

6.8) DAB at 0, 6, 9, and 12 hpi via infiltration of leaf halves opposite that of $MgCl_2$ or *Pst* DC3000 infiltration. Experiment was conducted once with 4 replicates per experimental or control group per time point per line (see Figure S3 for all 6 hpi replicates), and the scoring system depicts the number of leaves resembling the pictured leaf within each replicate set. Abbreviations: CFU = colony forming units, DAB = 3,3'-Diaminobenzidine, hpi = hours post-inoculation, and *Pst* DC3000 = *Pseudomonas syringae* pv. *tomato* DC3000.

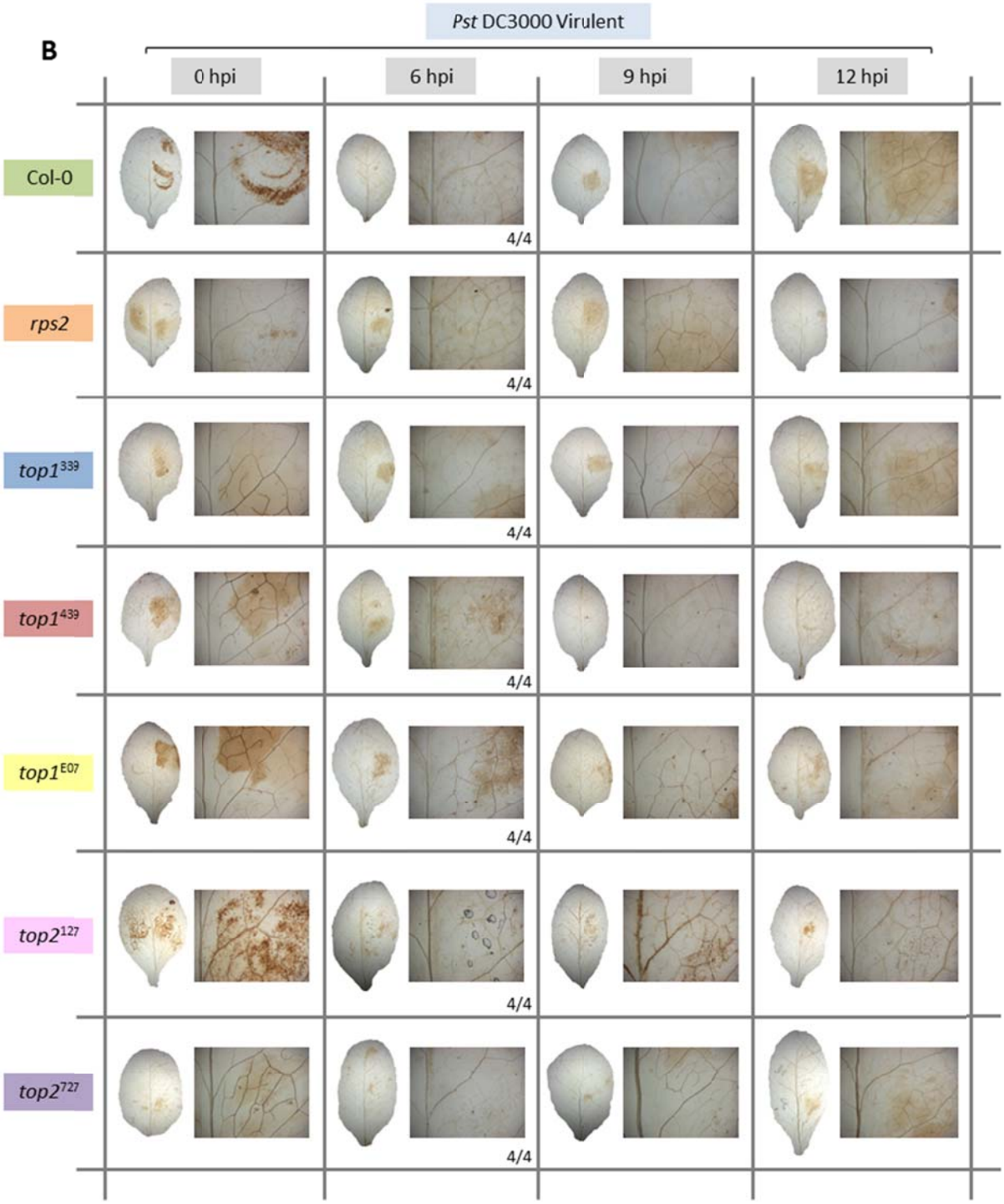

Figure 10 (*continued*): TOP1 and TOP2 may antagonistically regulate H_2O_2 accumulation during the oxidative burst. (B) *Pst* DC3000 virulent. Figure set is continued on the next 2 pages. See **(A)** for figure description.

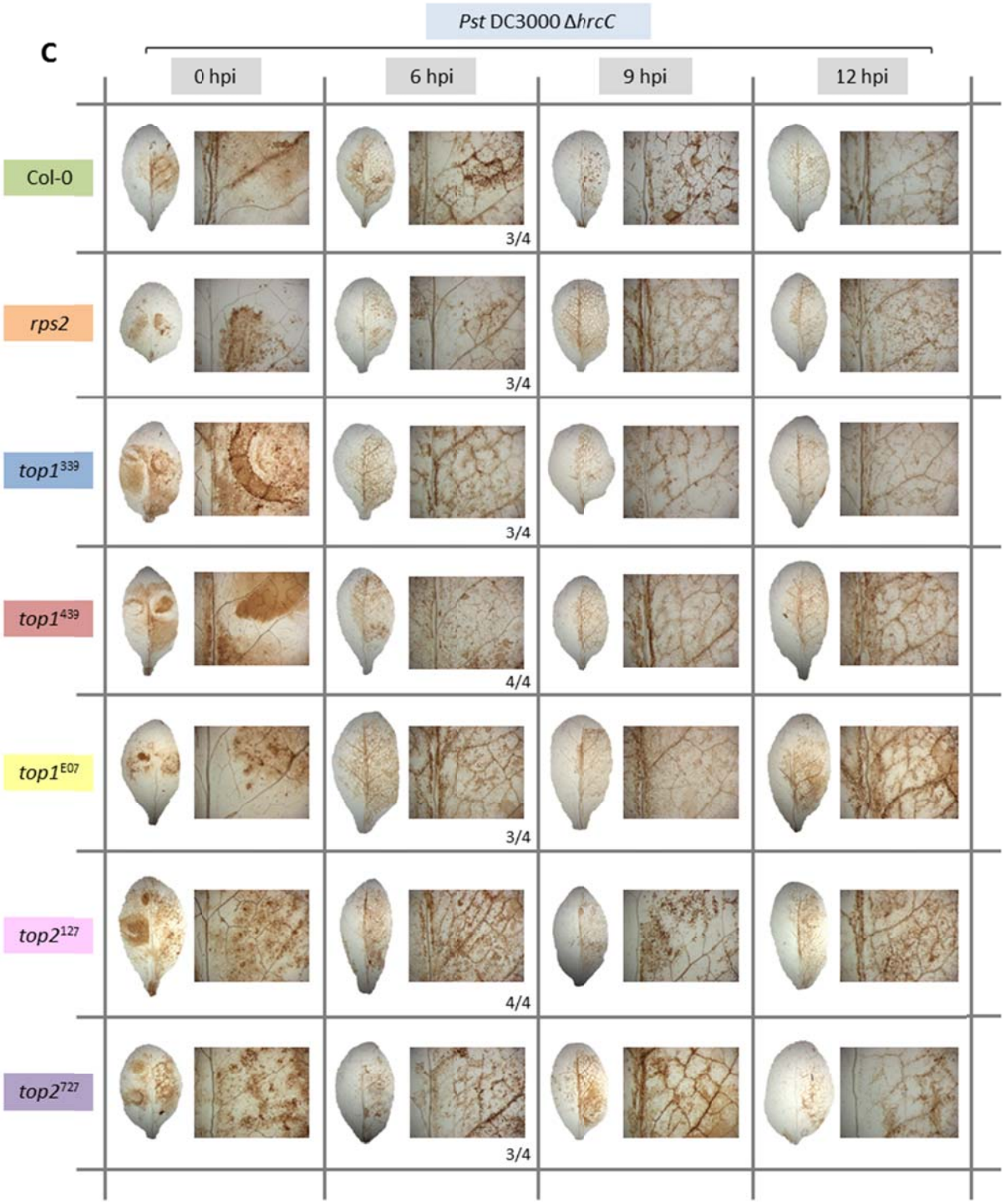

Figure 10 (*continued*): TOP1 and TOP2 may antagonistically regulate H_2O_2 accumulation during the oxidative burst. (C) *Pst* DC3000 Δ*hrcC*. Figure set is continued on the next page. See **(A)** for figure description.

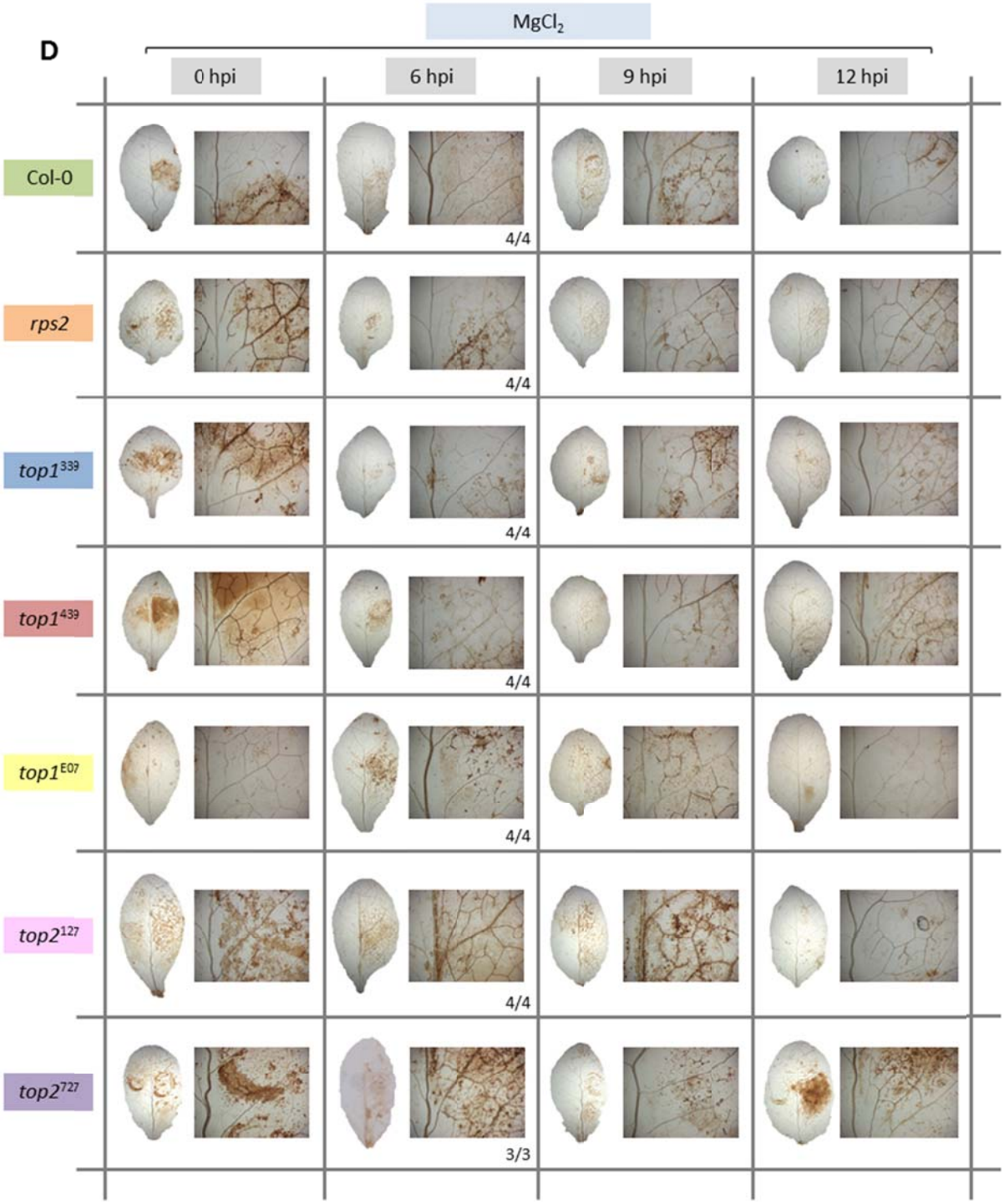

Figure 10 *(continued)*: TOP1 and TOP2 may antagonistically regulate H_2O_2 accumulation during the oxidative burst. (D) 10 mM $MgCl_2$. Figure set continued on the previous 3 pages. See **(A)** for figure description.

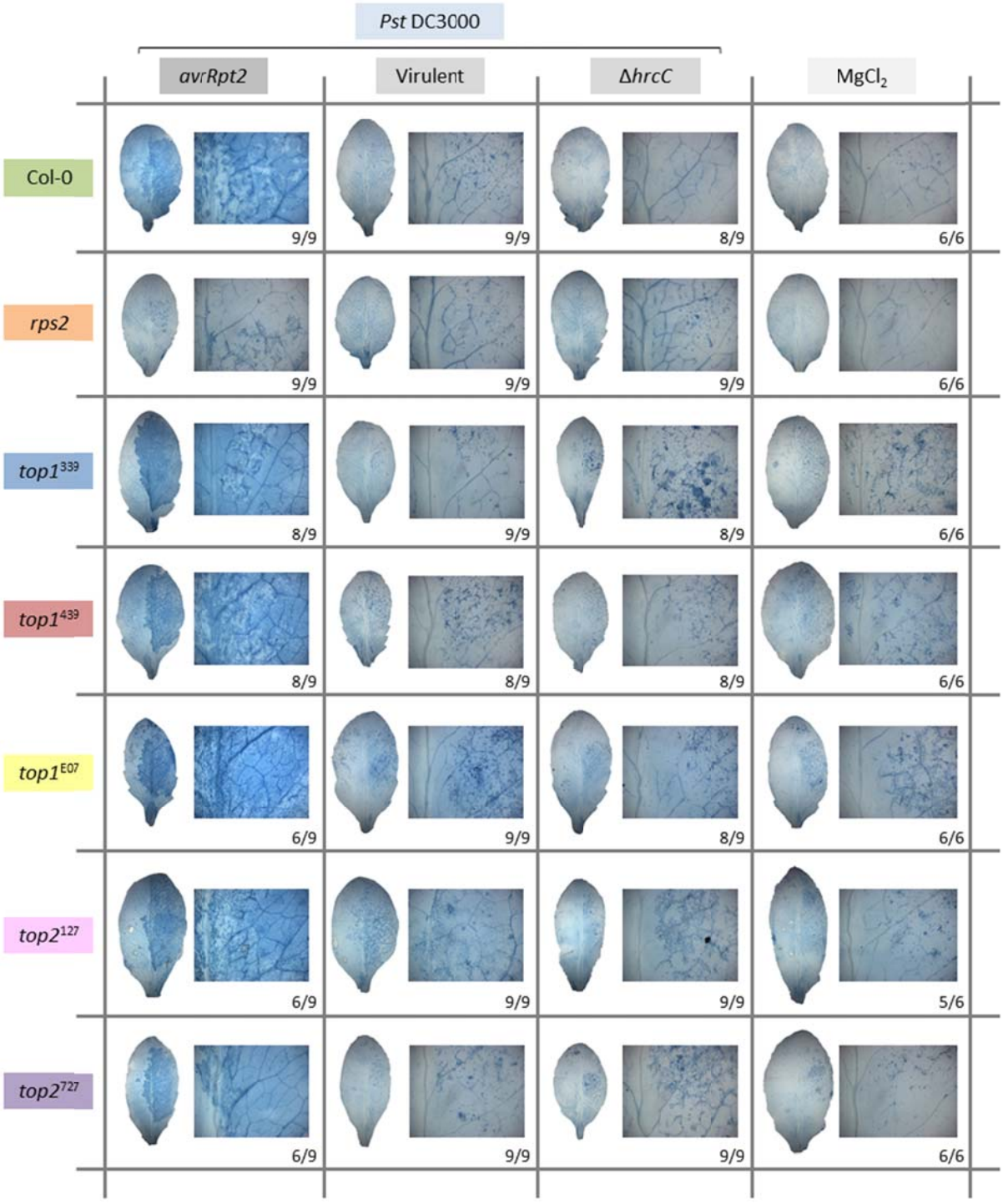

Figure 11: *top1* and *top2* single mutants have normal HR-PCD levels at 24 hpi. Plants of 3- to 4-weeks-old were syringe-infiltrated, 3 half-leaves per plant, with either 10 mM $MgCl_2$ or 1 x 10^6 CFU/mL *Pst* DC3000 *avrRpt2*, virulent, or Δ*hrcC*. Plants infiltrated with 10 mM $MgCl_2$

served as controls for symptom background caused by $MgCl_2$ and/or wounding caused by infiltration. Infiltrated leaves were collected 24 hpi and boiled in 0.33 mg/mL TB staining solution for 5-8 minutes. Experiment was conducted once with 9 replicates per experimental group per line and 6 replicates per $MgCl_2$ control group per line, and the scoring system depicts the number of leaves resembling the pictured leaf within each replicate set. Abbreviations: CFU = colony forming units, hpi = hours post-inoculation, HR = hypersensitive response, PCD = programmed cell death, *Pst* DC3000 = *Pseudomonas syringae* pv. *tomato* DC3000, and TB = Trypan Blue.

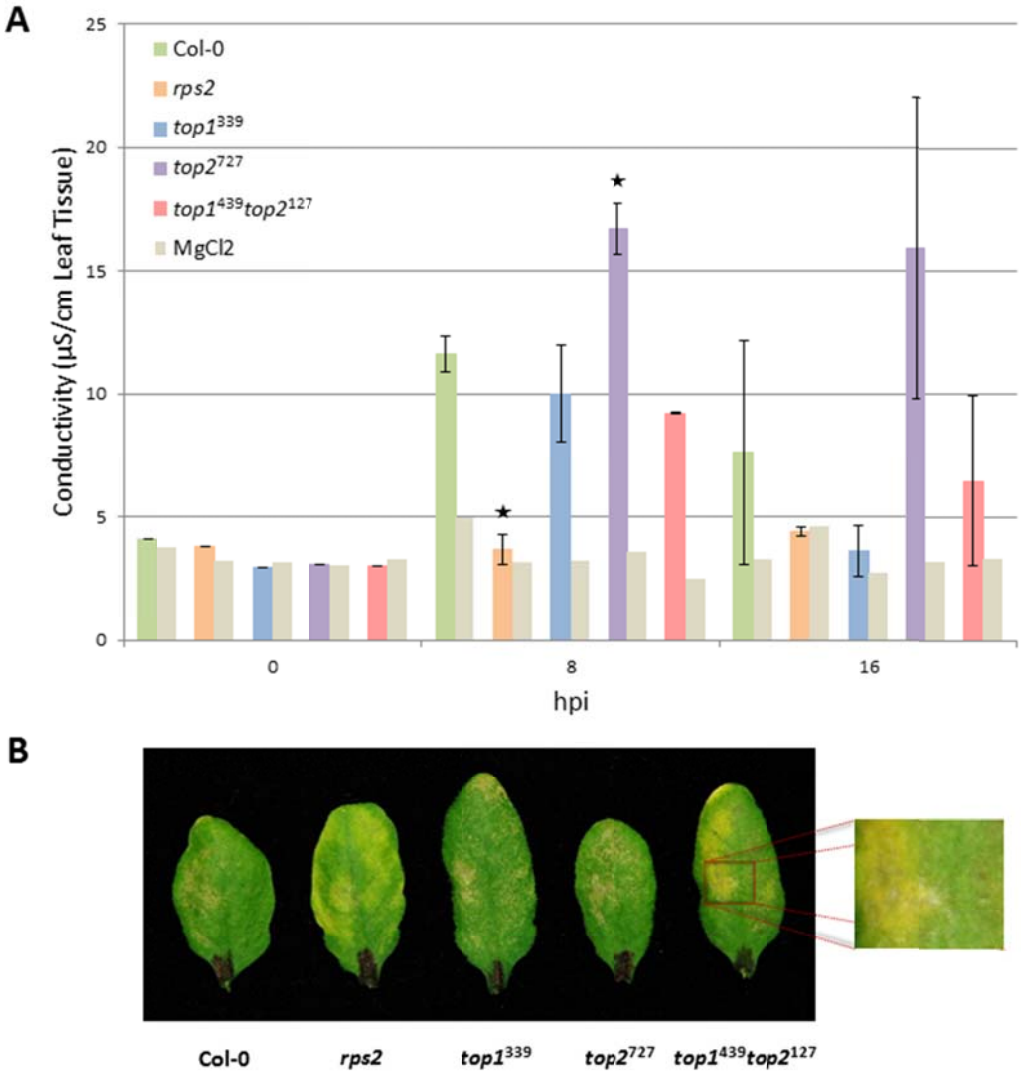

Figure 12: TOP1 and TOP2 may antagonistically regulate HR-PCD. Plants of 3- to 4-weeks-old were syringe-infiltrated, 5 leaves per plant, to saturation with 1 x 10^6 CFU/mL *Pst* DC3000 *avrRpt2* to elicit the HR. **(A)** Conductivity was used as a quantitative measure of PCD. For each replicate, 5 leaf discs—1 per each of the 5 inoculated leaves—were collected from non-infiltrated leaf halves at 0, 8, and 16 hpi and floated abaxial side up on 4 mL MQH_2O. Leaf discs were shaken at 100 rpm at room temperature for 2 hours before measuring conductivity of the bathing solutions. Plants infiltrated with 10 mM $MgCl_2$ served as controls for symptom background caused by $MgCl_2$ and/or wounding caused by infiltration. Stars represent significant differences in comparison to Col-0 (Student's *t*-test parameters: two-tailed distribution, two-sample unequal variance, ★ = $p < 0.01$). **(B)** *top1*^{339} and *top2*^{727} single mutants more closely

resemble the Col-0 positive control, whereas the *top1*^{439}*top2*^{127} double mutant more closely resembles the *rps2* negative control. Picture was taken 2-3 dpi. Abbreviations: CFU = colony forming units, hpi = hours post-inoculation, HR = hypersensitive response, PCD = programmed cell death, rpm = revolutions per minute, and µS = µSiemens.

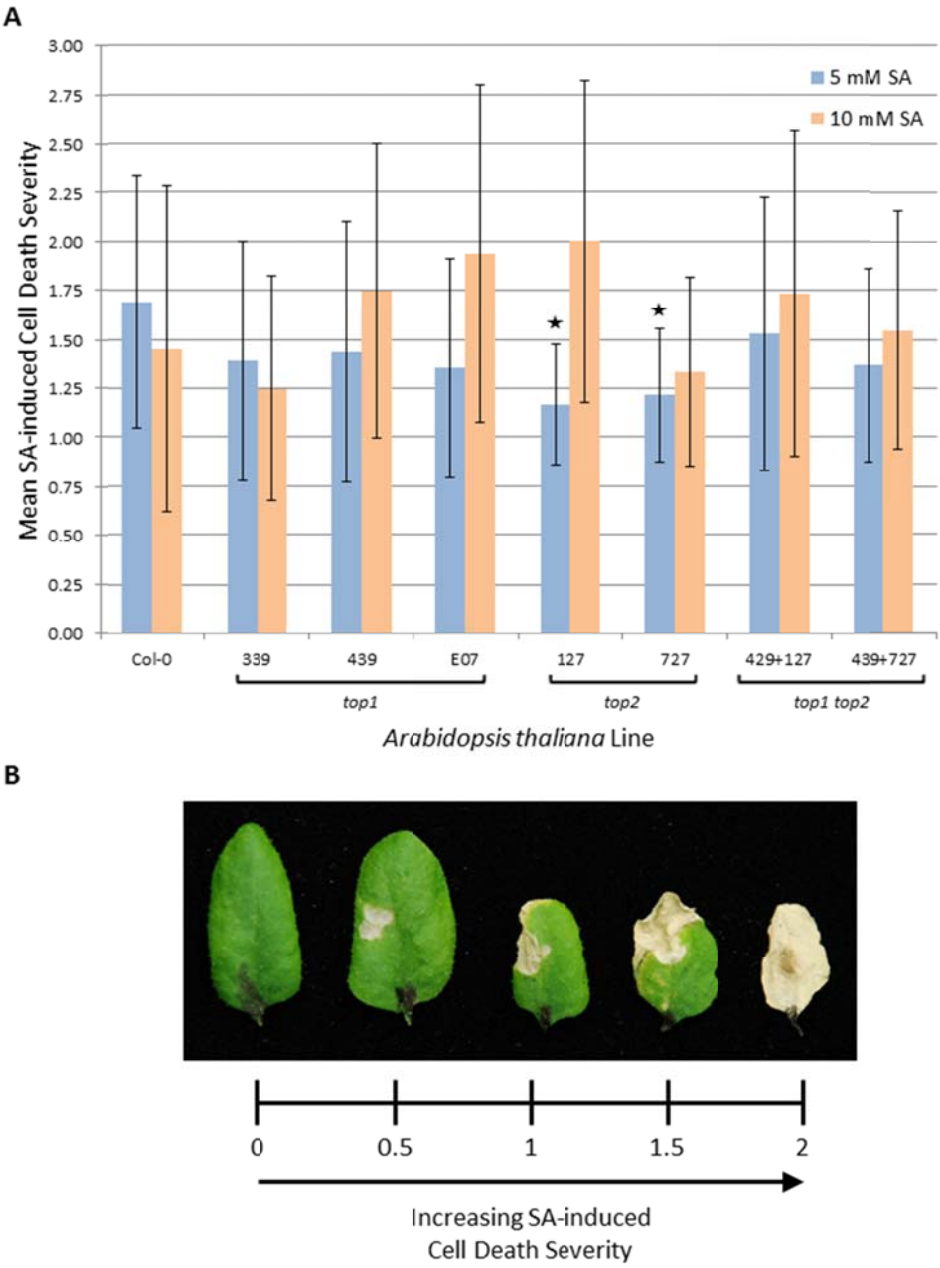

Figure 13: *top2* single mutants have decreased sensitivity to SA-induced cell death.

(A) Leaves of 18-days-old plants were infiltrated with 5 mM SA, 10 mM SA, or EtOH controls

(not shown). Approximately 3 leaves per plant were spot-infiltrated, with 5-8 plants used for both SA treatments and 4 plants used for both EtOH control treatments. Leaf phenotypes were scored 1 week post-infiltration. **(B)** Leaves were scored on a cell death severity scale of 0 (no symptoms) to 2 (total leaf collapse). EtOH controls were identical between all lines, showing very little or no cell death symptoms. Stars represent significant differences in comparison to Col-0 wild-type (Student's *t*-test parameters: two-tailed distribution, two-sample unequal variance, ★ = $p < 0.01$). EtOH = ethanol, HR = hypersensitive response, and SA = salicylic acid.

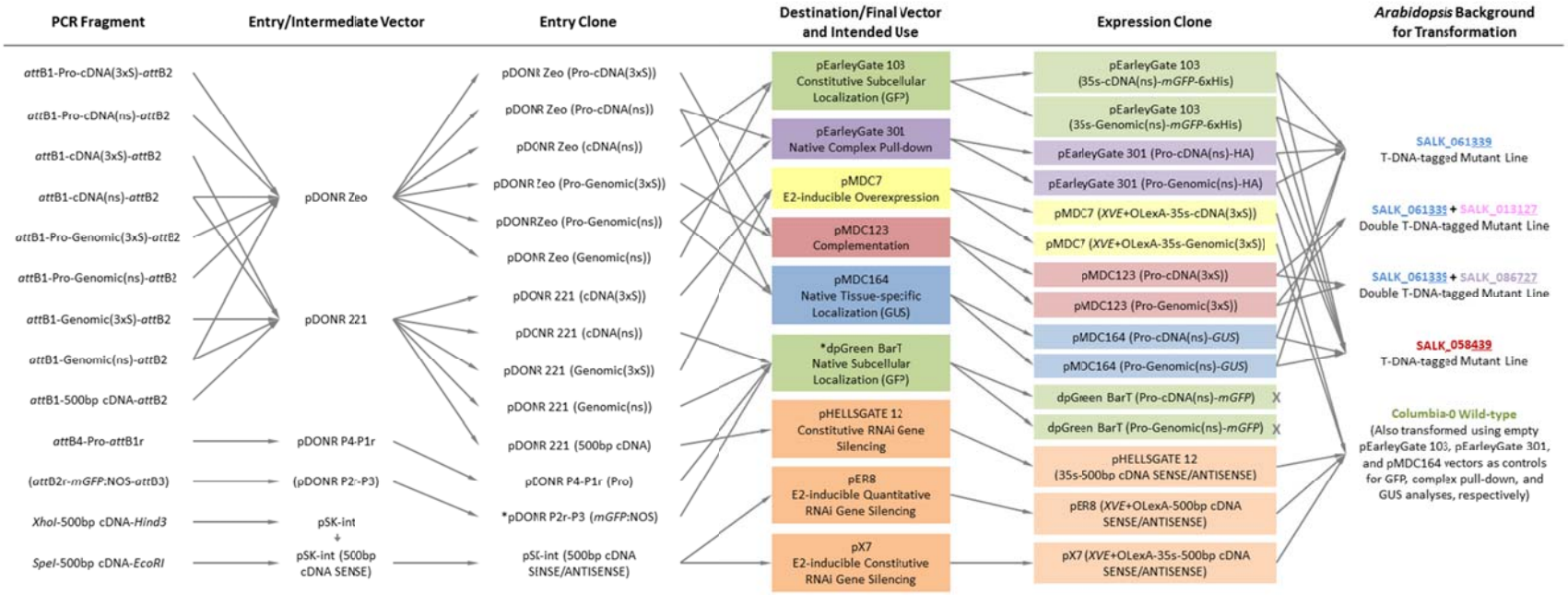

Figure 14: *TOP1* expression clones and transgenic *Arabidopsis* lines. Genomic = *TOP1* genomic DNA, cDNA = *TOP1* cDNA, Pro = 2 kbp *TOP1* predicted promoter, 500bp cDNA = *TOP1* sequence sharing 88% homology with *TOP2*, 3xS = 3 stop codons, ns = no stop codon, NOS = nopaline synthase terminator, *mGFP* = free green fluorescent protein marker, *GUS* = beta-glucuronidase reporter gene, HA = hemagglutinin tag, 6xHis = hexahistidine tag, 35s = CaMV constitutive promoter, and *XVE*+OLexA = E2-inducible expression system. *Generously provided by the Lee lab.

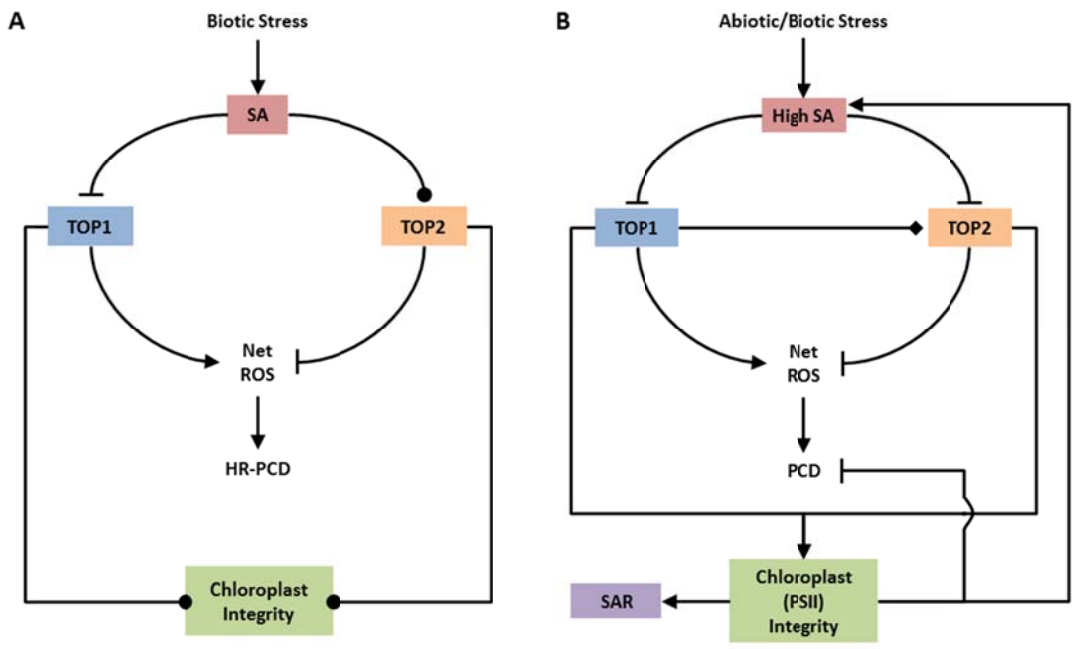

Figure 15: Models of TOP1 and TOP2 *in vivo* functions. Refer to main text for details regarding the working model **(A)** and speculative model **(B)**. Preliminary experiments revealed that SA inhibits TOP1 proteolytic activity (data not shown). TOP1 and TOP2 may enforce chloroplast integrity by regulating net ROS production and PCD, or may do so through other presently unknown mechanisms. Symbols: arrowheads = promotes, perpendicular lines = inhibits, circles = unknown whether upstream component promotes or inhibits, and diamond = epistatic to targeted connection. Abbreviations: HR = hypersensitive response, PCD = programmed cell death, PSII = Photosystem II, ROS = reactive oxygen species, SA = salicylic acid, and SAR = systemic acquired resistance.

Tables

Table 1: TOP1 and TOP2 may be paralogous within *Arabidopsis*. According to the Plant Proteome Database (PPDB) and Basic Local Alignment Search Tool (BLAST), TOP1 and TOP2 are also highly homologous with metalloendopeptidases found in *Oryza sativa*, *Zea mays*, and several algae and cyanobacteria species. Abbreviations: bp = base pair and aa = amino acid.

	TOP1	TOP2	Homology (%)*
Genomic DNA (bp)	3972	6907	45
cDNA (bp)	2514	2852	85
Coding Sequence (bp)	2376	2106	88
Protein (aa)	791	701	**82.3**

* % Homology was determined by sequence alignment between cDNAs or protein primary sequences using the DNASTAR Lasergene® SeqMan™ or MegAlign™ (Clustal W alignment) programs, respectively.

Table 2: TOP1 and TOP2 predicted subcellular localizations. Results were obtained using the TargetP subcellular localization neural network predictor (see Emanuelsson et al. (2007)). According to the SUB-cellular location database for *Arabidopsis* proteins (SUBA), other predictors designate TOP1 to the mitochondrion, nucleus, and peroxisome, and TOP2 to the cytosol and peroxisome.

	TOP1	TOP2
Protein Length (aa)	791	701
Chloroplast (CP) Transit Peptide	0.905	0.167
Mitochondrial (MT) Targeting Peptide	0.351	0.096
Signal Peptide (Endoplasmic Reticulum (ER))	0.000	0.075
Other	0.008	0.793
Predicted Subcellular Localization	CP	Any other location besides CP, MT, and ER
*Reliability Class	3	2

* Ranges from the strongest (1) to weakest (5) prediction; based on the size difference between the first and second highest prediction scores.

Figure and Table Legends

Figure 1: Screening for pSABPs using the functional protein microarray FPM-5000. **(A)** Detection of protein-4-AzSA interaction using the anti-SA antibody. **(I)** Molecular structure of 4-AzSA. **(II)** Method used to probe for pSABPs. (1) Printing: *Arabidopsis* proteins were adhered to the chip surface. (2) Probing: 4-AzSA fit into the binding pockets of compatible proteins. (3) UV light triggered cross-linking between the 4-AzSA azide group (N_3) and the bound protein; chips were washed to remove unbound and weakly bound 4-AzSA. (4) and (5) Hybridization: the anti-SA antibody recognized 4-AzSA, and the Cy5 secondary antibody recognized IgG. (6) Scanning: chip was scanned at 633 nm. Schematic created by Dr. Moreau. **(B)** Detection of 4-AzSA cross-linked to proteins on the FPM-5000. Microarrays were incubated with or without 1 mM 4-AzSA for 1 hour, cross-linked under 500 mJ UV light, and probed with the anti-SA antibody. Proteins printed on the microarray surface are clearly visible as distinct dots within the amplified box; proteins that bound 4-AzSA are colored yellow to white, whereas those that did not are colored green to violet (see color scale). Photos taken by Dr. Moreau. Abbreviations: 4-AzSA = 4-Azidosalicylic acid, pSABP = putative salicylic acid-binding protein, and IgG = immunoglobulin G.

Figure 2: Recombinant TOP1 binds 4-AzSA and SA with specificity. (A) Recombinant TOP1 purification from *Nicotiana benthamiana* and *Escherichia coli*. **(I)** Western blot following the purification of TOP1 from *Agrobacterium*-infiltrated *N. benthamiana* leaves. Lane 4 shows purified recombinant TOP1 (MW ≈ 89 + 25 kDa). Lanes 1-3 show the intermediate purification steps: 1 = crude extract, 2 = supernatant after TOP1 pull-down using IgG beads, and 4 = IgG beads after cleavage. **(II)** SDS PAGE gel following metal affinity chromatography purification of recombinant TOP1 (arrow; MW ≈ 89 kDa) from transgenic *E. coli* BL21 cells. Purification steps: FT = flow-through, W = wash, and E = eluted protein. Protein purifications were performed by Dr. Moreau and Giulio Zampogna. **(B)** SA can compete with 4-AzSA for binding recombinant TOP1. Recombinant TOP1 (MW = 89 + 25 kDa) purified from *N. benthamiana* was incubated with 500 µM 4-AzSA and cross-linked under 50 mJ UV light (3). After separation using SDS PAGE, the anti-SA antibody was used to probe for 4-AzSA. Control incubations lacking 4-AzSA (2) or without UV exposure (1) were also performed. Cross-linking in the

presence of 20 fold excess SA (4) revealed the specificity of the 4-AzSA-TOP1 interaction. Relative protein concentrations are represented in the Coomassie Brilliant Blue-stained membrane. Experiment conducted by Dr. Moreau. **(C)** TOP1-SA binding may be too weak to accurately calculate specificity using [^{3}H]SA exclusion chromatography. Incubations consisting of 20 μg protein in the presence of 600 nM [^{3}H]SA (total binding) were conducted on ice for 1 hour. Incubations in the presence of 8,000 fold excess SA (+ 5 mM SA) were performed to quantify nonspecific binding. Radioactivity was counted after gel filtration. Tobacco Salicylic Acid-binding Protein 2 (SABP2) serves as a positive control, whereas the SABP2 A13L deletion mutant and non-SABP glutathione peroxidase-like protein-1 (GPX1) serve as negative controls. The difference in dpm for TOP1 between the 600 nM [^{3}H]SA and 600 nM [^{3}H]SA + 5 mM SA treatments is not significantly different than that of the negative controls (Student's *t*-test parameters: two-tailed distribution, two-sample unequal variance, ★ = $p < 0.01$). Experiment was conducted by Dr. Moreau, with statistical analysis by Giulio Zampogna. Note: this experiment was repeated by Dr. Moreau and yielded significant results that confirm TOP1-SA binding specificity (data not shown).

Figure 3: *TOP1* and *TOP2* gene structures and characteristics. Triangles depict T-DNA insertion locations. Arrows indicate transcriptional direction. Blue = exons. Gray = introns. Purple = overlapping genes. Diagram is approximately to scale. Figure information was adapted from The *Arabidopsis* Information Resource (TAIR), *MEROPS* the Peptidase Database, the *Arabidopsis* Gene Regulatory Information Server (AGRIS), and Beers et al. (2000). Abbreviations: UTR = untranslated region, bp = base pair, and kbp = kilobase pair.

Figure 4: Predicted TOP1 and TOP2 protein structures. Diagram is to scale. Figure information was adapted from The *Arabidopsis* Information Resource (TAIR), *MEROPS* the Peptidase Database, and PROSITE Motif Scan. Motif logos and consensus sequence patterns were copied directly from PROSITE Motif Scan (http://myhits.isb-sib.ch/cgi-bin/motif_scan). Abbreviations: aa = amino acid, kDa = kilodalton, C = C-terminus, and N = N-terminus.

Figure 5: *top1*, *top2*, and *top1 top2* T-DNA-tagged mutant line zygosities. See Figure 2 and Table S2 for T-DNA insert locations and expected PCR product sizes. DNA was extracted from

rosette leaves of 2-weeks-old plants. PCR reactions to confirm T-DNA insertions in *top2*^{127}, *top1*^{339}*top2*^{127}, and *top1*^{439}*top2*^{127} revealed a second smaller, fainter DNA band below the expected-sized brighter band; this is most likely a cross-reaction of the T-DNA BP and 127 RP primer pair elsewhere in the genome rather than amplification of a second T-DNA insertion. DNA marker is shown in base pairs. Abbreviations: LP and RP = left and right genomic DNA primers, BP = T-DNA border primer, WT = wild-type, and HM = homozygous for the T-DNA insertion(s).

Figure 6: *TOP1* and *TOP2* cDNA alignment and semi-quantitative RT-PCR primer pair locations. Small arrows represent primers, and numbers 1-6 designate primer pairs used for semi-quantitative RT-PCR: (1) = 5′ *TOP1*, (2) = *TOP1* between 339 and 439 insertions, (3) = 3′ *TOP1*, (4) = 5′ *TOP2*, (5) = *TOP2* between 127 and 727 insertions, and (6) = 3′ *TOP2*. Red arrows represent primers that are unique to either *TOP1* or *TOP2*, whereas orange arrows represent primers that are identical between *TOP1* and *TOP2*. Diagram is approximately to scale. Figure information adapted from The *Arabidopsis* Information Resource (TAIR) and a *TOP1—TOP2* cDNA sequence alignment using the DNASTAR Lasergene® MegAlign™ (Clustal W alignment) program. Abbreviations: 5′ = 5′ untranslated region, 3′ = 3′ untranslated region, and bp = base pair.

Figure 7: Semi-quantitative RT-PCR of *top1*, *top2*, and *top1 top2* T-DNA-tagged mutant lines. RNA was extracted from rosette leaves of 2-weeks-old plants. Numbers 1-6 designate primer pairs used for semi-quantitative RT-PCR (see Figure 5). See Table S3 for expected PCR product sizes. Color outlines: red = no Col-0 wild-type control, blue = no *Actin-1* control, green = no Col-0 wild-type and *Actin-1* controls, and yellow = cDNA amplification products derived from the first row of RNA extracts. All PCR fragments without a yellow outline were derived from the second row of RNA extracts.

Figure 8: *top1* and *top2* single mutants do not display resistance phenotypes due to defects in MTI or ETI. Plants of 3- to 4-weeks-old were syringe-infiltrated, 3 leaves per plant, to saturation with either 10 mM $MgCl_2$ **(C)** or 1 x 10^5 CFU/mL *Pst* DC3000 virulent **(A)**, *Pst* DC3000 Δ*hrcC* **(B)**, *Pst* DC3000 *avrRpt2* **(D)**, or *Pst* DC3000 *avrRpm1* **(E)**. Pictures were taken

at 4 dpi. Chlorotic cell death disease symptoms signify susceptibility toward the infecting *Pst* strain. Col-0 wild-type = positive control and *rps2* and *rpm1* = negative controls. *Pst* DC3000 virulent = test for disease symptom defects or altered resistance. *Pst* DC3000 Δ*hrcC* strain = test for MTI defects. *Pst* DC3000 avirulent *avrRpt2* and *avrRpm1* = test for ETI defects. Plants infiltrated with 10 mM $MgCl_2$ served as controls for symptom background caused by $MgCl_2$ and/or wounding caused by infiltration. Abbreviations: CFU = colony forming units, dpi = days post-inoculation, ETI = effector-triggered immunity, MTI = microbe/pathogen-associated molecular pattern-triggered immunity, and *Pst* DC3000 = *Pseudomonas syringae* pv. *tomato* DC3000.

Figure 9: *Pst* DC3000 bacterial growth in *top1* and *top2* single mutant leaves is comparable to the wild-type. Plants were inoculated as described in Figure 8. Three leaf discs were collected from each of 8 plants per line at 0, 2, and 4 dpi and shaken at 300 rpm for 1 hour at room temperature in 10 mM $MgCl_2$ + 0.01% Silwet L-77 surfactant + appropriate antibiotic(s) to extract the bacteria. Dilutions were prepared and plated for colony growth analysis, thus giving 8 replicates per dilution per line for each dpi. Colony growth was observed and recorded for each line at the most discernible dilution ranges after 2 days incubation at 29°C. Mean CFU/cm^2 leaf tissue was calculated and plotted as above for **(A)** *Pst* DC3000 virulent, **(B)** *Pst* DC3000 Δ*hrcC*, **(C)** *Pst* DC3000 *avrRpt2*, and **(D)** *Pst* DC3000 *avrRpm1*. Experiments were repeated once (6-8 replicates) for (A), (B), and $top2^{127}$ and $top2^{727}$ in (C), and three times (20-24 replicates) for (C) and (D). Stars represent significant differences in comparison to Col-0 wild-type plants (Student's *t*-test parameters: two-tailed distribution, two-sample unequal variance, ★ = $p < 0.01$, ★★ = $p < 0.001$, and ★★★ = $p < 0.0001$). Abbreviations: CFU = colony forming units, dpi = days post-inoculation, rpm = revolutions per minute, and *Pst* DC3000 = *Pseudomonas syringae* pv. *tomato* DC3000.

Figure 10: TOP1 and TOP2 may antagonistically regulate H_2O_2 accumulation during the oxidative burst. Figure set is continued on the next 3 pages. Plants of 3- to 4-weeks-old were syringe-infiltrated, 4 half-leaves per plant, with either 10 mM $MgCl_2$ **(D)** or 5 x 10^7 CFU/mL *Pst* DC3000 *avrRpt2* **(A)**, virulent **(B)**, or Δ*hrcC* **(C)**. Leaves were stained with 1 mg/mL (pH 6.5-6.8) DAB at 0, 6, 9, and 12 hpi via infiltration of leaf halves opposite that of $MgCl_2$ or *Pst*

DC3000 infiltration. Experiment was conducted once with 4 replicates per experimental or control group per time point per line (see Figure S3 for all 6 hpi replicates), and the scoring system depicts the number of leaves resembling the pictured leaf within each replicate set. Abbreviations: CFU = colony forming units, DAB = 3,3'-Diaminobenzidine, hpi = hours post-inoculation, and *Pst* DC3000 = *Pseudomonas syringae* pv. *tomato* DC3000.

Figure 10 (*continued*): TOP1 and TOP2 may antagonistically regulate H_2O_2 accumulation during the oxidative burst. (B) *Pst* DC3000 virulent. Figure set is continued on the next 2 pages. See **(A)** for figure description.

Figure 10 (*continued*): TOP1 and TOP2 may antagonistically regulate H_2O_2 accumulation during the oxidative burst. (C) *Pst* DC3000 Δ*hrcC*. Figure set is continued on the next page. See **(A)** for figure description.

Figure 10 *(continued):* TOP1 and TOP2 may antagonistically regulate H_2O_2 accumulation during the oxidative burst. (D) 10 mM $MgCl_2$**.** Figure set continued on the previous 3 pages. See **(A)** for figure description.

Figure 11: *top1* and *top2* single mutants have normal HR-PCD levels at 24 hpi. Plants of 3- to 4-weeks-old were syringe-infiltrated, 3 half-leaves per plant, with either 10 mM $MgCl_2$ or 1 x 10^6 CFU/mL *Pst* DC3000 *avrRpt2*, virulent, or Δ*hrcC*. Plants infiltrated with 10 mM $MgCl_2$ served as controls for symptom background caused by $MgCl_2$ and/or wounding caused by infiltration. Infiltrated leaves were collected 24 hpi and boiled in 0.33 mg/mL TB staining solution for 5-8 minutes. Experiment was conducted once with 9 replicates per experimental group per line and 6 replicates per $MgCl_2$ control group per line, and the scoring system depicts the number of leaves resembling the pictured leaf within each replicate set. Abbreviations: CFU = colony forming units, hpi = hours post-inoculation, HR = hypersensitive response, PCD = programmed cell death, *Pst* DC3000 = *Pseudomonas syringae* pv. *tomato* DC3000, and TB = Trypan Blue.

Figure 12: TOP1 and TOP2 may antagonistically regulate HR-PCD. Plants of 3- to 4-weeks-old were syringe-infiltrated, 5 leaves per plant, to saturation with 1 x 10^6 CFU/mL *Pst* DC3000 *avrRpt2* to elicit the HR. **(A)** Conductivity was used as a quantitative measure of PCD. For each replicate, 5 leaf discs—1 per each of the 5 inoculated leaves—were collected from non-infiltrated leaf halves at 0, 8, and 16 hpi and floated abaxial side up on 4 mL MQH_2O. Leaf discs were shaken at 100 rpm at room temperature for 2 hours before measuring conductivity of the bathing solutions. Plants infiltrated with 10 mM $MgCl_2$ served as controls for symptom background caused by $MgCl_2$ and/or wounding caused by infiltration. Stars represent significant differences in comparison to Col-0 (Student's *t*-test parameters: two-tailed distribution, two-sample unequal variance, ★ = $p < 0.01$). **(B)** *top1*^{339} and *top2*^{727} single mutants phenotypically resemble the Col-0 positive control, whereas the *top1*^{439}*top2*^{127} double mutant phenotypically resembles the *rps2* negative control. Picture was taken 2-3 dpi. Abbreviations: CFU = colony forming units, hpi = hours post-inoculation, HR = hypersensitive response, PCD = programmed cell death, rpm = revolutions per minute, and µS = µSiemens.

Figure 13: *top2* single mutants have decreased sensitivity to SA-induced cell death. **(A)** Leaves of 18-days-old plants were infiltrated with 5 mM SA, 10 mM SA, or EtOH controls (not shown). Approximately 3 leaves per plant were spot-infiltrated, with 5-8 plants used for both SA treatments and 4 plants used for both EtOH control treatments. Leaf phenotypes were scored 1 week post-infiltration. **(B)** Leaves were scored on a cell death severity scale of 0 (no symptoms) to 2 (total leaf collapse). EtOH controls were identical between all lines, showing very little or no cell death symptoms. Stars represent significant differences in comparison to Col-0 wild-type (Student's *t*-test parameters: two-tailed distribution, two-sample unequal variance, ★ = $p < 0.01$). EtOH = ethanol, HR = hypersensitive response, and SA = salicylic acid.

Figure 14: *TOP1* expression clones and transgenic *Arabidopsis* lines. Genomic = *TOP1* genomic DNA, cDNA = *TOP1* cDNA, Pro = 2 kbp *TOP1* predicted promoter, 500bp cDNA = *TOP1* sequence sharing 88% homology with *TOP2*, 3xS = 3 stop codons, ns = no stop codon, NOS = nopaline synthase terminator, *mGFP* = free green fluorescent protein marker, *GUS* = beta-glucuronidase reporter gene, HA = hemagglutinin tag, 6xHis = hexahistidine tag, 35s =

CaMV constitutive promoter, and *XVE*+OLexA = E2-inducible expression system. *Generously provided by the Lee lab.

Figure 15: Models of TOP1 and TOP2 *in vivo* functions. Refer to main text for details regarding the working model **(A)** and speculative model **(B)**. Preliminary experiments revealed that SA inhibits TOP1 proteolytic activity (data not shown). TOP1 and TOP2 may enforce chloroplast integrity by regulating net ROS production and PCD, or may do so through other presently unknown mechanisms. Symbols: arrowheads = promotes, perpendicular lines = inhibits, circles = unknown whether upstream component promotes or inhibits, and diamond = epistatic to targeted connection. Abbreviations: HR = hypersensitive response, PCD = programmed cell death, PSII = Photosystem II, ROS = reactive oxygen species, SA = salicylic acid, and SAR = systemic acquired resistance.

Table 1: TOP1 and TOP2 may be paralogous within *Arabidopsis*. According to the Plant Proteome Database (PPDB) and Basic Local Alignment Search Tool (BLAST), TOP1 and TOP2 are also highly homologous with metalloendopeptidases found in *Oryza sativa*, *Zea mays*, and several algae and cyanobacteria species. Abbreviations: bp = base pair and aa = amino acid.

Table 2: TOP1 and TOP2 predicted subcellular localizations. Results were obtained using the TargetP subcellular localization neural network predictor (see Emanuelsson et al. (2007)). According to the SUB-cellular location database for *Arabidopsis* proteins (SUBA), other predictors designate TOP1 to the mitochondrion, nucleus, and peroxisome, and TOP2 to the cytosol and peroxisome.

Supplementary Figures

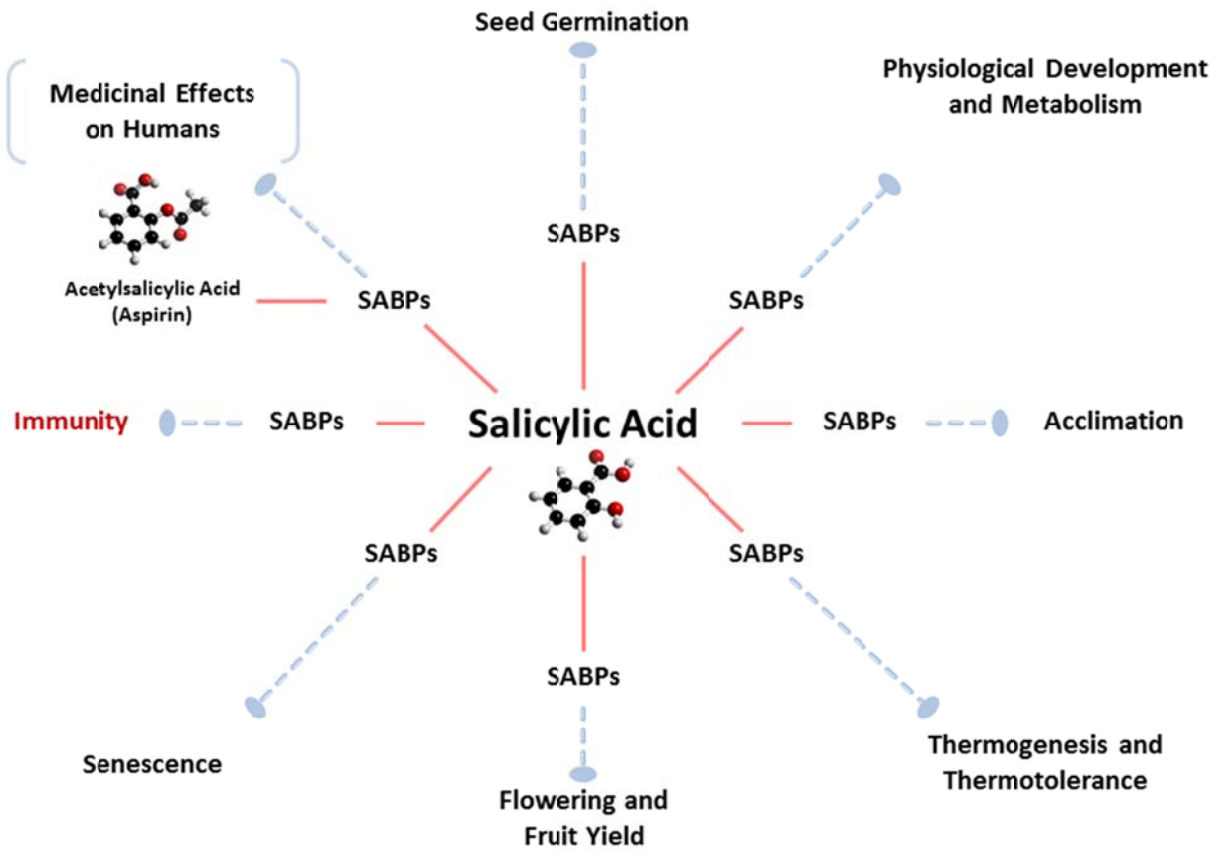

Figure S1: Salicylic acid functions and hypothetical signaling pathways. SA and Aspirin molecular structures were copied from 3Dchem.com (http://www.3dchem.com). Abbreviations: SABPs = salicylic acid-binding proteins.

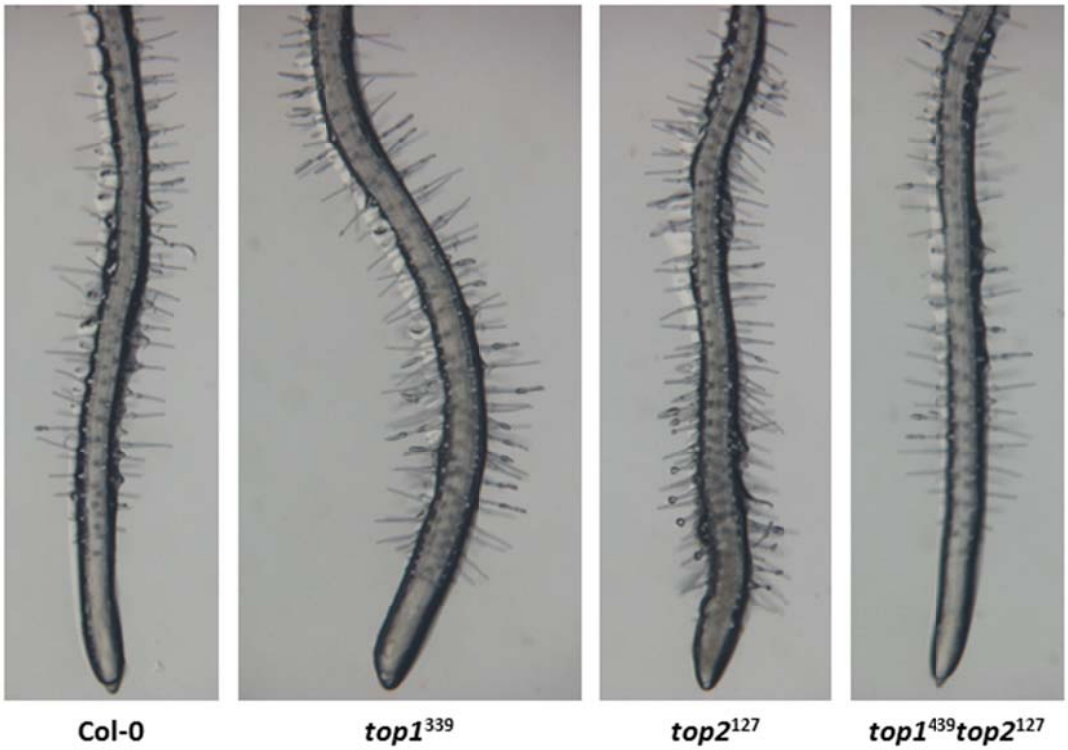

Figure S2: Root phenotypes of *top1*, *top2*, and *top1 top2* mutants. Roots of 20-days-old seedlings grown on nutrient media were visualized at 60X magnification. On average, *top1*^{339} may have had shorter root length (not shown) compared to the Col-0 wild-type, *top2*^{127}, and *top1*^{439}*top2*^{127}.

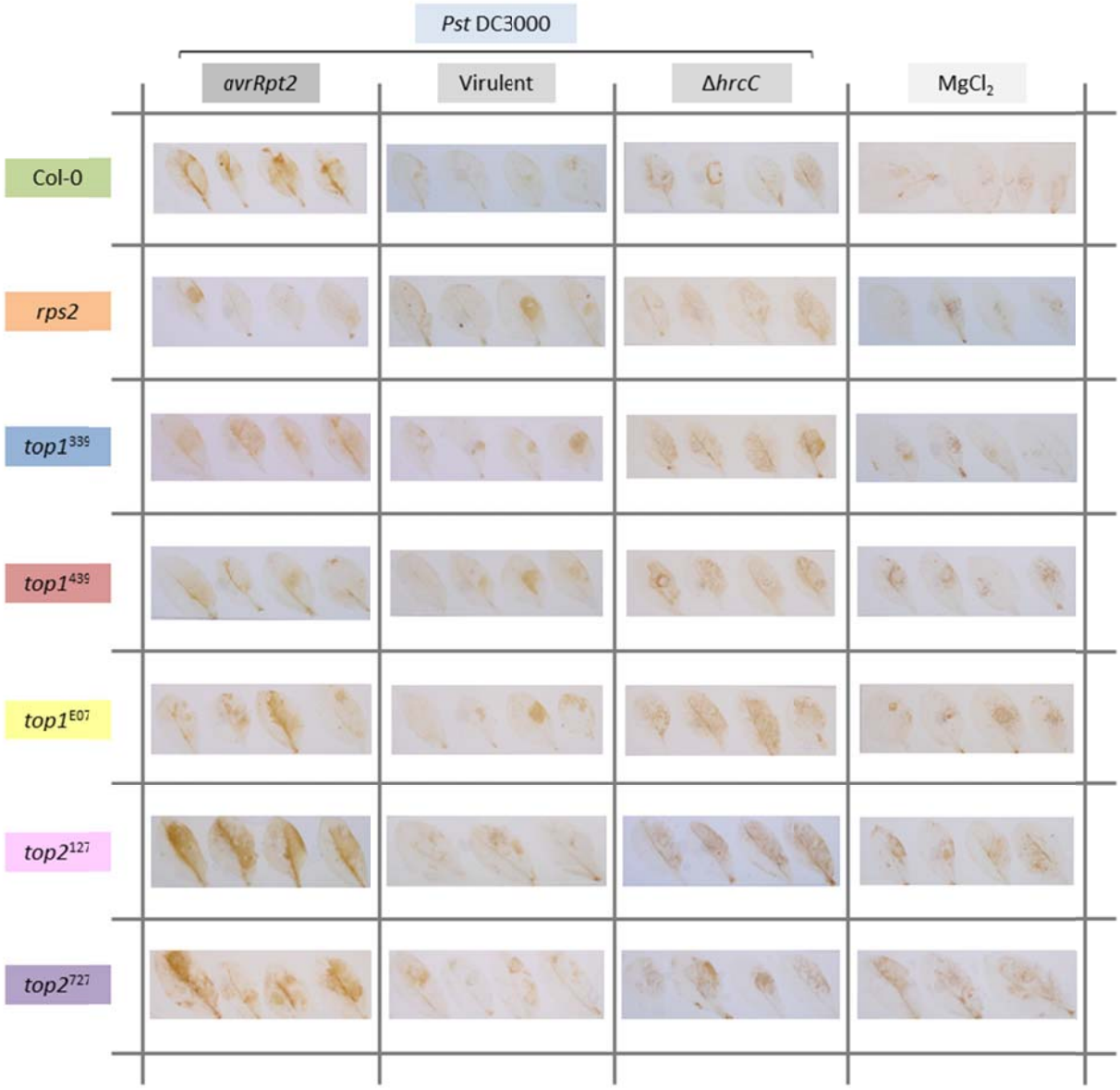

Figure S3: DAB staining replicate sets at 6 hours post-infiltration. See Figure 10 for a description of the experiment. Entire replicate sets at 0, 9, and 12 hpi were not documented, but the most representative leaves were photographed for display in Figure 10.

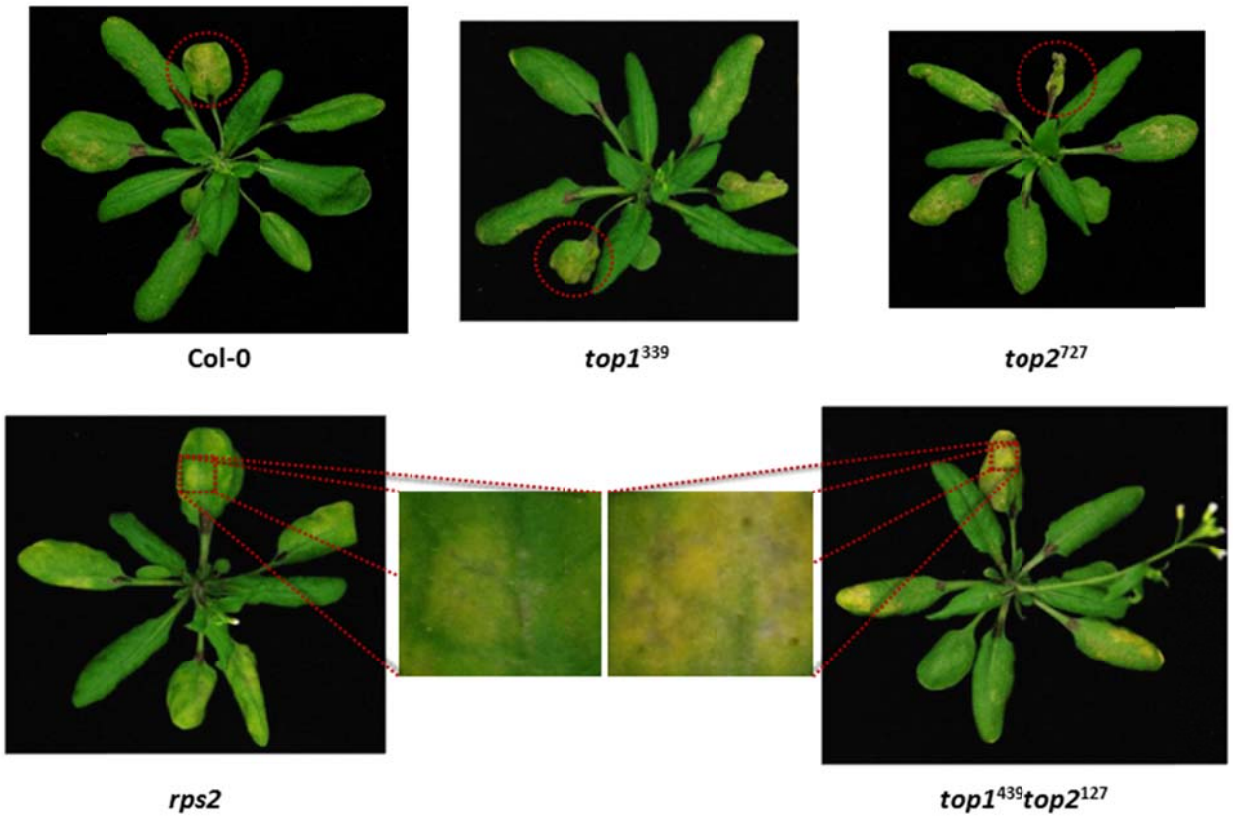

Figure S4: HR phenotypes of *top1*, *top2*, and *top1 top2* mutants. Plants of 3- to 4-weeks-old were photographed 2-3 dpi of whole leaves with 1 x 10^6 CFU/mL *Pst* DC3000 *avrRpt2*. Small leaves (circled) displayed severe disease symptoms or collapse, but are not representative of fully grown adult leaves; therefore, they should be discounted when interpreting the overall phenotypes. Abbreviations: CFU = colony forming units, dpi = days post-inoculation, and HR = hypersensitive response.

Supplementary Tables

Table S1: *TOP1* and *TOP2* T-DNA-tagged mutant lines. Table information was adapted from The *Arabidopsis* Information Resource (TAIR) and T-DNA Express: *Arabidopsis* Gene Mapping Tool. Abbreviations: bp = base pair, LP and RP = left and right genomic DNA primers, and BP = T-DNA border primer.

	T-DNA-tagged Mutant Line	LP+RP PCR Product Size (bp)	BP+RP PCR Product Size (bp)	Insert Size (bp)	Genomic DNA Insert Location (bp)
TOP1	SALK_061339.56.00.x	1000	488-788	365	Exon 6 1256
	SALK_058439.18.65.n	990	444-744	269	Exon 15 3467
	SAIL_879_E07	1218	534-834	948	5'UTR -11
	SAIL_227_G04	969	442-742	915	Exon 10 2368
TOP2	SALK_013127.55.50.x	1041	488-788	174	Intron 2 654
	SALK_086727.55.20.x	1151	501-801	387	Exon 5 1233
	SALK_138509.47.60.x	1106	555-872	440	Promoter -130
	SALK_127554.25.15.x	1106	555-872	458	Promoter -147

Table S2: Primers used for T-DNA insertion check, semi-quantitative RT-PCR, cloning, colony PCR check, and sequencing.
Abbreviations: FWD = forward primer, RV = reverse primer, LP = left border genomic primer, RP = right border genomic primer, BP = T-DNA border primer, Pro = 2 kbp *TOP1* predicted promoter, ORF = open reading frame, 500bp cDNA = *TOP1* sequence sharing 88% homology with *TOP2*, 3xS = 3 stop codons, ns = no stop codon, *att* = Gateway® recombination sites, and nt = nucleotide.

#	Gene, T-DNA, or Vector	Purpose	Nucleotide Sequence (5' to 3')	Description
1	TOP1	Promoter cloning	GGG GAC AAC TTT GTA TAG AAA AGT TGT CCG TAG CGA TGG AGG AAG AGA GAC A	FWD attB4-Pro
2	TOP1	Promoter cloning	GGG GAC TGC TTT TTT GTA CAA ACT TGC GTT TGC TAT TAC AAG CGT TGC CAT TAT TCT	RV Pro-attB1r
3	TOP1	Promoter-Genomic/cDNA cloning	AGT CGC CAT TAA CAT GTT TGC TAT TAC AAG CGT TGC CAT TAT TCT	FWD Pro-5'ORF (promoter with 5'ORF overhang for overlapping PCR)
4	TOP1	Promoter-Genomic/cDNA cloning	CTT GTA ATA GCA AAC ATG TTA ATG GCG ACT CCA ACG TCT CG	RV 3'Pro-ORF (ORF with 3'promoter overhang for overlapping PCR)
5	TOP1	Genomic/cDNA cloning	GGG GAC AAG TTT GTA CAA AAA AGC AGG CTT CAT GTT AAT GGC GAC TCC AAC GTC TCG	FWD attB1-ORF
6	TOP1	Colony PCR check	AGC AGA AGC AGA GGC AGC CAA	RV ORF(ns); used for colony PCR check
7	TOP1	Genomic/cDNA cloning	GGG GAC CAC TTT GTA CAA GAA AGC TGG GTC AGC AGA AGC AGA GGC AGC CAA G	RV ORF(ns)-attB2
8	TOP1	Genomic/cDNA cloning	TTA TTA TTA AGC AGA AGC AGA GGC AGC CAA	RV ORF(3xs)
9	TOP1	Genomic/cDNA cloning	GGG GAC CAC TTT GTA CAA GAA AGC TGG GTC TTA TTA TTA AGC AGA AGC AGA GGC AGC CAA	RV ORF(3xs)-attB2
10	TOP1	Colony PCR check	CCA ACC AGA GGC TAT TGC AA	RV 194 nt from 5' Pro
11	TOP1	Clone sequencing	CAG AGC ATA GAT CAG TGA TCC GGA CTC TG	FWD 694 nt from 5' Pro
12	TOP1	Clone sequencing	GGC TGG TTA TGG TTA AGC GGT CCA A	FWD 1175nt from 5' Pro
13	TOP1	Clone sequencing	AAG GAG GGG TCG AAC CTC CG	FWD 1701nt from 5' Pro
14	TOP1	Colony PCR check	ACG ACG GAT TCC ACG GCG	RV 269 nt from 5' ORF
15	TOP1	Clone sequencing	GGC TGT CAA GGA CAC ACC TGA GC	FWD 589 nt from 5' ORF
16	TOP1	Clone sequencing	GGA GGC GGT TCT CAT TGG TAT TGC TC	FWD 686 nt from 5' ORF
17	TOP1	Clone sequencing	GAT CGA GGG ATT GCC TCC ATC TGC	FWD 1184nt from 5' ORF
18	TOP1	Colony PCR check; clone sequencing	GTG CAT CCT GGG ATG CGG CTG	FWD 1192nt (cDNA) and 1705 nt (Genomic DNA) from 5' ORF
19	TOP1	Clone sequencing	CCA GTA GGT GAC AAG CCA AGC C	FWD 1656nt from 5' ORF
20	TOP1	Clone sequencing	CAG GAC AGA GAT TCA GAA ACA CCA	FWD 2230nt (cDNA) and 3598 nt (Genomic DNA) from 5' ORF
21	TOP1	Clone sequencing	GGA ACA ATG ATG TTC GGT TCT ACC GCG	FWD 2295nt from 5' ORF
22	TOP1	Colony PCR check; clone sequencing	CTC CTC GCC GCA AGA ACA TTC C	FWD 2945nt from 5' ORF
23	TOP1	Semi-quantitative RT-PCR	TCC TAC ATC CAC CAC TTC CA	FWD; 5'TOP1 (1); TOP1|TOP2 cDNA alignment location = 184 to 203
24	TOP2	Semi-quantitative RT-PCR	CTC ATT CTC TTT CTC GTC AAT CTC A	FWD; 5'TOP2 (4); TOP1|TOP2 cDNA alignment location = 257 to 281
25	TOP1 and TOP2	Semi-quantitative RT-PCR	TGA TTC ATC ATT CCC CAA ACA ACA G	RV; 5'TOP1|TOP2 (1|4); TOP1|TOP2 cDNA alignment location = 518 to 494
26	TOP1	Semi-quantitative RT-PCR	GGA ACC CAA TCG CTT ACT TT	FWD; 34 TOP1 (2); TOP1|TOP2 cDNA alignment location = 1517 to 1537
27	TOP1	Semi-quantitative RT-PCR	ATA CTT CCT CTG GGA GTG TT	RV; 34 TOP1 (2); TOP1|TOP2 cDNA alignment location = 1905 to 1924
28	TOP2	Semi-quantitative RT-PCR	GGA CAG AGC AAA CCC ATT TAC A	FWD; 17 TOP2 (5); TOP1|TOP2 cDNA alignment location = 604 to 625
29	TOP2	Semi-quantitative RT-PCR	TGT TAA ATT CTT CCC TCT TAT CAT CTT C	RV; 17 TOP2 (5); TOP1|TOP2 cDNA alignment location = 763 to 736
30	TOP1 and TOP2	Semi-quantitative RT-PCR	CAG GAC AGA GAT TCA GAA ACA C	FWD; 3'TOP1|TOP2 (3|6); TOP1|TOP2 cDNA alignment location = 2252 to 2272
31	TOP1	Semi-quantitative RT-PCR	CAA TGC AAT GTA TTA GAT GTA AAT GGT TG	RV; 3'TOP1 (3) TOP1|TOP2 cDNA alignment location = 2513 to 2485
32	TOP2	Semi-quantitative RT-PCR	CTC TGT TCG TTT CGT TTA TGA ACC	RV; 3'TOP2 (6); TOP1|TOP2 cDNA alignment location = 2571 to 2548
33	SALK Line T-DNA	T-DNA insertion check	ATT TTG CCG ATT TCG GAA C	BP (FWD) LBb1.3 T-DNA border in SALK lines
34	SAIL Line T-DNA	T-DNA insertion check	GCC TTT TCA GAA ATG GAT AAA TAG CCT TGC TTC C	BP (FWD) LB1 T-DNA border in SAIL lines
35	TOP1 T-DNA	T-DNA insertion check	ACA TTG GTC TTA TGC AGC CAG	LP (FWD) SALK_061339
36	TOP1 T-DNA	T-DNA insertion check	CAG GAT GCA CTA CGA AGC TTC	RP (RV) SALK_061339
37	TOP1 T-DNA	T-DNA insertion check	GCT GAA CAG AGG GTG AGA GTG	LP (FWD) SALK_058439
38	TOP1 T-DNA	T-DNA insertion check	GTA CCA GGA GGA CCA GAG TCC	RP (RV) SALK_058439
39	TOP1 T-DNA	T-DNA insertion check	AAG CGG TCC AAT CAT AAT TCT C	LP (FWD) SAIL_879_E07
40	TOP1 T-DNA	T-DNA insertion check	TGT GAA CAT ACG AGA TGC TGC	RP (RV) SAIL_879_E07
41	TOP1 T-DNA	T-DNA insertion check	AAT GGT CAG ATC AAA ACG CAC	LP (FWD) SAIL_227_G04
42	TOP1 T-DNA	T-DNA insertion check	CAA AGA TTC TTC TGG GAA CCC	RP (RV) SAIL_227_G04
43	TOP2 T-DNA	T-DNA insertion check	GCT TCC CTC AGA TTC ACT TCC	LP (FWD) SALK_013127
44	TOP2 T-DNA	T-DNA insertion check	GAG CAA TAC CAC TCA GAA CCG	RP (RV) SALK_013127
45	TOP2 T-DNA	T-DNA insertion check	GCT GCC ATT GAA GAA GTT CAG	LP (FWD) SALK_086727
46	TOP2 T-DNA	T-DNA insertion check	AAG CTT AGC CTT TTC CAG TCG	RP (RV) SALK_086727
47	TOP2 T-DNA	T-DNA insertion check	AAT GGG TGA ACA AGC AGA GTC	LP (FWD) SALK_138509 and SALK_127554
48	TOP2 T-DNA	T-DNA insertion check	AAA TCG TTT CAC ACA AAT GGC	RP (RV) SALK_138509 and SALK_127554
49	TOP1	RNAi cloning	CCC GGC TCG AGG GGA CAC CAC TTT CTG GAG TGA GAG	FWD XhoI-500 bp cDNA Sense Arm
50	TOP1	RNAi cloning	GGG CCA AGC TTG ATA TTT CGG ATA CCA GCA ACT AGC CC	RV 500 bp cDNA-HindIII Sense Arm
51	TOP1	RNAi cloning	GGG CCA CTA GTG GGA CAC CAC TTT CTG GAG TGA GAG	FWD SpeI-500 bp cDNA Antisense Arm
52	TOP1	RNAi cloning	GGG CCG AAT TCG ATA TTT CGG ATA CCA GCA ACT AGC CC	RV 500 bp cDNA-EcoRI Antisense Arm
53	TOP1	RNAi cloning	GGG GAC AAG TTT GTA CAA AAA AGC AGG CTT CGG GAC ACC ACT TTC TGG AGT GAG AG	FWD attB1-500 bp cDNA Sense/Antisense Arms
54	TOP1	RNAi cloning	GGG GAC CAC TTT GTA CAA GAA AGC TGG GTC GAT ATT TCG GAT ACC AGC AAC TAG C	RV 500 bp cDNA-attB2 Sense/Antisense Arms
55	Vector	Clone sequencing	GTAAAACGACGGCCAG	FWD M13; 5' sequencing of multiple entry clones
56	Vector	Clone sequencing	CAGGAAACAGCTATGAC	RV M13, 3' sequencing of multiple entry clones
57	Vector	Clone sequencing	TAA TAC GAC TCA CTA TAG GG	RV T7; 5' sequencing of dpGreen Bar-T multisite Gateway expression clone
58	Vector	Clone sequencing	ATT AAC CCT CAC TAA AGG GA	FWD T3; 3' sequencing of dpGreen Bar-T multisite Gateway expression clone
59	Vector	Clone sequencing	GGG ATG ACG CAC AAT CC	FWD; 5' sequencing of pHELLSGATE 12 clone; designed by Helliwell and Waterhouse (2003)
60	Vector	Clone sequencing	GAG CTA CAC ATG CTC AGG	RV; 3' sequencing of pHELLSGATE 12 clone; designed by Helliwell and Waterhouse (2003)
61	TOP1	Colony PCR check; clone sequencing	GGG ACA CCA CTT TCT GGA	FWD; colony PCR check; 5' sequencing of RNAi expression clones
62	TOP1	Colony PCR check; clone sequencing	GAT ATT TCG GAT ACC AGC AAC TAG	RV; colony PCR check; 3' sequencing of RNAi expression clones
63	ccdB	Emptyvector check	ATG CAG TTT AAG GTT TAC ACC TAT	FWD ccdB; for confirming empty Gateway vectors
64	ccdB	Emptyvector check	TTA TAT TCC CCA GAA CAT CAG GT	RV ccdB; for confirming empty Gateway vectors

Table S3: Expected semi-quantitative RT-PCR product sizes for wild-type *TOP1* and *TOP2*. Numbers 1-6 designate primer pairs: (1) = 5′ *TOP1*, (2) = *TOP1* between 339 and 439 insertions, (3) = 3′ *TOP1*, (4) = 5′ *TOP2*, (5) = *TOP2* between 127 and 727 insertions, and (6) = 3′ *TOP2*. *Actin 1* was amplified as an endogenous control.

***TOP1* Primer Pair**	**PCR Product Size (bp)**		***TOP2* Primer Pair**
	***TOP1* cDNA**	***TOP2* cDNA**	
1	334	261	4
2	407	159	5
3	256	318	6
Actin 1	391		*Actin 1*

Table S4: Vectors used for *TOP1* cloning. Abbreviations: ABRC = *Arabidopsis* Biological Resource Center, and ihp = intron-containing hairpin.

Vector	Purpose	Cloning Method	Source	Creators and References
pDONR™ 221	Entry/Intermediate Clone	Gateway®	Invitrogen	Invitrogen
pDONR™ /Zeo	Entry/Intermediate Clone	Gateway®	Invitrogen	Invitrogen
pDONR™ P4-P1r	Entry/Intermediate Clone	Gateway®	Invitrogen	Invitrogen
pDONR™ P2R-P3	Entry/Intermediate Clone	Gateway®	Invitrogen	Invitrogen
pEarleyGate 103	Constitutive Subcellular Localization	Gateway®	ABRC	Earley et al. (2006)
pEarleyGate 301	Native Complex Pull-down	Gateway®	ABRC	Earley et al. (2006)
pMDC7	Inducible Overexpression	Gateway®	Institute of Plant Biology and Zürich-Basel Plant Science Centre	Curtis and Grossniklaus (2003)
pMDC123	Complementation	Gateway®	ABRC	Curtis and Grossniklaus (2003)
pMDC164	Native Tissue-specific Localization	Gateway®	ABRC	Curtis and Grossniklaus (2003)
dpGreen BarT	Native Subcellular Localization	MultiSite Gateway®	Ji-Young Lee Lab	Lee Lab at the Boyce Thompson Institute for Plant Research
pSK-int	ihp-RNA-encoding Intermediate	Restriction Digestion-Ligation	Rockefeller University	Guo et al. (2003), Zuo et al. (2000), and Zuo et al. (2006)
pX7	Inducible-constitutive RNAi	Restriction Digestion-Ligation	Rockefeller University	Zuo et al. (2006)
pER8	Inducible-quantitative RNAi	Restriction Digestion-Ligation	Rockefeller University	Zuo et al. (2006)
pHELLSGATE 12	Constitutive RNAi	Gateway®	CSIRO Plant Industry	Helliwell and Waterhouse (2003) and Wesley et al. (2001)

Table S5: TOP1 and TOP2 homology with *Homo sapiens* and *Mus musculus* proteins.

Homo sapiens	Homology (%)*				*Mus muculus*
	TOP1	TOP2	TOP1	TOP2	
Thimet Oligopeptidase	**20.1**	**24.8**	**27.4**	**27.2**	Thimet Oligopeptidase
Mitochondrial Neurolysin	**23.7**	**30.3**	**27.2**	**27.3**	Mitochondrial Neurolysin Precursor
Mitochondrial Intermediate Peptidase	**22.1**	**32.1**	**23.7**	**24.0**	Mitochondrial Intermediate Peptidase Precursor

* % Homology was determined by sequence alignment between protein primary sequences using the DNASTAR Lasergene® MegAlign™ (Clustal W alignment) program.

Supplementary Figure and Table Legends

Figure S1: Salicylic acid functions and hypothetical signaling pathways. SA and Aspirin molecular structures were copied from 3Dchem.com (http://www.3dchem.com). Abbreviations: SABPs = salicylic acid-binding proteins.

Figure S2: Root phenotypes of *top1*, *top2*, and *top1 top2* mutants. Roots of 20-days-old seedlings grown on nutrient media were visualized at 60X magnification. On average, *top1*^{339} may have had shorter root length (not shown) compared to the Col-0 wild-type, *top2*^{127}, and *top1*^{439}*top2*^{127}.

Figure S3: DAB staining replicate sets at 6 hours post-infiltration. See Figure 10 for a description of the experiment. Entire replicate sets at 0, 9, and 12 hpi were not documented, but the most representative leaves were photographed for display in Figure 10.

Figure S4: HR phenotypes of *top1*, *top2*, and *top1 top2* mutants. Plants of 3- to 4-weeks-old were photographed 2-3 dpi of whole leaves with 1 x 10^6 CFU/mL *Pst* DC3000 *avrRpt2*. Small leaves (circled) displayed severe disease symptoms or collapse, but are not representative of fully grown adult leaves; therefore, they should be discounted when interpreting the overall phenotypes. Abbreviations: CFU = colony forming units, dpi = days post-inoculation, and HR = hypersensitive response.

Table S1: *TOP1* and *TOP2* T-DNA-tagged mutant lines. Table information was adapted from The *Arabidopsis* Information Resource (TAIR) and T-DNA Express: *Arabidopsis* Gene Mapping Tool. Abbreviations: bp = base pair, LP and RP = left and right genomic DNA primers, and BP = T-DNA border primer.

Table S2: Primers used for T-DNA insertion check, semi-quantitative RT-PCR, cloning, colony PCR check, and sequencing. Abbreviations: FWD = forward primer, RV = reverse primer, LP = left border genomic primer, RP = right border genomic primer, BP = T-DNA border primer, Pro = 2 kbp *TOP1* predicted promoter, ORF = open reading frame,

500bp cDNA = *TOP1* sequence sharing 88% homology with *TOP2*, 3xS = 3 stop codons, ns = no stop codon, *att* = Gateway® recombination sites, and nt = nucleotide.

Table S3: Expected semi-quantitative RT-PCR product sizes for wild-type *TOP1* and *TOP2*. Numbers 1-6 designate primer pairs: (1) = 5′ *TOP1*, (2) = *TOP1* between 339 and 439 insertions, (3) = 3′ *TOP1*, (4) = 5′ *TOP2*, (5) = *TOP2* between 127 and 727 insertions, and (6) = 3′ *TOP2*. *Actin 1* was amplified as an endogenous control.

Table S4: Vectors used for *TOP1* cloning. Abbreviations: ABRC = *Arabidopsis* Biological Resource Center, and ihp = intron-containing hairpin.

Table S5: TOP1 and TOP2 homology with *Homo sapiens* and *Mus musculus* proteins.

References

Ahlert, D., Stegemann, S., Kahlau, S., Ruf, S., and Bock, R. (2009). Insensitivity of chloroplast gene expression to DNA methylation. Mol. Genet. Genomics **282:** 17-24.

Aiken, C.T., Kaake, R.M., Wang, X., and Huang, L. (2011). Oxidative stress-mediated regulation of proteasome complexes. Molecular & Cellular Proteomics **10:** 1-11.

Altschup, S.F., Gish, W., Miller, W., Myers, E.W., & Lipman, D.J. (1990). Basic local alignment search tool. J. Mol. Biol. **215:** 403-410.

An, C., and Mou, Z. (2011). Salicylic acid and its function in plant immunity. Journal of Integrative Plant Biology **53:** 412-428.

Attaran, E., Zeier, T.E., Griebel, T., and Zeier, J. (2009). Methyl salicylate production and jasmonate signaling are not essential for systemic acquired resistance in *Arabidopsis*. The Plant Cell **21:** 954-971.

Ausubel, F.M. (2005). Are innate immune signaling pathways in plants and animals conserved? Nature Immunology **6:** 973-9.

Beers, E.P., Woffenden, B.J., and Zhao, C. (2000). Plant proteolytic enzymes: possible roles during programmed cell death. Plant Molecular Biology **44:** 399-415.

Block, A., Schmelz, E., O'Donnell, P.J., Jones, J.B., and Klee, H.J. (2005). Systemic acquired tolerance to virulent bacterial pathogens in tomato. Plant Physiology **138:** 1481-1490.

Book, A.J., Gladman, N.P., Lee, S., Scalf, M., Smith, L.M., and Vierstra, R.D. (2010). Affinity purification of the *Arabidopsis* 26 S proteasome reveals a diverse array of plant proteolytic complexes. The Journal of Biological Chemistry **285:** 25554-25569.

Boyes, D.C., Nam, J., and Dangl, J.L. (1998). The *Arabidopsis thaliana* RPM1 disease resistance gene product is a peripheral plasma membrane protein that is degraded coincident with the hypersensitive response. PNAS **95:** 15849-15854.

Brodersen, P., Malinovsky, F.G., Hématy, K., Newman, M., and Mundy, J. (2005). The role of salicylic acid in the induction of cell death. Plant Physiology **138:** 1037-1045.

Canet, J.V., Dobón, A., Ibáñez, F., Perales, L., and Tornero, P. (2010). Resistance and biomass in *Arabidopsis*: a new model for salicylic acid perception. Plant Biotechnology Journal **8:** 126-141.

Cao, H., Glazebrook, J., Clarke, J.D., Volko, S., and Dong, X. (1997). The *Arabidopsis* NPR1 gene that controls systemic acquired resistance encodes a novel protein containing ankyrin repeats. Cell **88:** 57-63.

Chen, F., D'Auria, J.C., Tholl, D., Ross, J.R., Gershenzon, J., Noel, J.P., and Pichersky, E. (2003). An *Arabidopsis thaliana* gene for methylsalicylate biosynthesis, identified by a biochemical genomics approach, has a role in defense. The Plant Journal **36:** 577-588.

Chen, Z., Ricigliano, J.W., and Klessig, D.F. (1993a). Purification and characterization of a soluble salicylic acid-binding protein from tobacco. PNAS **90:** 9533-9537.

Chen, Z., Silva, H., and Klessig, D.F. (1993b). Active oxygen species in the induction of plant systemic acquired resistance by salicylic acid. Science **262:** 1883-1885.

Chi, W., Sun, X., and Zhang, L. (2012). The roles of chloroplast proteases in the biogenesis and maintenance of photosystem II. Biochimica et Biophysica Acta **1817:** 239-246.

Clough, S.J., and Bent, A.F. (1998). Floral dip: a simplified method for *Agrobacterium*-mediated transformation of *Arabidopsis thaliana*. The Plant Journal **16:** 735-743.

Coll, N.S., Epple, P., and Dangl, J.L. (2011). Programmed cell death in the plant immune system. Cell Death and Differentiation **18:** 1247-1256.

Cunha, F.M., Berti, D.A., Ferreira, Z.S., Klitzke, F., Markus, R.P., and Ferro, E.S. (2008). Intracellular peptides as natural regulators of cell signaling. Journal of Biological Chemistry **283:** 24448-24459.

Curtis, M.D., and Grossniklaus, U. (2003). A Gateway cloning vector set for high-throughput functional analysis of genes in planta. Plant Physiology **133:** 462-469.

Dangl, J.L., Dietrich, R.A., and Richberg, M.H. (1996). Death don't have no mercy: cell death programs in plant-microbe interactions. The Plant Cell **8:** 1793-1807.

Dao, T.T.H., Puig, R.C., Kim, H.K., Erkelens, C., Lefeber, A.W.M., Linthorst, H.J.M., Choi, Y.H., and Verpoorte, R. (2009). Effect of benzothiadiazole on the metabolome of *Arabidopsis thaliana*. Plant Physiology and Biochemistry **47:** 146-152.

Davies, M.J. (2005). The oxidative environment and protein damage. Biochimica et Biophysica Acta **1703:** 93-109.

Davuluri, R.V., Sun, H., Palaniswamy, S.K., Matthews, N., Molina, C., Kurtz, M., and Grotewold, E. (2003). AGRIS: *Arabidopsis* Gene Regulatory Information Server, an information resource of *Arabidopsis* cis-regulatory elements and transcription factors. BMC Bioinformatics **4:** 1-11.

De Pinto, M.C., Locato, V., and De Gara, L. (2011). Redox regulation in plant programmed cell death. Plant, Cell and Environment **35:** 234-244.

Delledonne, M., Zeier, J., Marocco, A., and Lamb, C. (2001). Signal interactions between nitric oxide and reactive oxygen intermediates in the plant hypersensitive disease resistance response. PNAS **98:** 13454-13459.

Dielen, A., Badaoui, S., Candresse, T., and German-Retana, S. (2010). The ubiquitin/26S proteasome system in plant-pathogen interactions: a never-ending hide-and-seek game. Molecular Plant Pathology **11:** 293-308.

Dietrich, R.A., Delaney, T.P., Uknes, S.J., Ward, E.R., Ryals, J.A., and Dangl, J.L. (1994). *Arabidopsis* mutants simulating disease resistance response. Cell **77:** 565-577.

Dodds, P.N., and Rathjen, J.P. (2010). Plant immunity: towards an integrated view of plant-pathogen interactions. Nature Reviews Genetics **11:** 539-548.

Du, H., and Klessig, D.F. (1997). Identification of a soluble, high-affinity salicylic acid-binding protein in tobacco. Plant Physiology **113:** 1319-1327.

Durner, J., and Klessig, D.F. (1995). Inhibition of ascorbate peroxidase by salicylic acid and 2,6-dichloroisonicotinic acid, two inducers of plant defense responses. PNAS **92:** 11312-11316.

Durrant, W.E., and Dong, X. (2004). Systemic acquired resistance. Ann. Rev. Phytopathol. **42:** 185-209.

Earley, K.W., Haag, J.R., Pontes, O., Opper, K., Juehne, T., Song, K., and Pikaard, C.S. (2006). Gateway-compatible vectors for plant functional genomics and proteomics. The Plant Journal **45:** 616-629.

Eckardt, N.A. (2006). Programmed cell death in plants: a role for mitochondrial-associated hexokinases. The Plant Cell **18:** 2097-2099.

Eder, J., and Fersht, A.R. (1995). Pro-sequence-assisted protein folding. Molecular Microbiology **16:** 609-614.

Emanuelsson, O., Brunak, S., von Heijne, G., and Nielsen, H. (2007). Locating proteins in the cell using TargetP, SignalP and related tools. Nature Protocols **2:** 953-971.

Fariduddin, Q., Hayat, S., and Ahmad, A. (2003). Salicylic acid influences net photosynthetic rate, carboxylation efficiency, nitrate reductase activity, and seed yield in *Brassica juncea*. Photosynthetica **41:** 281-284.

Fojtová, M., Kovařík, A., and Matyášek, R. (2001). Cytosine methylation of plastid genome in higher plants. Fact or artefact? Plant Science **160:** 585-593.

Fragnière, C., Serrano, M., Abou-Mansour, E., Métraux, J., and L'Haridon, F. (2011). Salicylic acid and its location in response to biotic and abiotic stress. FEBS Letters **585:** 1847-1852.

Gadjev, I., Stone, J.M., and Gechev, T.S. (2008). Programmed cell death in plants : new insights into redox regulation and the role of hydrogen peroxide. International Review of Cell and Molecular Biology **270:** 87-144.

Gimenez-Ibanez, S., and Rathjen, J.P. (2010). The case for the defense: plants versus *Pseudomonas syringae*. Microbes and Infection **12:** 428-437.

Greenberg, J.T., and Yao, N. (2004). The role and regulation of programmed cell death in plant-pathogen interactions. Cellular Microbiology **6:** 201-211.

Guo, H., Fei, J., Xie, Q., and Chua, N. (2003). A chemical-regulated inducible RNAi system in plants. The Plant Journal **34:** 383-392.

Hall, D.A, Ptacek, J., and Snyder, M. (2007). Protein microarray technology. Mechanisms of Ageing and Development **128:** 161-167.

Hatsugai, N., Iwasaki, S., Tamura, K., Kondo, M., Fuji, K., Ogasawara, K., Nishimura, M., and Hara-Nishimura, I. (2009). A novel membrane fusion-mediated plant immunity against bacterial pathogens. Genes & Development **23:** 2496-2506.

Heazlewood, J.L., Tonti-Filippini, J., Verboom, R.E., and Millar, A.H. (2005). Combining experimental and predicted datasets for determination of the subcellular location of proteins. Bioinformatics **139:** 598-609.

Heazlewood, J.L., Verboom, R.E., Tonti-Filippini, J., Small, I., and Millar, A.H. (2007). SUBA: the *Arabidopsis* subcellular database. Nucleic Acids Research **35:** D213-D218.

Helliwell, C., and Waterhouse, P. (2003). Constructs and methods for high-throughput gene silencing in plants. Methods **30:** 289-295.

Huala, E., Dickerman, A.W., Garcia-Hernandez, M., Weems, D., Reiser, L., LaFond, F., Hanley, D., Kiphart, D., Zhuang, M., Huang, W., Mueller, L.A., Bhattacharyya, D., Bhaya, D., Sobral, B.W., Beavis, W., Meinke, D.W., Town, C.D., Somerville, C., and Rhee, S.Y. (2001). The *Arabidopsis* Information Resource (TAIR): a comprehensive database and web-based information retrieval, analysis, and visualization system for a model plant. Nucleic Acids Research **29:** 102-105.

Huang, J., Wang, H., Xie, X., Zhang, D., Liu, Y., and Guo, G. (2010). Roles of DNA methyltransferases in *Arabidopsis* development. African Journal of Biotechnology **9:** 8506-8514.

Jaspers, P. and Kangasjärvi, J. (2010). Reactive oxygen species in abiotic stress signaling. Physiologia Plantarum **138:** 405-413.

Jelenska, J., Yao, N., Vinatzer, B.A., Wright, C.M., Brodsky, J.L., and Greenberg, J.T. (2007). A J domain virulence effector of *Pseudomonas syringae* remodels host chloroplasts and suppresses defenses. Current Biology **17:** 499-508.

Jones, J.D.G., and Dangl, J.L. (2006). The plant immune system. Nature Reviews **444:** 323-329.

Jongeneel, C.V., Bouvier, J., & Bairoch, A. (1989). A unique signature identifies a family of zinc-dependent metallopeptidases. FEBS Letters **242:** 211-214.

Katagiri, F. (2004). A global view of defense gene expression regulation - a highly interconnected signaling network. Current Opinion in Plant Biology **7:** 506-511.

Katagiri, F., Thilmony, R., and He, S.Y. (2002). The *Arabidopsis* Book: The *Arabidopsis thaliana-Pseudomonas syringae* interaction. The American Society of Plant Biologists **1:** e0039.

Kawasaki, T., Nam, J., Boyes, D.C., Holt, B.F., Hubert, D.A., Wiig, A., and Dangl, J.L. (2005). A duplicated pair of *Arabidopsis* RING-finger E3 ligases contribute to the RPM1- and RPS2-mediated hypersensitive response. The Plant Journal **33:** 258-270.

Keogh, R.C., Deverall, B.J., and McLeod, S. (1980). Comparison of histological and physiological responses to *Phakopsora pachyrhizi* in resistant and susceptible soybean. Trans. Br. Mycol. Soc. **74:** 329-333.

Kessler, J.H., Khan, S., Seifert, U., Le Gall, S., Chow, K.M., Paschen, A., Bres-Vloemans, S.A., de Ru, A., van Montfoort, N., Franken, K.L.M.C., Benckhuijsen, W.E., Brooks, J.M., van Hall, T., Ray, K., Mulder, A., Doxiadis, I.I.N., van Swieten, P.F., Overkleeft, H.S., Prat, A., Tomkinson, B., Neefjes, J., Kloetzel, P.M., Rodgers, D.W., Hersh, L.B., Drijfhout, J.W., vanVeelen, P.A., Ossendorp, F., and Melief, C.J.M. (2011). Antigen processing by nardilysin and thimet oligopeptidase generates cytotoxic T cell epitopes. Nature Immunology **12:** 45-53.

Kest, B., Orlowski, M., and Bodnar, R.J. (1991). Increases in opioid-mediated swim antinociception following endopeptidase 24.15 inhibition. Physiology & Behavior **50:** 843-845.

Kim, S.I., Pabon, A., Swanson, T.A., and Glucksman, M.J. (2003). Regulation of cell-surface major histocompatibility complex class I expression by the endopeptidase EC3.4.24.15 (thimet oligopeptidase). Biochem. J. **375:** 111-120.

Kloetzel, P., and Ossendorp, F. (2004). Proteasome and peptidase function in MHC-class-I-mediated antigen presentation. Current Opinion in Immunology **16:** 76-81.

Koch, E., and Slusarenko, A. (1990). *Arabidopsis* is susceptible to infection by a downy mildew fungus. The Plant Cell **2:** 437-445.

Krysan, P.J., Young, J.C., and Sussman, M.R. (1999). T-DNA as an insertional mutagen in *Arabidopsis*. The Plant Cell **11:** 2283-2290.

Kunkel, B.N., and Brooks, D.M. (2002). Cross talk between signaling pathways in pathogen defense. Current Opinion in Plant Biology **5:** 325-331.

Kwon, H., Yokoyama, R., and Nishitani, K. (2005). A proteomic approach to apoplastic proteins involved in cell wall regeneration in protoplasts of *Arabidopsis* suspension-cultured cells. Plant Cell Physiol. **46:** 843-857.

Levine, A., Tenhaken, R., Dixon, R., and Lamb, C. (1994). H_20_2 from the oxidative burst orchestrates the plant hypersensitive disease resistance response. Cell **79:** 583-593.

Liu, P., Yang, Y., Pichersky, E., and Klessig, D.F. (2010a). Altering expression of benzoic acid/salicylic acid carboxyl methyltransferase 1 compromises systemic acquired resistance and PAMP-triggered immunity in *Arabidopsis*. MPMI **23:** 82-90.

Liu, P., von Dahl, C.C., and Klessig, D.F. (2011a). The extent to which methyl salicylate is required for signaling systemic acquired resistance is dependent on exposure to light after infection. Plant Physiology **157:** 2216-2226.

Liu, P., von Dahl, C.C., Park, S., and Klessig, D.F. (2011b). Interconnection between methyl salicylate and lipid-based long-distance signaling during the development of systemic acquired resistance in *Arabidopsis* and tobacco. Plant Physiology **155:** 1762-1768.

Liu, P., Bhattacharjee, S., Klessig, D.F., and Moffett, P. (2010b). Systemic acquired resistance is induced by R gene-mediated responses independent of cell death. Molecular Plant Pathology **11:** 155-160.

Liu, Y., Schiff, M., Czymmek, K., Tallóczy, Z., Levine, B., and Dinesh-Kumar, S.P. (2005). Autophagy regulates programmed cell death during the plant innate immune response. Cell **121:** 567-577.

Loake, G., and Grant, M. (2007). Salicylic acid in plant defence - the players and protagonists. Current Opinion in Plant Biology **10:** 466-472.

Logemann, E., Birkenbihl, R.P., Ulker, B., and Somssich, I.E. (2006). An improved method for preparing *Agrobacterium* cells that simplifies the *Arabidopsis* transformation protocol. Plant Methods **2:** 1-5.

Love, A.J., Milner, J.J., and Sadanandom, A. (2008). Timing is everything: regulatory overlap in plant cell death. Trends in Plant Science **13:** 589-595.

Martinez, C., Baccou, J.C., Bresson, E., Baissac, Y., Daniel, J.F., Jalloul, A., Montillet, J.L., Geiger, J., Assigbetsé, K., and Nicole, M. (2000). Salicylic acid mediated by the oxidative burst is a key molecule in local and systemic responses of cotton challenged by an avirulent race of *Xanthomonas campestris* pv *malvacearum*. Plant Physiology **122:** 757-766.

Masek, T., Vopalensky, V., Suchomelova, P., and Pospisek, M. (2005). Denaturing RNA electrophoresis in TAE agarose gels. Analytical Biochemistry **336:** 46-50.

McCarty, M.F., and Block, K.I. (2006). Preadministration of high-dose salicylates, suppressors of NF-kB activation, may increase the chemosensitivity of many cancers: an example of proapoptotic signal modulation therapy. Integrative Cancer Therapies **5:** 252-268.

Mecey, C., Hauck, P., Trapp, M., Pumplin, N., Plovanich, A., Yao, J., and He, S.Y. (2011). Critical role of STAYGREEN/Mendel's I locus in disease symptom development during *Pseudomonas syringae* pv. *tomato* infection of *Arabidopsis*. Plant Physiology **157:** 1965-1974.

Meher, H.C., Gajbhiye, V.T., and Singh, G. (2011). A GC-ECD method for estimation of free and bound amino acids, γ-aminobutyric acid, salicylic acid, and acetyl salicylic acid from *Solanum lycopersicum* (L.). Journal of AOAC International **94:** 232-243.

Melotto, M., Underwood, W., Koczan, J., Nomura, K., and He, S.Y. (2006). Plant stomata function in innate immunity against bacterial invasion. Cell **126:** 969-980.

Miao, Y., Laun, T.M., Smykowski, A., and Zentgraf, U. (2007). *Arabidopsis* MEKK1 can take a short cut: it can directly interact with senescence-related WRKY53 transcription factor on the protein level and can bind to its promoter. Plant Mol. Biol. **65:** 63-76.

Miller, G., Shulaev, V., and Mittler, R. (2008). Reactive oxygen signaling and abiotic stress. Physiologia Plantarum **133:** 481-489.

Miner, J., and Hoffhines, A. (2007). The discovery of aspirin's antithrombotic effects. Tex. Heart Inst. J. **34:** 179-186.

Mitchell, J.A., Akarasereenont, P., Thiemermann, C., Flower, R.J., and Vane, J.R. (1993). Selectivity of nonsteroidal antiinflammatory drugs as inhibitors of constitutive and inducible cyclooxygenase. PNAS **90:** 11693-11697.

Mittler, R., Vanderauwera, S., Gollery, M., and Van Breusegem, F. (2004). Reactive oxygen gene network of plants. Trends in Plant Science **9:** 490-498.

Moharekar, S.T., Lokhande (Moharekar), S.D., Hara, T., Tanaka, R., Tanaka, A., and Chavan, P.D. (2003). Effect of salicylic acid on chlorophyll and carotenoid contents of wheat and moong seedlings. Photosynthetica **41:** 315-317.

Mubarakshina, M.M., Ivanov, B.N., Naydov, I.A., Hillier, W., Badger, M.R., and Krieger-Liszkay, A. (2010). Production and diffusion of chloroplastic H_2O_2 and its implication to signalling. Journal of Experimental Botany **61:** 3577-3587.

Mur, L.A.J., Aubry, S., Mondhe, M., Kingston-Smith, A., Gallagher, J., Thomas, H., Timms-Taravella, E., James, C., Papp, I., Hörtensteiner, S., Thomas, H., and Ougham, H. (2010). Accumulation of chlorophyll catabolites photosensitizes the hypersensitive response elicited by *Pseudomonas syringae* in *Arabidopsis*. New Phytologist **188:** 161-174.

Mur, L.A.J., Kenton, P., Lloyd, A.J., Ougham, H., and Prats, E. (2008). The hypersensitive response; the centenary is upon us but how much do we know? Journal of Experimental Botany **59:** 501-520.

Nakagami, H., Soukupová, H., Schikora, A., Žárský, V., and Hirt, H. (2006). A mitogen-activated protein kinase kinase kinase mediates reactive oxygen species homeostasis in *Arabidopsis*. The Journal of Biological Chemistry **281:** 38697-38704.

Nakamura, S., Mano, S., Tanaka, Y., Ohnishi, M., Nakamori, C., Araki, M., Niwa, T., Nishimura, M., Kaminaka, H., Nakagawa, T., Sato, Y., and Ishiguro, S. (2010). Gateway binary vectors with the bialaphos resistance gene, bar, as a selection marker for plant transformation. Biosci. Biotechnol. Biochem. **74:** 1315-1319.

Nakazawa, M., and Matsui, M. (2003). Selection of hygromycin-resistant *Arabidopsis* seedlings. BioTechniques **34:** 28-30.

Nishimura, M.T., and Dangl, J.L. (2010). *Arabidopsis* and the plant immune system. The Plant Journal **61:** 1053-1066.

Nixon, P.J., Barker, M., Boehm, M., de Vries, R., and Komenda, J. (2005). FtsH-mediated repair of the photosystem II complex in response to light stress. Journal of Experimental Botany **56:** 357-363.

Norman, M.U., Reeve, S.B., Dive, V., Smith, A.I., and Lew, R.A. (2003). Endopeptidases 3.4.24.15 and 24.16 in endothelial cells: potential role in vasoactive peptide metabolism. Am. J. Physiol. Heart Circ. Physiol. **284:** H1978-H1984.

Padmanabhan, M.S., and Dinesh-Kumar, S.P. (2010). All hands on deck - the role of chloroplasts, endoplasmic reticulum, and the nucleus in driving plant innate immunity. MPMI **23:** 1368-1380.

Pancheva, T.V., and Popova, L.P. (1998). Effect of salicylic acid on the synthesis of ribulose-1,5-bisphosphate carboxylase/oxygenase in barley leaves. Journal of Plant Physiology **152:** 381-386.

Park, S., Kaimoyo, E., Kumar, D., Mosher, S., and Klessig, D.F. (2007a). Methyl salicylate is a critical mobile signal for plant systemic acquired resistance. Science **318:** 113-116.

Park, S., Yu, J., Park, J., Li, J., Yoo, S., Lee, N., Lee, S., Jeong, S., Seo, H.S., Koh, H., Jeon, J., Park, Y., and Paek, N. (2007b). The senescence-induced staygreen protein regulates chlorophyll degradation. The Plant Cell **19:** 1649-1664.

Paschoalin, T., Carmona, A.K., Oliveira, V., Juliano, L., and Travassos, L.R. (2005). Characterization of thimet- and neurolysin-like activities in *Escherichia coli* M3A peptidases and description of a specific substrate. Archives of Biochemistry and Biophysics **441:** 25-34.

Paschoalin, T., Carmona, A.K., Rodrigues, E.G., Oliveira, V., Monteiro, H.P., Juliano, M.A., Juliano, L., and Travassos, L.R. (2007). Characterization of thimet oligopeptidase and neurolysin activities in B16F10-Nex2 tumor cells and their involvement in angiogenesis and tumor growth. Molecular Cancer **6:** 1-14.

Paterson, J., Baxter, G., Lawrence, J., and Duthie, G. (2006). Is there a role for dietary salicylates in health? Proceedings of the Nutrition Society **65:** 93-96.

Pavlopoulou, A., and Kossida, S. (2007). Plant cytosine-5 DNA methyltransferases: structure, function, and molecular evolution. Genomics **90:** 530-541.

Polge, C., Jaquinod, M., Holzer, F., Bourguignon, J., Walling, L., and Brouquisse, R. (2009). Evidence for the existence in *Arabidopsis thaliana* of the proteasome proteolytic pathway: activation in response to cadmium. The Journal of Biological Chemistry **284:** 35412-35424.

Popescu, S.C., Snyder, M., and Dinesh-Kumar, S.P. (2007). *Arabidopsis* protein microarrays for the high-throughput identification of protein-protein interactions. Plant Signaling & Behavior **2:** 416-420.

Postel, S., Küfner, I., Beuter, C., Mazzotta, S., Schwedt, A., Borlotti, A., Halter, T., Kemmerling, B., and Nürnberger, T. (2010). The multifunctional leucine-rich repeat receptor kinase BAK1 is implicated in *Arabidopsis* development and immunity. European Journal of Cell Biology **89:** 169-174.

Rao, M.V., Paliyath, G., Ormrod, D.P., Murr, D.P., and Watkins, C.B. (2012). Influence of salicylic acid on H_20_2 production, oxidative stress, and H_20_2-metabolizing enzymes. Plant Physiology **115:** 137-149.

Rate, D.N., and Greenberg, J.T. (2001). The *Arabidopsis* aberrant growth and death2 mutant shows resistance to *Pseudomonas syringae* and reveals a role for NPR1 in suppressing hypersensitive cell death. The Plant Journal **27:** 203-211.

Rawlings, N.D., Morton, F.R., Kok, C.Y., Kong, J., and Barrett, A.J. (2008). MEROPS: the peptidase database. Nucleic Acids Research **36:** D320-D325.

Rawlings, N.D. and Barrett, A.J. (1995). Evolutionary families of metallopeptidases. Methods in Enzymology **248:** 183-228.

Ray, K., Hines, C.S., Coll-Rodriguez, J., and Rodgers, D.W. (2004). Crystal structure of human thimet oligopeptidase provides insight into substrate recognition, regulation, and localization. The Journal of Biological Chemistry **279:** 20480-20489.

Robert-Seilaniantz, A., Grant, M., and Jones, J.D.G. (2011). Hormone crosstalk in plant disease and defense: more than just jasmonate-salicylate antagonism. Annu. Rev. Phytopathol. **49:** 317-343.

Rock, K.L., York, I.A., and Goldberg, A.L. (2004). Post-proteasomal antigen processing for major histocompatibility complex class I presentation. Nature Immunology **5:** 670-677.

Roine, E., Wei, W., Yuan, J., Nurmiaho-Lassila, E.L., Kalkkinen, N., Romantschuk, M., and He, S.Y. (1997). Hrp pilus: an hrp-dependent bacterial surface appendage produced by *Pseudomonas syringae* pv. *tomato* DC3000. PNAS **94:** 3459-3464.

Saric, T., Graef, C.I., and Goldberg, A.L. (2004). Pathway for degradation of peptides generated by proteasomes: a key role for thimet oligopeptidase and other metallopeptidases. The Journal of Biological Chemistry **279:** 46723-46732.

Sarry, J., Kuhn, L., Ducruix, C., Lafaye, A., Junot, C., Hugouvieux, V., Bastien, O., Fievet, J.B., Vailhen, D., Amekraz, B., Moulin, C., Ezan, E., Garin, J., and Bourguignon, J. (2006). The early responses of *Arabidopsis thaliana* cells to cadmium exposure explored by protein and metabolite profiling analyses. Proteomics **6:** 2180-2198.

Scotter, M.J., Roberts, D.P.T., Wilson, L.A., Howard, F.A.C., Davis, J., and Mansell, N. (2007). Free salicylic acid and acetyl salicylic acid content of foods using gas chromatography-mass spectrometry. Food Chemistry **105:** 273-279.

Seo, S., Okamoto, M., Iwai, T., Iwano, M., Fukui, K., Isogai, A., Nakajima, N., and Ohashi, Y. (2000). Reduced levels of chloroplast FtsH protein in tobacco mosaic virus-infected tobacco leaves accelerate the hypersensitive reaction. The Plant Cell **12:** 917-932.

Sigrist, C.J.A., Cerutti, L., de Castro, E., Langendijk-Genevaux, P.S., Bulliard, V., Bairoch, A., and Hulo, N. (2010). PROSITE, a protein domain database for functional characterization and annotation. Nucleic Acids Research **38:** D161-D166.

Silva, C.L., Portaro, F.C.V., Camargo, A.C.M.D., and Ferro, E.S. (1999). Thimet oligopeptidase (EC 3.4.24.15), a novel protein on the route of MHC class I antigen presentation. Biochemical and Biophysical Research Communications **255:** 591-595.

Slaymaker, D.H., Navarre, D.A., Clark, D., del Pozo, O., Martin, G.B., and Klessig, D.F. (2002). The tobacco salicylic acid-binding protein 3 (SABP3) is the chloroplast carbonic anhydrase, which exhibits antioxidant activity and plays a role in the hypersensitive defense response. PNAS **99:** 11640-11650.

Snyrychová, I., Ayaydin, F., and Hideg, E. (2009). Detecting hydrogen peroxide in leaves in vivo - a comparison of methods. Physiologia Plantarum **135:** 1-18.

Sokolenko, A., Pojidaeva, E., Zinchenko, V., Panichkin, V., Glaser, V.M., Herrmann, R.G., and Shestakov, S.V. (2002). The gene complement for proteolysis in the cyanobacterium *Synechocystis* sp . PCC 6803 and *Arabidopsis thaliana* chloroplasts. Curr. Genet. **41:** 291-310.

Spoel, S.H., Mou, Z., Tada, Y., Spivey, N.W., Genschik, P., and Dong, X. (2009). Proteasome-mediated turnover of the transcription coactivator NPR1 plays dual roles in regulating plant immunity. Cell **137:** 860-872.

Straus, M.R., Rietz, S., van Themaat, E.V.L., Bartsch, M., and Parker, J.E. (2010). Salicylic acid antagonism of EDS1-driven cell death is important for immune and oxidative stress responses in *Arabidopsis*. The Plant Journal **62:** 628-640.

Sun, Q., Zybailov, B., Majeran, W., Friso, G., Olinares, P.D.B., and van Wijk, K.J. (2009). PPDB, the Plant Proteomics Database at Cornell. Nucleic Acids Research **37:** D969-D974.

Swanson, S., and Gilroy, S. (2010). ROS in plant development. Physiologia Plantarum **138:** 384-392.

Takahashi, S., and Murata, N. (2008). How do environmental stresses accelerate photoinhibition? Trends in Plant Science **13:** 178-182.

Tenhaken, R, Levine, A., Brisson, L.F., Dixon, R.A., and Lamb, C. (1995). Function of the oxidative burst in hypersensitive disease resistance. PNAS **92:** 4158-4163.

Thordal-Christensen, H., Zhang, Z., Wei, Y., and Collinge, D.B. (1997). Subcellular localization of H_2O_2 in plants. H_2O_2 accumulation in papillae and hypersensitive response during the barley-powdery mildew interaction. The Plant Journal **11:** 1187-1194.

Torres, M.A. (2010). ROS in biotic interactions. Physiologia Plantarum **138:** 414-429.

Torres, M.A., Dangl, J.L., and Jones, J.D.G. (2002). Arabidopsis gp91 phox homologues AtrbohD and AtrbohF are required for accumulation of reactive oxygen intermediates in the plant defense response. PNAS **99:** 517-522.

Torres, M.A., Jones, J.D.G., and Dangl, J.L. (2005). Pathogen-induced, NADPH oxidase-derived reactive oxygen intermediates suppress spread of cell death in *Arabidopsis thaliana*. Nature Genetics **37:** 1130-1134.

Vallad, G.E., and Goodman, R.M. (2004). Systemic acquired resistance and induced systemic resistance in conventional agriculture. Crop Sci. **44:** 1920-1934.

van Bentem, S.F., Anrather, D., Dohnal, I., Roitinger, E., Csaszar, E., Joore, J., Buijnink, J., Carreri , A., Forzani, C., Lorkovic, Z.J., Barta, A., Lecourieux, D., Verhounig, A., Jonak, C., and Hirt, H. (2008). Site-specific phosphorylation profiling of *Arabidopsis* proteins by mass spectrometry and peptide chip analysis. Journal of Proteome Research **7:** 2458-2470.

Van Breusegem, F., Bailey-Serres, J., and Mittler, R. (2008). Unraveling the tapestry of networks involving reactive oxygen species in plants. Plant Physiology **147:** 978-984.

Vanacker, H., Lu, H., Rate, D.N., and Greenberg, J.T. (2001). A role for salicylic acid and NPR1 in regulating cell growth in *Arabidopsis*. The Plant Journal **28:** 209-216.

Vane, J.R., and Botting, R.M. (2003). The mechanism of action of aspirin. Thrombosis Research **110:** 255-258.

Vicente, M.R., and Plasencia, J. (2011). Salicylic acid beyond defence: its role in plant growth and development. Journal of Experimental Botany **62:** 3321-3338.

Villiers, F., Ducruix, C., Hugouvieux, V., Jarno, N., Ezan, E., Garin, J., Junot, C., and Bourguignon, J. (2011). Investigating the plant response to cadmium exposure by proteomic and metabolomic approaches. Proteomics **11:** 1650-1663.

Vision, T.J., Brown, D.G., and Tanksley, S.D. (2000). The origins of genomic duplications in *Arabidopsis*. Science **290:** 2114-2117.

Vlot, A.C., Klessig, D.F., and Park, S. (2008a). Systemic acquired resistance: the elusive signal(s). Current Opinion in Plant Biology **11:** 436-442.

Vlot, A.C., Dempsey, D.M.A., and Klessig, D.F. (2009). Salicylic acid, a multifaceted hormone to combat disease. Annu. Rev. Phytopathol. **47:** 177-206.

Vlot, A.C., Liu, P., Cameron, R.K., Park, S., Yang, Y., Kumar, D., Zhou, F., Padukkavidana, T., Gustafsson, C., Pichersky, E., and Klessig, D.F. (2008). Identification of likely orthologs of tobacco salicylic acid-binding protein 2 and their role in systemic acquired resistance in *Arabidopsis thaliana*. The Plant Journal **56:** 445-456.

Walters, D., Walsh, D., Newton, A., and Lyon, G. (2005). Induced resistance for plant disease control: maximizing the efficacy of resistance elicitors. Phytopathology **95:** 1368-1373.

Wang, X., Wang, Q., Ives, K.L., and Evers, B.M. (2009a). Curcumin inhibits neruotensin-mediated interleukin-8 production and migration of HCT116 human colon cancer cells. Clin. Cancer Res. **12:** 5346-5355.

Wang, Y.H. (2008). How effective is T-DNA insertional mutagenesis in *Arabidopsis*? J. Biochem. Tech. **1:** 11-20.

Wang, Y., Zhang, W., Song, L., Zou, J., Su, Z., and Wu, W. (2008). Transcriptome analyses show changes in gene expression to accompany pollen germination. Plant Physiology **148:** 1201-1211.

Wang, Y., Feechan, A., Yun, B., Shafiei, R., Hofmann, A., Taylor, P., Xue, P., Yang, F., Xie, Z., Pallas, J.A., Chu, C., and Loake, G.J. (2009b). S-nitrosylation of AtSABP3 antagonizes the expression of plant immunity. The Journal of Biological Chemistry **284:** 2131-2137.

Watanabe, N., and Lam, E. (2006). *Arabidopsis* Bax inhibitor-1 functions as an attenuator of biotic and abiotic types of cell death. The Plant Journal **45:** 884-894.

Watanabe, N., and Lam, E. (2008). BAX inhibitor-1 modulates endoplasmic reticulum stress-mediated programmed cell death in *Arabidopsis*. The Journal of Biological Chemistry **283:** 3200-3210.

Watanabe, N., and Lam, E. (2011). *Arabidopsis* metacaspase 2d is a positive mediator of cell death induced during biotic and abiotic stresses. The Plant Journal **66:** 969-982.

Wesley, S.V., Helliwell, C.A., Smith, N.A., Wang, M.B., Rouse, D.T., Liu, Q., Gooding, P.S., Singh, S.P., Abbott, D., Stoutjesdijk, P.A., Robinson, S.P., Gleave, A.P., Green, A.G., and Waterhouse, P.M. (2001). Construct design for efficient, effective and high-throughput gene silencing in plants. The Plant Journal **27:** 581-590.

Winter, D., Vinegar, B., Nahal, H., Ammar, R., Wilson, G.V., and Provart, N. J. (2007). An "Electronic Fluorescent Pictograph" browser for exploring and analyzing large-scale biological data sets. PLoS ONE **2:** e718.

Wolf-Yadlin, A., Sevecka, M., and MacBeath, G. (2009). Dissecting protein function and signaling using protein microarrays. Current Opinion in Chemical Biology **13:** 398-405.

Wolfe, J., Hutcheon, C.J., Higgins, V.J., and Cameron, R.K. (2000). A functional gene-for-gene interaction is required for the production of an oxidative burst in response to infection with avirulent *Pseudomonas syringae* pv. *tomato* in *Arabidopsis thaliana*. Physiological and Molecular Plant Pathology **56:** 253-261.

Xiang, C., Han, P., & Oliver, D.J. (1999). In solium selection for *Arabidopsis* transformants resistant to kanamycin. Plant Molecular Biology Reporter **17:** 59-65.

York, I.A., Mo, A.X.Y., Lemerise, K., Zeng, W., Shen, Y., Abraham, C.R., Saric, T., Goldberg, A.L., and Rock, K.L. (2003). The cytosolic endopeptidase, thimet oligopeptidase, destroys antigenic peptides and limits the extent of MHC class I antigen presentation. Immunity **18:** 429-440.

Yoshimoto, K., Jikumaru, Y., Kamiya, Y., Kusano, M., Consonni, C., Panstruga, R., Ohsumi, Y., and Shirasu, K. (2009). Autophagy negatively regulates cell death by controlling NPR1-dependent salicylic acid signaling during senescence and the innate immune response in *Arabidopsis*. The Plant Cell **21:** 2914-2927.

Yoshioka, M., and Yamamoto, Y. (2011). Quality control of photosystem II: where and how does the degradation of the D1 protein by FtsH proteases start under light stress? - facts and hypotheses. Journal of Photochemistry and Photobiology B: Biology **104:** 229-235.

Zhang, C., Gutsche, A.T., and Shapiro, A.D. (2004). Feedback control of the *Arabidopsis* hypersensitive response. MPMI **17:** 357-365.

Zhang, W., and Chen, W. (2011). Role of salicylic acid in alleviating photochemical damage and autophagic cell death induction of cadmium stress in *Arabidopsis thaliana*. Photochem. Photobiol. Sci. **10:** 947-955.

Zhang, Y., Xu, S., Ding, P., Wang, D., Cheng, Y.T., He, J., Gao, M., Xu, F., Li, Y., Zhu, Z., Li, X., and Zhang, Y. (2010). Control of salicylic acid synthesis and systemic acquired resistance by two members of a plant-specific family of transcription factors. PNAS **107:** 18220-18225.

Zuo, J., Niu, Q., and Chua, N. (2000). Technical advance: An estrogen receptor-based transactivator XVE mediates highly inducible gene expression in transgenic plants. The Plant Journal **24:** 265-273.

Zuo, J., Hare, P.D., and Chua, N. (2006). Applications of chemical-inducible expression systems in functional genomics and biotechnology. Methods in Molecular Biology **323:** 329-342.